AD NUMBER
AD127331
CLASSIFICATION CHANGES
TO: unclassified
FROM: confidential
LIMITATION CHANGES
TO: Distribution authorized to DoD only; Test and Evaluation; MAR 1957. Other requests shall be referred to David Taylor Model Basin, Washington, DC. Pre-dates formal DoD distribution statements. Treat as DoD only.
FROM: Controlling DoD Organization: David Taylor Model Basin, Washington, DC.
AUTHORITY
31 Mar 1969, DoDD 5200.10; Pre-dates formal DoD distribution statements. Treat as DoD only.

NAVY DEPARTMENT

THE DAVID W. TAYLOR MODEL BASIN

AERODYNAMICS LABORATORY

WASHINGTON 7, D.C.

WIND-TUNNEL INVESTIGATION OF THE DRAG OF A PROPOSED BOUNDARY-LAYER-CONTROLLED AIRSHIP

(Title Unclassified)

by

Peter A. Gerrard

Symbols

A	wake area
C_{D_w}	wake drag coefficient
C_{D_w}'	wake point drag coefficient
C_{D_s}	suction pump drag coefficient
C_{D_t}	total drag coefficient
C_p	pressure coefficient
g	distance between aft end of main body of BLC airship and tail cone, shroud, or annular airfoil
L	body length
M	stream Mach number
m	suction mass flow
p	static pressure
p_t	total head pressure
R	Reynolds number ($U_1 L/\nu$)
r	body radius
U	velocity
u	velocity parallel to surface in the boundary layer
V	airship volume
W_s	power supplied by suction pump
x	axial station measured from nose
γ	ratio of specific heats (1.4)
δ	boundary-layer thickness
δ^*	boundary-layer displacement thickness

Symbols (Concluded)

ρ	density
ξ	coordinate normal to and measured outward from the body surface
η	angle between the tangent to the body surface and the body axis
θ	boundary-layer momentum thickness
ν	kinematic viscosity

Subscripts

1	refers to free-stream conditions
w	refers to conditions at the wake station
b	refers to conditions at surface of body
δ	refers to conditions at outer edge of boundary layer

TABLE OF CONTENTS

TABLE OF CONTENTS (Concluded)

AERODYNAMICS LABORATORY
DAVID TAYLOR MODEL BASIN
UNITED STATES NAVY
WASHINGTON, D. C.

WIND-TUNNEL INVESTIGATION OF THE DRAG OF A PROPOSED BOUNDARY-LAYER-CONTROLLED AIRSHIP

by

Peter A. Cerreta

SUMMARY

An investigation of the drag of a proposed boundary-layer-controlled airship has been made in the 7- by 10-Foot Transonic Wind Tunnel at the David Taylor Model Basin. The tests covered a Reynolds number range of 4,000,000 to 12,000,000. Included in the investigation was a limited number of tests of an XZS2G-1 airship.

Two means of boundary-layer control were tested. Investigations were made of an annular airfoil and an annular suction slot, both located at approximately the 85-percent station.

The drag of the BLC airship is compared with that of the XZS2G-1 airship. The drag of the annular airfoil configuration is higher than that of the XZS2G-1. For the suction configuration, results indicate that a saving in drag of approximately 20 percent over that of the XZS2G-1 could be realized.

INTRODUCTION

The Goodyear Aircraft Company has proposed a design for an airship using boundary-layer control on the aft portion of the airship. Although several other advantageous features are attributed by the designer to this airship, the tests reported

herein are primarily to provide experimental verification of the theoretically anticipated reduction in drag due to boundary-layer control.

Two alternative methods of boundary-layer control are presented in the proposed design. The first employs the technique of internal suction applied to the boundary layer through a circumferential gap located on the aft portion of the airship where boundary-layer separation for this particular configuration is normally expected. In the second method the suction gap is replaced by a small annular airfoil which encircles the airship. The anticipated result in either case is a significant reduction in drag due to the elimination or delay of flow separation.

In Reference 1, wind-tunnel tests were requested and authorized for a 0.0144-scale model of the Goodyear boundary-layer-control airship to determine its drag characteristics. Drag measurements of a model of the XZS2G-1 airship to serve as a standard of comparison were also requested in Reference 1. These tests were conducted in the TMB 7- by 10-Foot Transonic Wind Tunnel during July, August, and September of 1956.

DESCRIPTION OF APPARATUS

The investigation was conducted in the TMB 7- by 10-Foot Transonic Wind Tunnel. The tunnel has a slotted throat and, at the time of testing, was capable of speeds up to a Mach number of 0.8. The Mach number variation in the test region was ±0.005. The free-stream turbulence level as measured with a hot-wire anemometer varied from 0.01 percent at M = 0.1 to 0.04 percent at M = 0.4. Measurements indicated that the flow angularity in the test section was within ±0.1° in both the pitch and yaw direction.

Drag values were determined from a survey of the momentum deficit in the wake. A wake rake was located approximately 3 feet downstream of the model and was used to measure the total-head deficit and static pressure in the wake. The general arrangement of the wake rake is shown in Figures 1a and 1b. The vertical and horizontal arms of the rake contained 61 and 106 total-head tubes, respectively. Wake static pressures were measured at seven stations along the horizontal arm. It was possible to adjust both the horizontal and vertical position of the rake during a run. By observing the wake total-head distribution on the manometer boards, it was possible to position the center of the rake on the center of the wake. This procedure was followed for each run.

Because of the limited number of manometer tubes, it was not possible to use all the tubes in the rake simultaneously. For this reason only 31 tubes in the vertical arm were used. The 106 tubes in the horizontal arm of the rake were, in reality, four rakes consolidated into one arm. By using a switching arrangement it was possible to select the proper rake for the size of wake to be measured. By this method it was possible to obtain a minimum of 12 total-head readings in the wake for wake radii varying from 3.5 inches to 20 inches. All wake static tubes were used.

A calibrated Venturi meter was used to determine the suction flow rate. By measuring the total and static pressure in the throat of the venturi and the temperature of the stream, the suction flow rate could be determined from the calibration curves.

Transition was fixed at the 10-percent station on both models by a double row of staggered, discrete, conical

turbulence-stimulating elements, which are clearly visible in the photograph of Figure 2b. A sublimation technique was used to check the effectiveness of the turbulence stimulators. The subliming solution was a mixture of acenaphthene and acetone. The solution was dry-sprayed onto the model and the coating was brushed lightly to remove any large particles which might have accumulated during spraying. Figure 2a shows the BLC airship after coating. During a run, the coating sublimates in the turbulent region earlier than in the laminar region. Figure 2b is a photograph of the coating after a run was completed. The technique showed that transition was occurring, as desired, at the 10-percent station. Boundary-layer-turbulence stimulation was used for all tests except for one run to determine the pressure distribution of the XZS2G-1.

Both airship models were supported from the wall of the tunnel by a strut. The XZS2G-1 mounted on this strut is shown in Figure 1a. The strut, which was constructed with a symmetrical low-speed airfoil section, was hollow in order to provide a passageway for air removed from the boundary layer by suction. For configurations with no suction, the passageway was closed off to prevent undesired back-flow through it.

A visual observation of the flow direction over the complete model and the model-strut junction was made by the standard tuft method. Tufts showed no excessive change of flow direction on the model in the vicinity of the strut. The method did indicate, however, that the flow separated several inches upstream of the suction slot when no suction was applied to the model. When sufficient suction was applied to the model the flow was attached well aft of the suction gap.

MODELS AND TESTS

Tests were performed on two models, the XZS2G-1 and the BLC airship. Reynolds numbers for these tests, based on a body length of 58.8 inches, varied from 4,000,000 to 12,000,000.

A model of the XZS2G-1 was constructed and tested to provide a basis of comparison for the drag of the proposed BLC airship. The model was constructed in three sections - nose, center, and tail. The nose and tail sections were made of spun aluminum. The center section was constructed with a fiber glass skin attached to aluminum bracing. The model was supported from the center section by a strut. A photograph of the model installed in the tunnel is given in Figure 1a. Pressure distribution over the model was measured at 43 stations along a generatrix in the horizontal plane of the support but diametrically opposite. Table 1 gives the coordinates of the model for stations corresponding to the location of the static pressure orifices.

Tests of the XZS2G-1 were made for both natural and tripped boundary layers. For both conditions the pressure distributions over the body were recorded and in the case of the tripped boundary layer the velocity distribution in the wake was recorded.

The BLC airship was constructed in two main sections - body and tail cone. The body was constructed in three sub-sections - nose, center, and aft portions. The tail cone was attached to the body by means of three uniformly spaced 3/8-inch rods. These rods were actuated by a drive mechanism housed in the body section so that the axial position of the tail cone could be varied with respect to the body. In this manner a suction gap of adjustable width was formed between the body and the tail cone.

In addition, the geometry of the suction gap was also altered by attaching a shroud to the forward end of the adjustable tail cone. This shroud formed a lip which extended the contour of the tail cone in the upstream direction.

When testing the annular airfoil, an alternate tail cone was used in the gap-closed position forming the basic BLC airship configuration. This tail cone permitted the actuating rods to extend through it. Thus, with the airfoil supported by the rods, it was possible to vary the axial position of the airfoil by means of the same actuating mechanism previously used to vary the tail cone position.

The ducting for the suction system was internally housed in the body section and passed through the supporting strut to the exterior of the test section where it was connected to the piping system associated with a conventional suction pump. The air withdrawn from the tunnel flow in this way was eventually discharged into the atmosphere.

The aft subsection of the body section was easily removable to provide access to the suction ducting and drive mechanism which are housed within the body.

As in the case of the XZS2G-1, the basic BLC airship model is equipped with 43 static-pressure orifices distributed along the generatrix in the horizontal plane opposite the supporting strut. A sketch of the basic BLC airship configuration and the coordinates associated with each orifice location are given in Table 2.

Besides the basic BLC configuration, a total of three other major configurations were tested – the tail cone suction gap with and without shroud and the annular airfoil. These three additional configurations are sketched, in part, in Table 3. Also shown for each configuration is a list of the

positions of the appropriate components at which experimental data were obtained. The Reynolds number was also varied during the test of each configuration and, for the two cases of boundary-layer suction, the suction conditions, in addition, were systematically varied.

The BLC airship was also instrumented for boundary-layer measurements. Two boundary-layer rakes were mounted on the airship, one upstream and one downstream of the suction slot. The upstream rake was used in all runs of the BLC airship. A similar rake was located on the suction tail cone. In the basic and annular airfoil tests two rakes were installed on the tail cone. These rakes were spaced so that one rake was located at the leading edge and one at the trailing edge of the airfoil. Figure 2a shows the upstream rake and two tail-cone rakes installed on the basic configuration.

All runs of the BLC airship were made with the boundary layer tripped. For each run, body static-pressure distributions, boundary-layer profiles, and velocity distributions in the wake were determined. For runs with suction, sufficient data were taken to calculate the suction flow rate.

REDUCTION OF DATA

The equations used in reducing the data, together with a brief description of the underlying theoretical considerations and assumptions, are given below.

PRESSURE COEFFICIENT

The pressure coefficient, C_p, was calculated from measurements of body static pressure, p_b, and free-stream static pressure, p_1, in accordance with the following relation:

$$C_p = \frac{p_b - p_1}{\frac{1}{2}\rho_1 U_1^2} = \frac{p_b - p_1}{\frac{\gamma}{2} p_1 M_1^2}$$

DRAG COEFFICIENTS

The wake drag coefficient, C_{D_w}, was determined from a simplified form of the integral of the momentum loss over the wake. The method, essentially, consists of an integration of the wake point drag coefficient, C'_{D_w}, over the wake area, A_w; i.e.,

$$C_{D_w} = \frac{D_w}{\frac{1}{2}\rho_1 U_1^2 V^{2/3}} = \frac{1}{V^{2/3}} \int_{A_w} C'_{D_w} \, dA_w$$

where,

$$C'_{D_w} = 2 \frac{\rho_w}{\rho_1} \frac{U_w}{U_1} \left(1 - \frac{U_w}{U_1}\right)$$

$$= 2 \left(\frac{p_{t_w} - p_w}{p_{t_1} - p_1}\right)^{\frac{1}{2}} \left(\frac{p_w}{p_1}\right)^{\frac{1}{2\gamma}} \left[1 + 0.625 \left(\frac{p_{t_1}}{p_1}\right)^{\frac{2(\gamma-1)}{\gamma}} - 0.625 \left(\frac{p_{t_w}}{p_w}\right)^{\frac{2(\gamma-1)}{\gamma}}\right]^{\frac{1}{2}} \times$$

$$\left[\left(\frac{p_{t_w}}{p_{t_1}}\right)^{\frac{\gamma-1}{2\gamma}} - \left(\frac{p_{t_w} - p_1}{p_{t_1} - p_1}\right)^{\frac{1}{2}}\right] \left[1 + 0.625 \left(\frac{p_{t_1}}{p_1}\right)^{\frac{2(\gamma-1)}{\gamma}} - 0.625 \left(\frac{p_{t_w}}{p_1}\right)^{\frac{2(\gamma-1)}{\gamma}}\right]^{\frac{1}{2}}$$

The suction pump drag coefficient, C_{D_s}, was determined from energy balance considerations in which the pump work required to restore that portion of the boundary layer that was withdrawn by the suction system to free-stream total head is converted to an equivalent drag. The assumptions made in deriving the relation for the suction pump drag coefficient which is given on the following page are:

(1) That the flow in the boundary layer is adiabatically related to the flow in the free stream, and

(2) That the pump isentropically restores the mass removed from the boundary layer by the suction system to its free-stream total-head condition.

$$C_{D_s} = \frac{D_s}{\frac{1}{2}\rho_1 U_1^2 V^{2/3}} = \frac{W_s}{\frac{1}{2}\rho_1 U_1^3 V^{2/3}}$$

$$= \frac{2\pi}{V^{2/3}}\left[\frac{2}{(\gamma-1)M_1^2} + 1\right]\int_0^{-y} \frac{\rho}{\rho_1}\frac{U}{U_1}\left[\left(\frac{p_{t_1}}{p_t}\right)^{\frac{\gamma-1}{\gamma}} - 1\right](r+\xi\cos\eta)d\xi$$

The upper limit of integration, y, was determined in each case by integrating the mass flow in the boundary layer from the body surface outward to a point at which the integrated value equaled the value independently recorded by a flow meter as the mass flow withdrawn from the boundary layer by the suction system. Also, in the actual performance of the suction-pump-drag calculations, the flow was considered incompressible, i.e. $\rho/\rho_1 = 1$. For purposes of clarification, it is pointed out that the incremental area element of the suction-pump-drag integral is equal to $2\pi(r + \xi\cos\eta)d\xi$, which, as can be seen in Figure 3, reflects the fact that the integration is over the surface of a truncated cone under axially symmetric conditions. The integration of the suction-pump-drag coefficient was carried out with the body radius, r, equal to 7.44 inches and the angle, η, equal to 27°.

The total drag coefficient, C_{D_t}, is then equal to the sum of the wake-drag coefficient, C_{D_w}, and the suction-pump-drag coefficient, C_{D_s}, i.e.,

$$C_{D_t} = C_{D_w} + C_{D_s}$$

Note that for configurations without suction $C_{D_s} = 0$, and hence $C_{D_t} = C_{D_w}$.

The reference areas used in computing the drag coefficients are the two-thirds power of the volumes of the airships and are equal to 326.9 square inches for the XZS2G-1 and 493.9 square inches for the BLC airship.

BOUNDARY-LAYER CHARACTERISTICS

The displacement thickness, δ^*, and the momentum thickness, θ, were calculated as though the boundary layer were two-dimensional. Hence,

$$\delta^* = \int_0^{\delta} \left(1 - \frac{u}{U_\delta}\right) d\xi$$

and

$$\theta = \int_0^{\delta} \frac{u}{U_\delta}\left(1 - \frac{u}{U_\delta}\right) d\xi$$

It is again pointed out that the flow in the boundary layer is regarded as incompressible for the purposes of the present tests. It is felt that the error introduced by such an assumption is negligible for the conditions of the present tests.

RESULTS AND DISCUSSION

Drag coefficients determined from wake measurements and suction-pump-drag coefficients determined from boundary-layer

measurements are presented in Table 4. Values of boundary-layer displacement and momentum thickness calculated from boundary-layer surveys made upstream of the suction gap are also included in Table 4. The above values are tabulated for each test configuration.

The drag coefficients are presented as functions of Reynolds number in Figures 4 through 6. Drag coefficients for the XZS2G-1 and the basic BLC airship appear in Figure 4. The basic BLC airship has neither suction gap nor annular airfoil but represents essentially the airship envelope with no appendages. The drag coefficient for the basic BLC airship is approximately 50 percent higher than that of the standard airship, i.e. the XZS2G-1.

The variation of drag coefficient with Reynolds number for the BLC airship with varying amounts of suction is given in Figure 5. It can be seen that there is a sharp rise in drag coefficient at a Reynolds number of 10,000,000 in the case where no suction was applied to the model, but where a suction gap existed. At present no explanation for this increase can be given. The rise is present for both the cone and cone-shroud configurations.

At the time that sufficient suction was applied to attach the flow on the model upstream of the suction gap, a significant decrease in drag was realized. The minimum suction rate used in these tests was that just necessary to attach the flow. There is an indication, however, that after initially attaching the flow the suction rate can be slightly reduced while still maintaining attached flow. Nevertheless, for the purposes of the present tests, minimum suction rate refers to the condition required to attach the flow initially.

Data are also presented for two suction values above the minimum. It is evident from Figure 5 that no advantage is gained by applying suction beyond the minimum amount needed for initial flow attachment. As the Reynolds number was increased, the amount of suction required for attachment increased; and, at the higher speeds, the amount of suction available was not sufficient to attach the flow on the tail cone configuration. The Reynolds number range over which the available suction was sufficient to attach the flow was slightly extended, however, by placing a shroud on the tail cone. The shroud also had the effect of reducing the minimum suction required. In this regard, it is of interest to note that for the same gap dimensions (defined in Table 3), the drag of both the tail cone configuration and the tail cone with shroud configuration exhibit the same variation with Reynolds number; i.e., when plotted as a function of Reynolds number, the drag data for both configurations fall on a single curve.

The results of tests with the annular airfoil are presented in Figure 6. Contrary to expectations, the airfoil did not, in general, prevent separation on the airship. It is seen that the drag for this configuration is higher than that of the basic BLC airship. The increased drag can be attributed in part to the additional drag of the airfoil itself.

The results of Figures 4 through 6 are summarized in Figure 7. In this figure an average of the drag curves for the model with suction and the minimum drag obtained for the airfoil configuration are presented. The results indicate that of the two boundary-layer-control methods tested the suction method is far superior and, in fact, is the only one that shows a drag reduction. In particular, the drag of the

BLC airship with suction is at least 20 percent lower than that of the XZS2G-1 throughout the entire Reynolds number range of the tests.

The pressure distributions for each test configuration appear in Figures 8 through 12. Figure 8 presents the pressure distribution data for the XZS2G-1 for natural transition and with transition fixed at the 10-percent body station. The distribution for the basic BLC airship is given in Figure 9. A favorable pressure gradient exists over the first 60 percent of the body. Figures 10 and 11 show the distribution with varying amounts of suction applied to the cone and cone-shroud configurations, respectively. In both cases the application of suction extends the favorable gradient to about the 80-percent station.

The distribution for tests with the annular airfoil are given in Figure 12. The distribution is essentially the same as that of the basic BLC body except that there is less pressure recovery on the aft portion of the airship. This is indicative of a higher form drag, which, combined with the parasite drag of the annular airfoil, accounts for the drag behavior shown in Figure 7.

Boundary-layer measurements were taken upstream of the suction gap station and the velocity profiles derived from them are presented in Figures 13 through 16. The curves presented were calculated from faired data points and, consequently, the symbols shown represent interpolated values rather than actual experimental points.

To obtain these curves the measured total-head distributions were plotted to an enlarged scale, faired, and values from the resultant curves tabulated at intervals of 0.02 inch. The velocity ratio at each of these interpolated points was then

calculated under the assumption that the boundary-layer flow is incompressible. The displacement thickness, momentum thickness, and their ratio were than determined according to the definitions given in the previous section entitled, "Reduction of Data."

As stated previously, rakes were also placed on the suction tail cone and fore and aft of the airfoil. No calculations were made for these rakes since they were located in a separated region both in the case of no suction and for the airfoil configuration. In the case where suction was applied, the boundary layer on the tail cone was too thin to be measured with the rakes that were installed.

Aerodynamics Laboratory
David Taylor Model Basin
Washington, D. C.
March 1957

REFERENCE

1. BUAER ltr Aer-AD-312/226 TED No. TMB AD-3198 of 13 Jan 1955.

Table 1

XZS2G-1 Airship Coordinates
for Orifice Locations

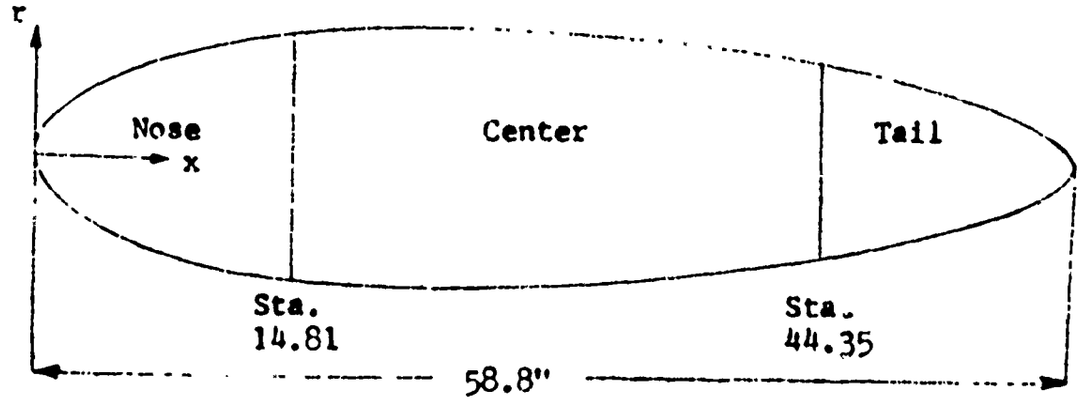

Orifice	x in inches	r in inches	Orifice	x in inches	r in inches
1	0	0	23	33.000	6.680
2	1.002	2.125	24	35.002	6.495
3	2.003	2.952	25	37.002	6.280
4	3.003	3.590	26	39.003	6.052
5	4.003	4.096	27	40.996	5.792
6	5.016	4.516	28	42.999	5.483
7	6.010	4.855	29	44.998	5.151
8	7.017	5.163	30	46.492	4.888
9	8.003	5.448	31	47.497	4.691
10	9.001	5.714	32	48.502	4.487
11	10.002	5.948	33	49.500	4.266
12	11.000	6.139	34	50.499	4.038
13	13.007	6.452	35	51.490	3.793
14	15.501	6.705	36	52.503	3.513
15	17.000	6.815	37	53.515	3.218
16	18.994	6.934	38	54.494	2.926
17	21.001	6.991	39	55.486	2.578
18	23.003	7.017	40	56.513	2.151
19	25.006	7.006	41	57.496	1.622
20	26.999	6.961	42	58.495	0.793
21	29.003	6.895	43	58.8	0
22	31.002	6.800			

Table 3

Test Configurations
(L = 58.8 Inches)

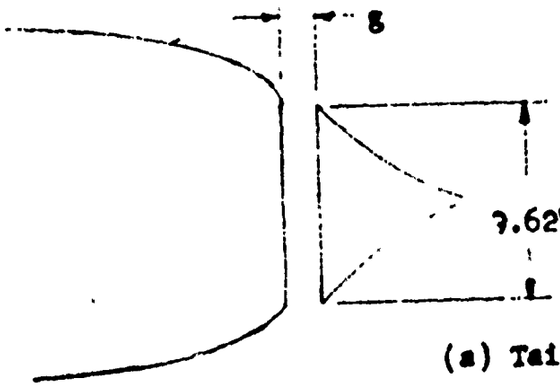

g/L = 0.004, 0.008, 0.012, 0.016

(a) Tail Cone Configuration

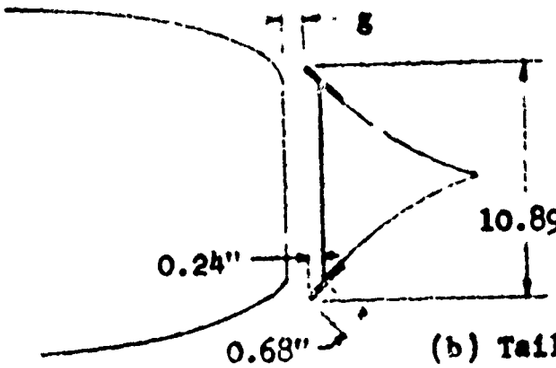

g/L = 0.004, 0.008, 0.012

(b) Tail Cone With Shroud

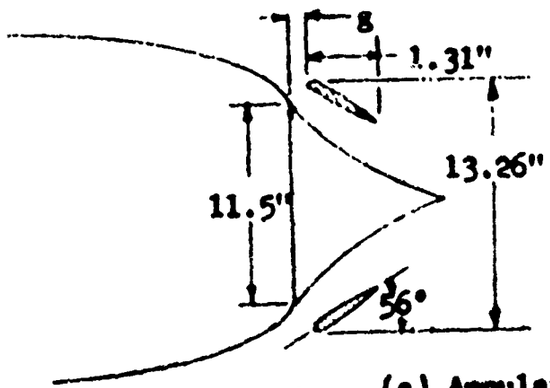

g/L = 0.007, 0.013, 0.018, 0.022

(c) Annular Airfoil Configuration

Table 4

Summary of Test Configurations and Calculated Results

Model	Airfoil	Shroud	BL	g/L	Rx10^{-6}	$\dot{m}$ in $\frac{\text{lb-sec}}{\text{ft}}$	C_{D_s}	C_{D_w}	C_{D_T}	δ^*	θ	H
XZS2G-1	None	None	Tripped	0	4.65	0	0	0.0284	0.0284	--	--	--
					8.57			0.0262	0.0262	--	--	--
					12.6			0.0267	0.0267	--	--	--
					18.3			0.0239	0.0239	--	--	--
BLC Airship	None	None	Tripped	0	4.31	0	0	0.0403	0.0403	0.2465	0.1423	1.7322
					7.00			0.0438	0.0438	0.1852	0.1076	1.7211
					9.85			0.0391	0.0391	0.1720	0.1010	1.7029
					12.4			0.0481	0.0481	0.1677	0.0987	1.6990
				0.016	4.36	0	0	0.0359	0.0359	0.2022	0.1155	1.7506
					4.61	0.03813	0.0203	0.0040	0.0243	0.1048	0.0696	1.5057
					4.61	0.04987	0.0230	0.0016	0.0246	0.1022	0.0676	1.5118
					4.71	0.06028	0.0235	0.0008	0.0243	0.0947	0.0627	1.5103
					6.95	0	0	0.0372	0.0372	0.1836	0.1030	1.7825
					6.95	0	0	0.0308	0.0308	0.1770	0.0987	1.7933
					7.15	0.05868	0.0188	0.0032	0.0220	0.0964	0.0651	1.4807
					7.10	0.07623	0.0209	0.0018	0.0227	0.0920	0.0623	1.4767
					7.25	0.08713	0.0219	0.0007	0.0226	0.0883	0.0602	1.4667
					9.9	0	0	0.0438	0.0438	0.1657	0.0974	1.7012
					9.8	0.08208	0.0182	0.0014	0.0196	0.0906	0.0620	1.4612
					10.2	0.08411	0.0180	0.0013	0.0193	0.0883	0.0606	1.4570
					10.1	0.08431	0.0182	0.0014	0.0196	0.0870	0.0595	1.4621
					12.6	0	0	0.0255	0.0255	0.1667	0.0950	1.7547

CONFIDENTIAL

Table 4 (Continued)

Model.	Airfoil	Shroud	BL	g/L	Rx10^{-6}	$\dot{m}$ in $\frac{\text{lb-sec}}{\text{ft}}$	C_{D_s}	C_{D_w}	C_{D_T}	δ^*	θ	H
BLC Airship	None	None	Tripped	0.012	4.46	0	0	0.0484	0.0484	0.2218	0.1136	1.9524
					4.36	0	0	0.0314	0.0314	0.1648	0.1051	1.5680
					4.36	0.03245	0.0182	0.0042	0.0224	0.1055	0.0698	1.5114
					4.41	0.04419	0.0206	0.0026	0.0232	0.0940	0.0627	1.4992
					4.46	0.05897	0.0231	0.0008	0.0239	0.0922	0.0623	1.4799
					7.10	0	0	0.0350	0.0350	0.2177	0.1079	2.0176
					7.15	0.04936	0.0156	0.0041	0.0197	0.0936	0.0641	1.4602
					7.06	0.06755	0.0192	0.0018	0.0210	0.0850	0.0584	1.4554
					7.01	0.08207	0.0211	0.0013	0.0224	0.0826	0.0570	1.4491
					10.2	0	0	0.0558	0.0558	0.1739	0.0999	1.7407
					10.3	0.07000	0.0191	0.0054	0.0245	0.1157	0.0778	1.4871
					9.95	0.08162	0.0173	0.0032	0.0205	0.0854	0.0566	1.5088
					9.85	--	--	0.0027	--	0.0781	0.0544	1.4356
		Attached	Tripped	0.012	4.51	0.03095	0.0171	0.0040	0.0211	0.0963	0.0631	1.5261
					4.41	0.04263	0.0214	0.0022	0.0236	0.0929	0.0618	1.5032
					4.36	0.05922	0.0309	0.0007	0.0316	0.0918	0.0620	1.4806
					7.00	0.04281	0.0146	0.0052	0.0198	0.0898	0.0605	1.4842
					6.95	0.06850	0.0193	0.0017	0.0210	0.0840	0.0575	1.4608
					7.10	0.08487	0.0212	0.0010	0.0222	0.0837	0.0579	1.4455
					6.90	0.06826	0.0190	0.0014	0.0204	0.0833	0.0568	1.4665
					10.1	0.06286	0.0147	0.0027	0.0174	0.0854	0.0575	1.4852
					10.0	0.07410	0.0164	0.0027	0.0191	0.0870	0.0588	1.4795
					10.0	0.08385	0.0175	0.0049	0.0224	0.0788	0.0543	1.4511
					11.3	0.06667	0.0144	0.0026	0.0170	0.0826	0.0567	1.4567
					11.3	0.07998	0.0161	0.0019	0.0180	0.0794	0.0550	1.4436
					11.2	0.09470	0.0165	0.0019	0.0184	0.0793	0.0547	1.4497

CONFIDENTIAL

Table 4 (Continued)

Model	Airfoil	Shroud	BL	g/L	$Rx10^{-6}$	$\frac{m}{\text{in}}$ $\frac{\text{lb-sec}}{\text{ft}}$	C_{D_s}	C_{D_w}	C_{D_T}	δ^*	θ	H
BLC Airship	None	None	Tripped	0.008	4.56	0	0	0.0326	0.0326	0.1692	0.1042	1.6238
					4.51	0.03891	0.0209	0.0028	0.0237	0.1047	0.0705	1.4851
					4.41	0.05273	0.0229	0.0018	0.0247	0.0947	0.0622	1.5225
					4.51	0.05447	0.0224	0.0009	0.0233	0.0888	0.0609	1.4581
					4.60	0.08263	0.0239	0.0003	0.0242	0.0827	0.0553	1.4954
					7.20	0	0	0.0274	0.0274	0.2104	0.1082	1.9445
					7.15	0.05677	0.0178	0.0030	0.0208	0.0948	0.0624	1.5192
					7.20	0.07491	0.0192	0.0014	0.0206	0.0833	0.0572	1.4552
					7.10	0.07409	0.0193	0.0010	0.0203	0.0802	0.0562	1.4270
					7.10	0.08112	0.0205	0.0009	0.0214	0.0878	0.0584	1.5034
					10.15	0	0	0.0574	0.0574	0.1910	0.1011	1.8892
					10.15	0.07788	0.0169	0.0019	0.0288	0.0848	0.0563	1.5062
					10.0	0.07925	0.0165	0.0020	0.0185	0.0793	0.0553	1.4339
					4.31	0	0	0.0291	0.0291	0.2252	0.1154	1.9582
					4.36	0.08315	0.0259	0.0005	0.0264	0.0833	0.0582	1.4312
					6.85	0	0	0.0291	0.0291	0.2020	0.1142	1.7686
					6.95	0.05558	0.0176	0.0024	0.0200	0.0880	0.0608	1.4473
					7.10	0.07286	0.0198	0.0013	0.0211	0.0846	0.0581	1.4561
					7.05	0.08372	0.0213	0.0008	0.0221	0.0799	0.0558	1.4318
			Attached	Tripped	6.95	0.08493	0.0210	0.0009	0.0219	0.0819	0.0562	1.4572
					9.9	0	0	0.0557	0.0557	0.1766	0.1011	1.7467
					9.8	0.07397	0.0163	0.0027	0.0190	0.0795	0.0550	1.4454
					10.2	0.08011	0.0167	0.0026	0.0193	0.0777	0.0537	1.4469
					10.1	0.08126	0.0172	0.0026	0.0198	0.0791	0.0552	1.4329
					11.3	0	0	0.0500	0.0500	0.1726	0.0989	1.7451
					11.3	0.07974	0.0158	0.0020	0.0178	0.0786	0.0547	1.4369

CONFIDENTIAL

Table 4 (Concluded)

Model	Airfoil	Shroud	BL	g/L	Rx10^{-6}	$\frac{m}{\text{in}}$ $\frac{\text{lb-sec}}{\text{ft}}$	C_{D_s}	C_{D_w}	C_{D_T}	δ^*	θ	H
BLC Airship	None	None	Tripped	0.004	4.36	0	0	0.0901	0.0901	0.1931	0.1107	1.7443
					4.31	0.04474	0.0215	0.0014	0.0229	0.0906	0.0615	1.4731
					4.31	0.04864	0.0214	0.0019	0.0233	0.0856	0.0582	1.4707
	None	Attached	Tripped	0.004	4.51	0	0	0.0325	0.0325	0.2214	0.1208	1.8327
					4.60	0.05055	0.0219	0.0029	0.0248	0.0903	0.0625	1.4448
					4.55	0.06346	0.0242	0.0024	0.0266	0.0904	0.0603	1.4991
					4.55	0.06565	0.0229	0.0005	0.0234	0.0827	0.0572	1.4458
					6.90	0	0	0.0286	0.0286	0.1941	0.1048	1.8520
					7.05	0.05878	0.0189	0.0033	0.0222	0.0854	0.0584	1.4623
					6.95	0.07826	0.0205	0.0035	0.0240	0.0805	0.0558	1.4426
					7.15	0	0	0.0288	0.0288	0.2047	0.1074	1.9059
	Attached	None	Tripped	0.007	4.36	0	0	0.0465	0.0465	0.1726	0.1025	1.6904
					7.01			0.0472	0.0472	0.1605	0.0970	1.6546
					9.75			0.0503	0.0503	0.1446	0.0888	1.6283
					12.82			0.0472	0.0472	0.1463	0.0879	1.6643
				0.013	4.56	0	0	0.0485	0.0485	0.1769	0.1013	1.7462
					6.76			0.0554	0.0554	0.1567	0.0961	1.6305
					9.80			0.0633	0.0633	0.1546	0.0912	1.6951
					12.82			0.0580	0.0580	0.1436	0.0878	1.6355
				0.018	4.41	0	0	0.0587	0.0587	0.1688	0.1000	1.6880
					6.95			0.0587	0.0587	0.1607	0.0970	1.6567
					9.75			0.0755	0.0755	0.1494	0.0906	1.6490
					12.69			0.0623	0.0628	0.1468	0.0905	1.6220
				0.022	4.56	0	0	0.0607	0.0607	0.1770	0.1066	1.6604
					7.01			0.0622	0.0622	0.1589	0.0955	1.6638
					9.80			0.0557	0.0557	0.1648	0.0949	1.7365
					12.69			0.0639	0.0639	0.1492	0.0896	1.6651

CONFIDENTIAL

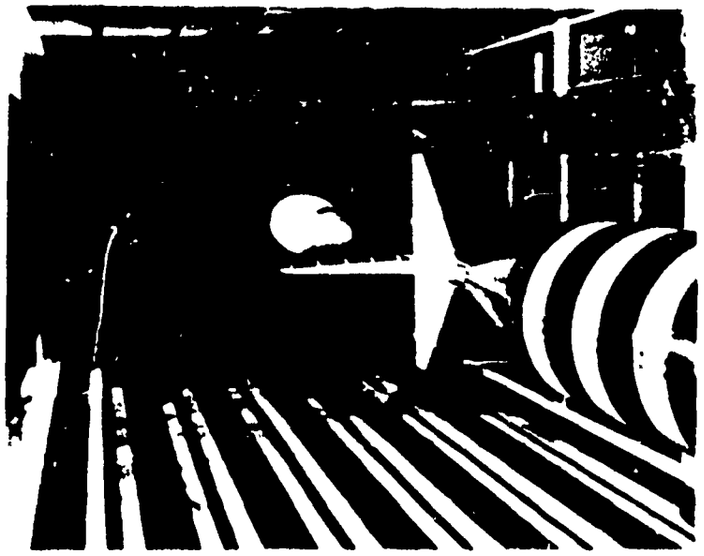

PSD-200,030

(a) XZS2G-1 Airship Model

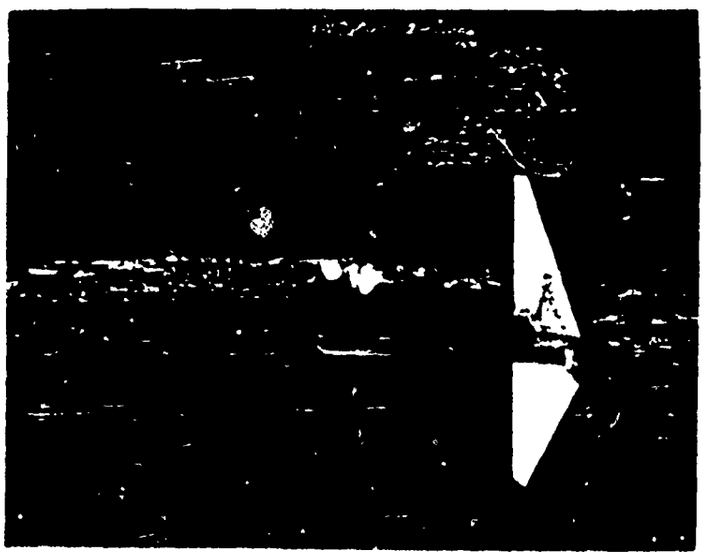

PSD-200,031

(b) Boundary-Layer-Control Airship

Figure 1 - Installation of Airship Models in 7- by 10-Foot Transonic Wind Tunnel

PSD-200,033

(a) Transition Coating Before Development

PSD-200,034

(b) Transition Coating After Development

Figure 2 - Boundary-Layer Transition Indication

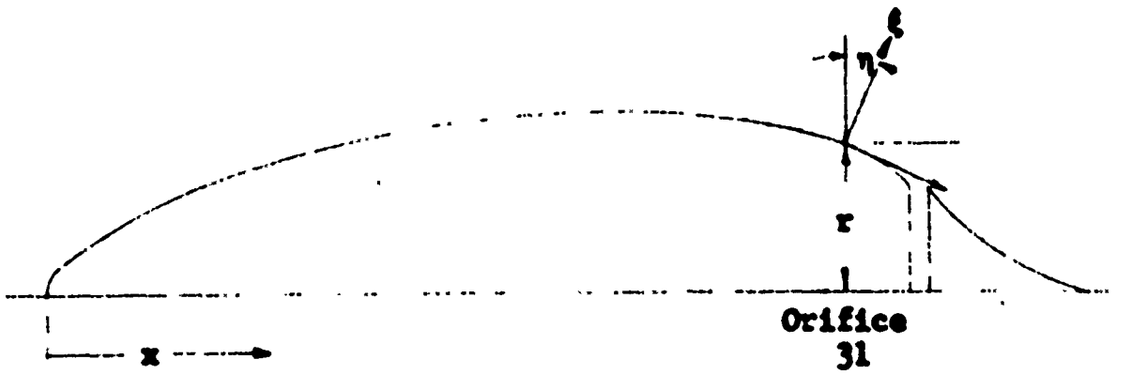

Figure 3 - Sketch of ELC Airship Showing Location of Forward Boundary-Layer Rake

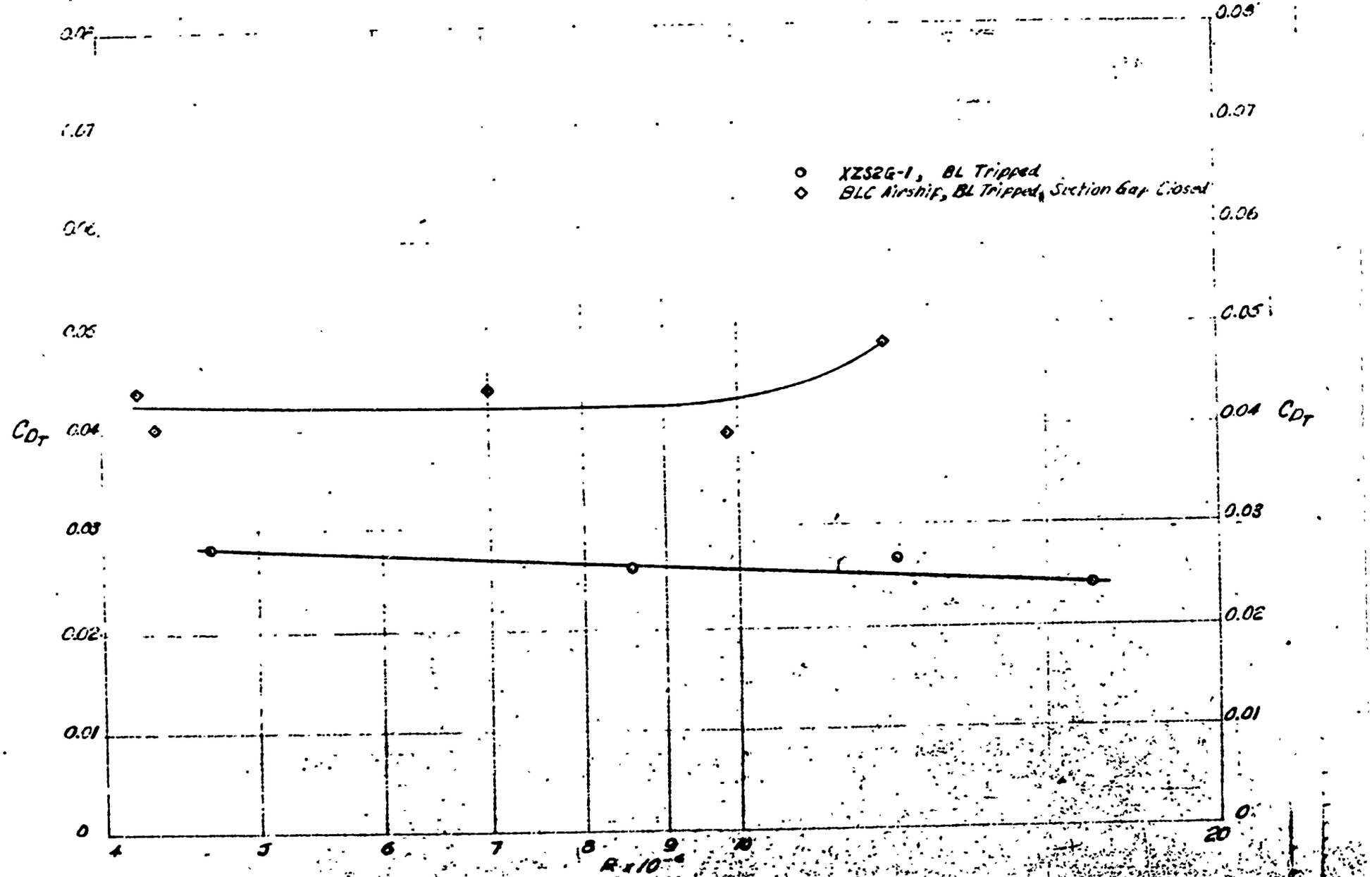

Figure 4 - Variation of Drag Coefficient With Reynolds Number for XZS2G-1 and Basic BLC Airship Configuration

FIGURE 4

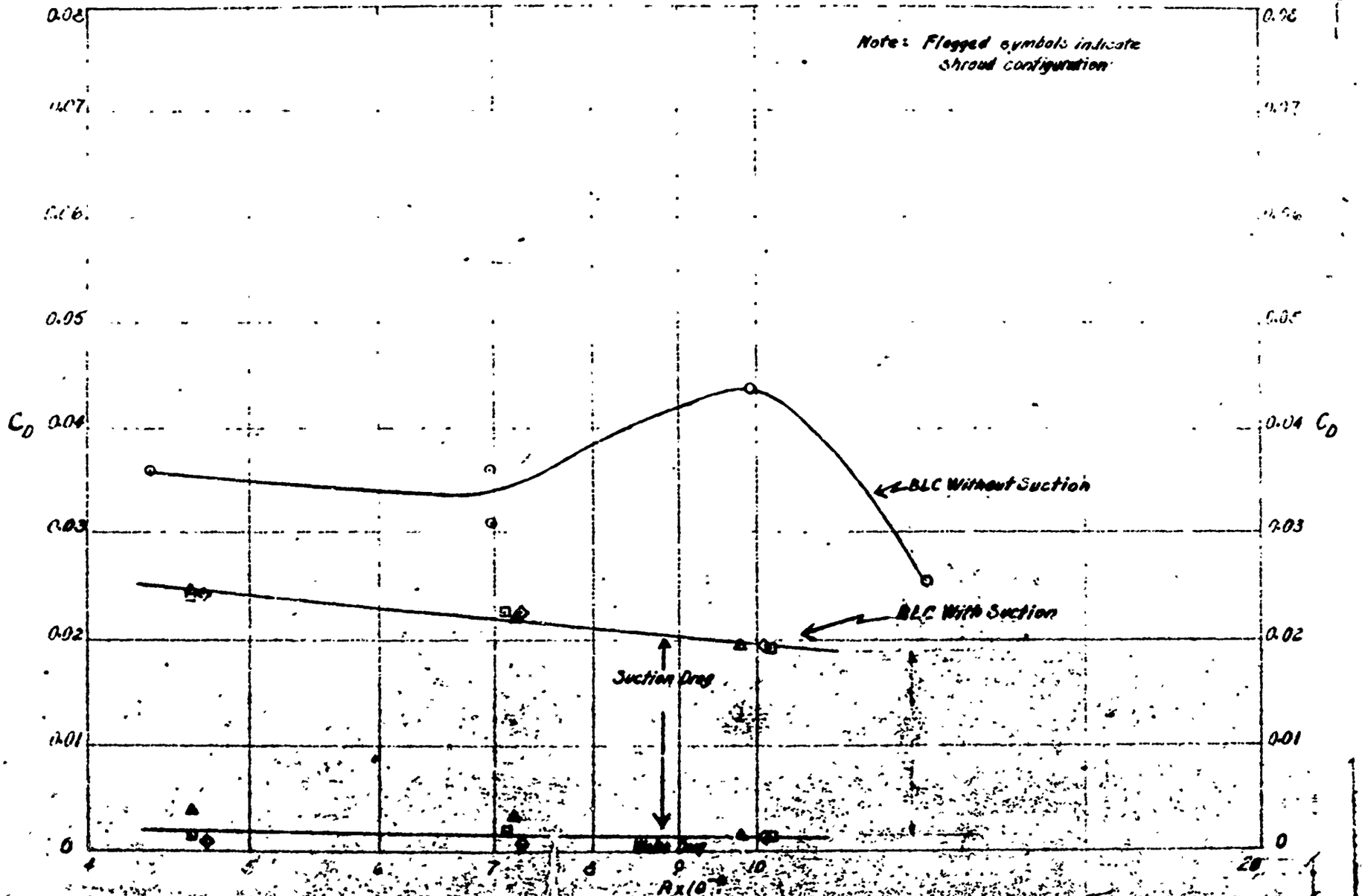

Figure 5.- Variation of Drag Coefficient With Reynolds Number for BLC Nacelle With Varying Suction

FIGURE 5a

914

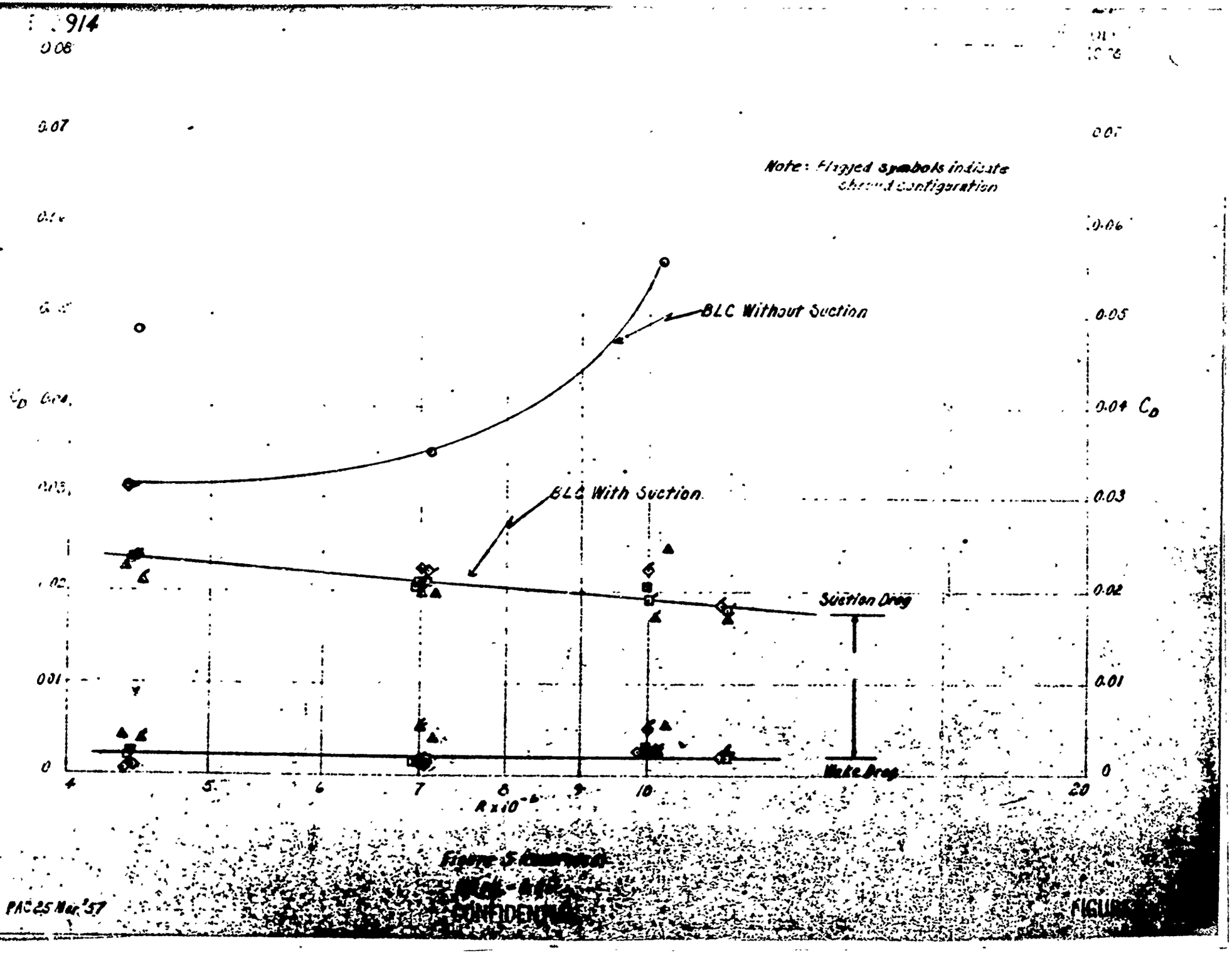
Note: Flagged symbols indicate
clean configuration
BLC Without Suction
BLC With Suction
Suction Drag
Wake Drag
C_D
$R \times 10^{-6}$
0.08
0.07
0.06
0.05
0.04
0.03
0.02
0.01
0
4
5
6
7
8
9
10
20

NACA 914

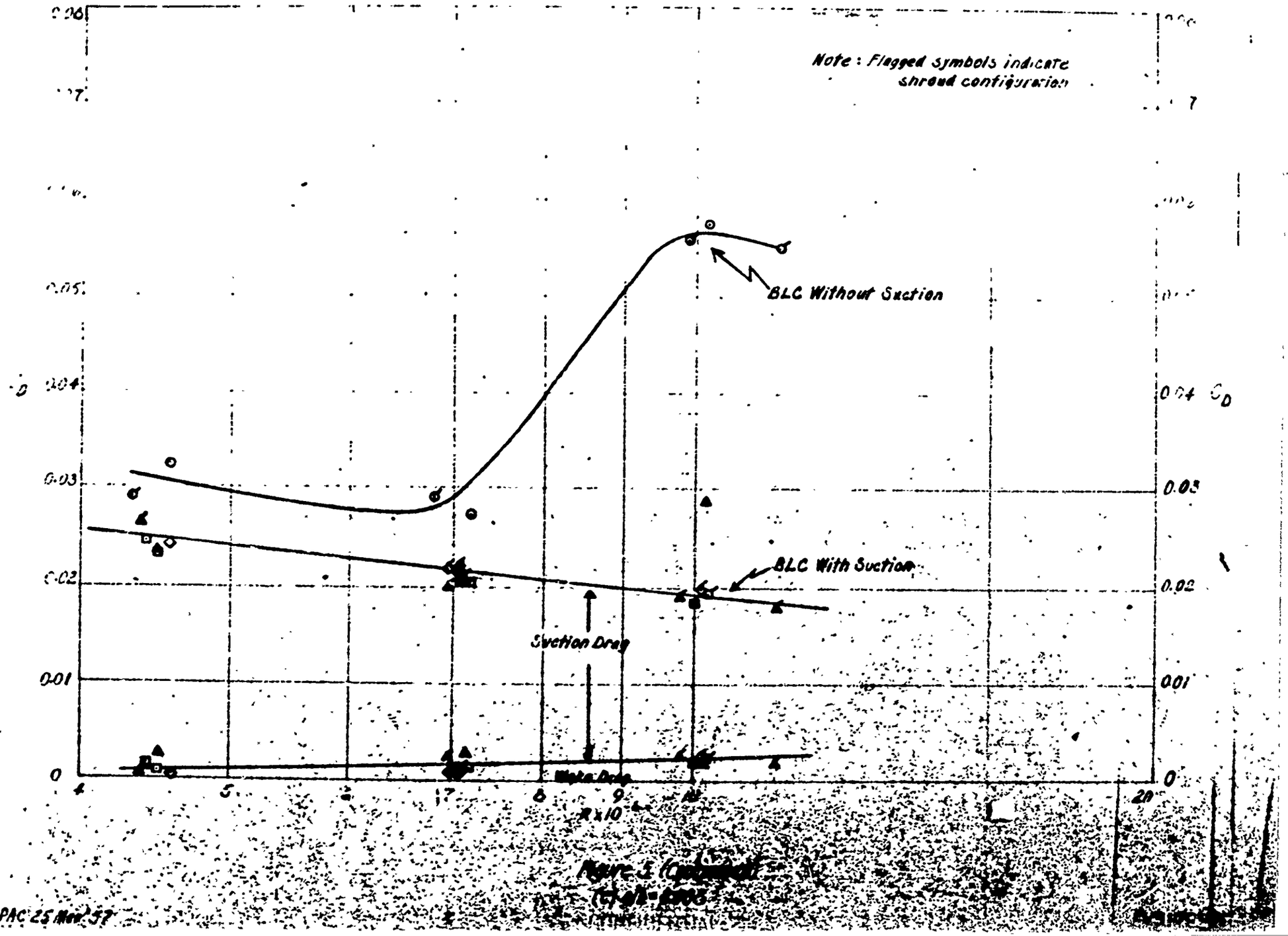

Figure 5 (Continued)

SERO 9/4

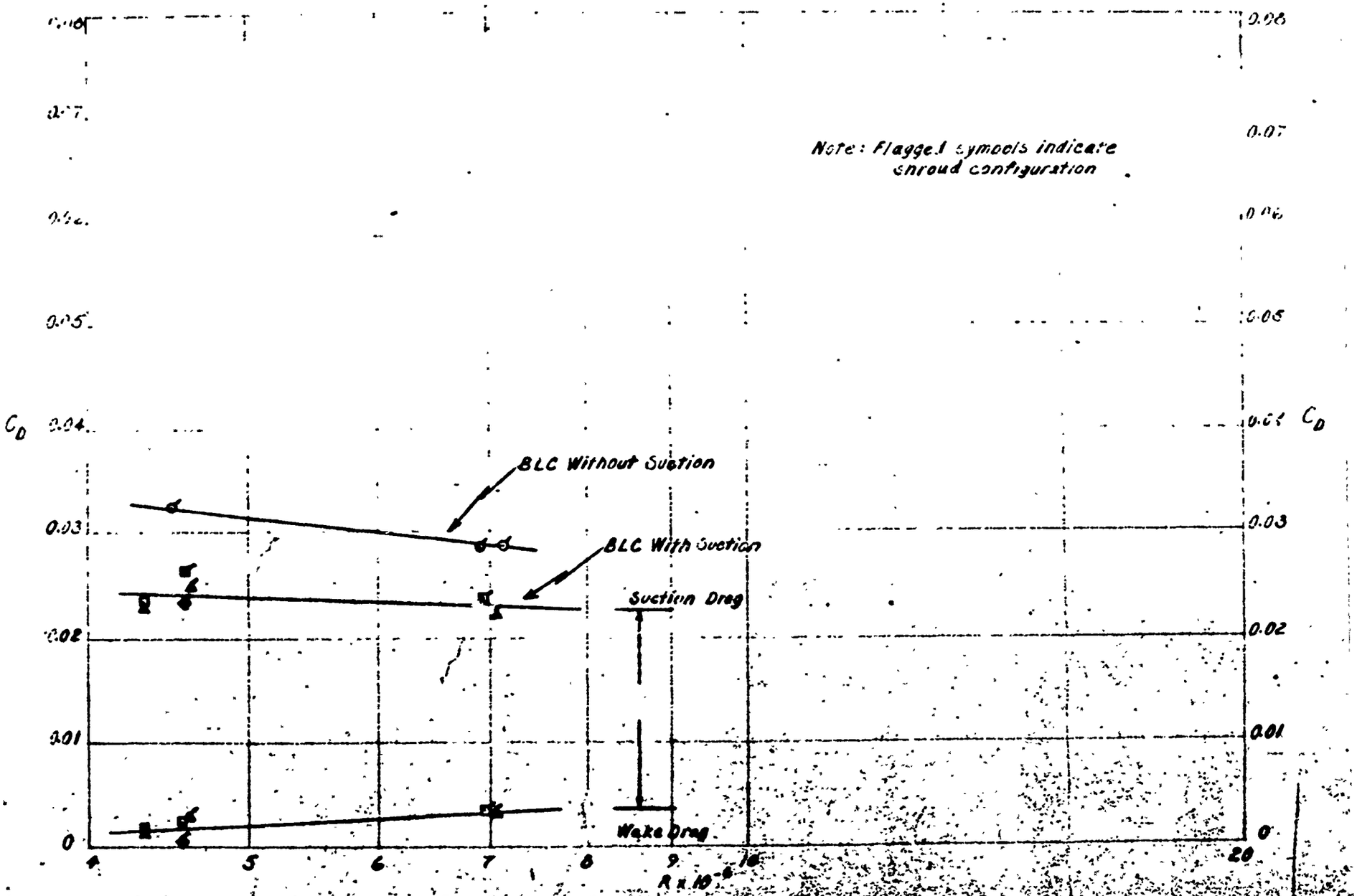

Figure 5 (Concluded)
@ $\delta k = 0.064$

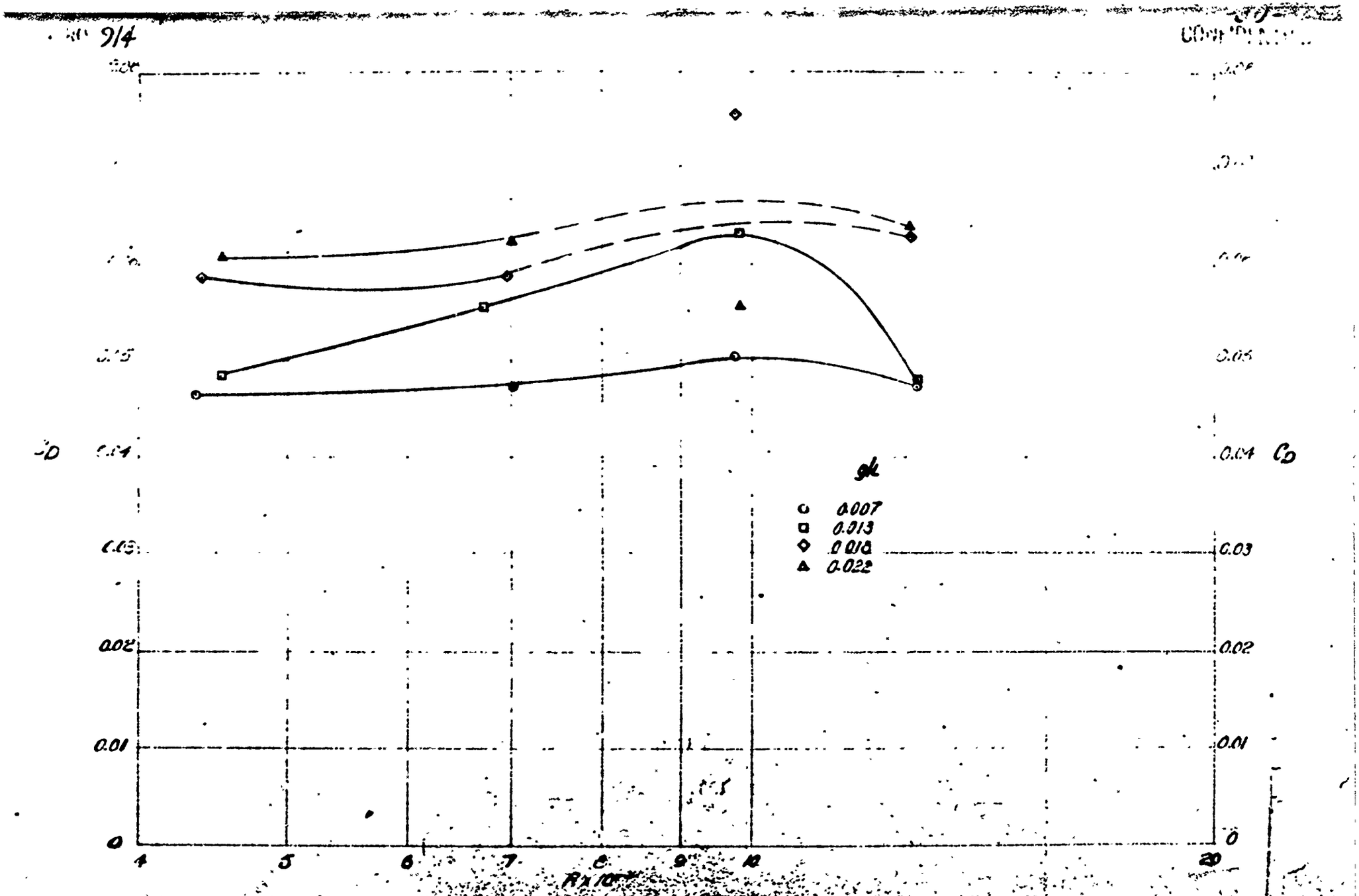

Figure 6 - Variation of Drag Coefficient With Reynolds Number For BLC Airship With Annular Airfoil

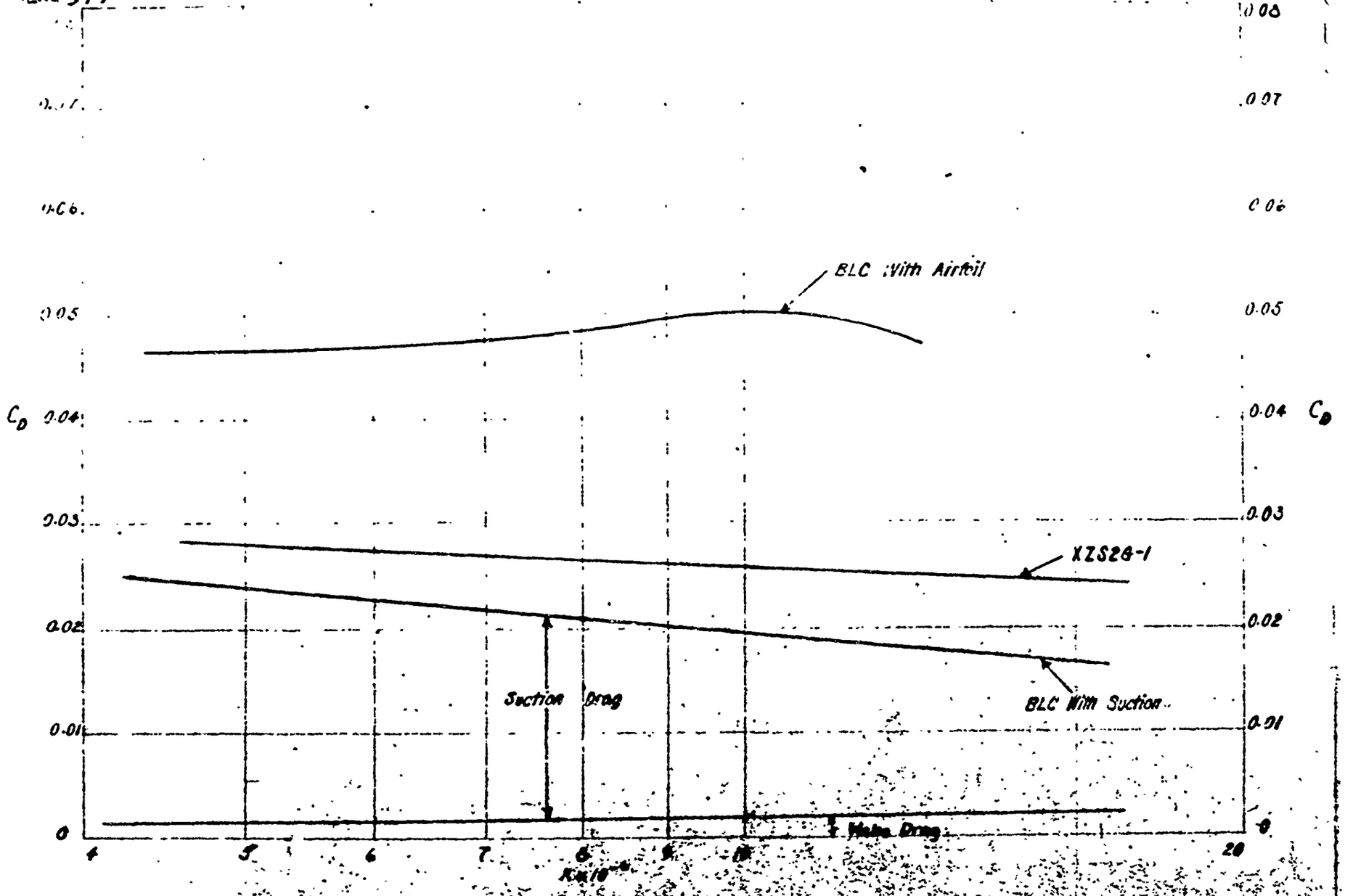

Figure 7 – Variation of Drag Coefficient with Reynolds Number for Various Test Configurations

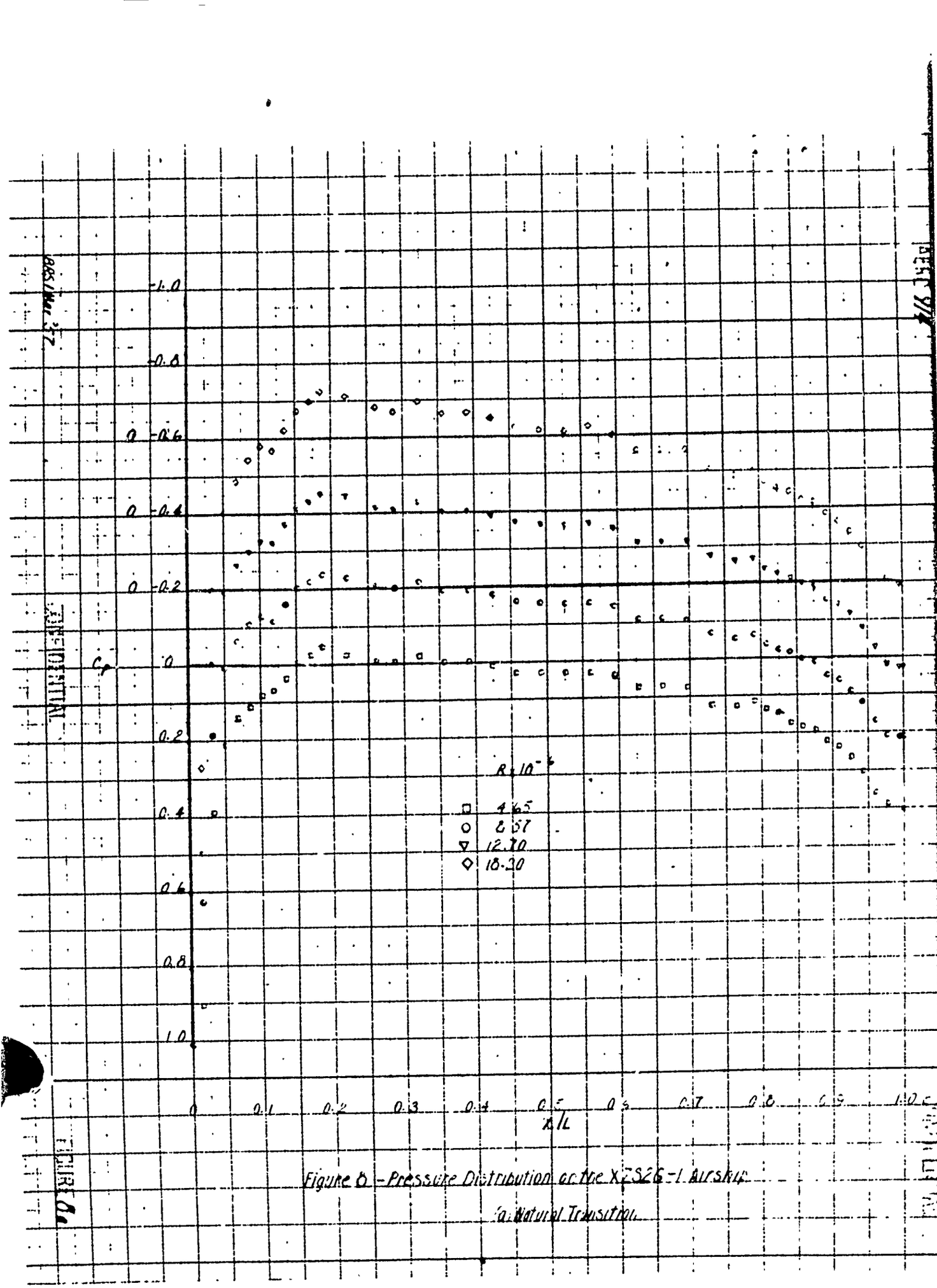

Figure 6 – Pressure Distribution on the XZS26-1 Airship

(a) Natural Transition

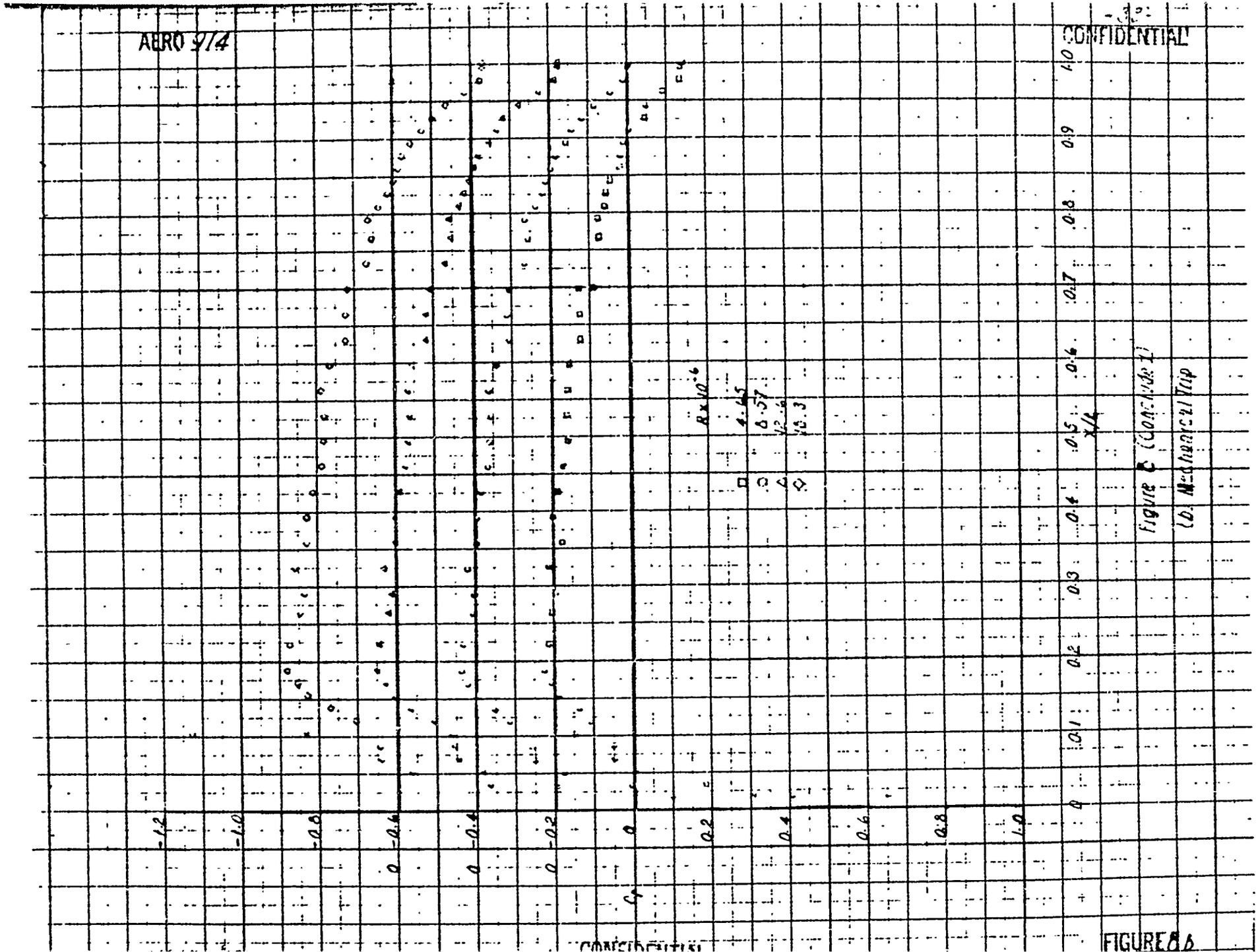

Figure 6 (Concluded)

(b) Mechanical flap

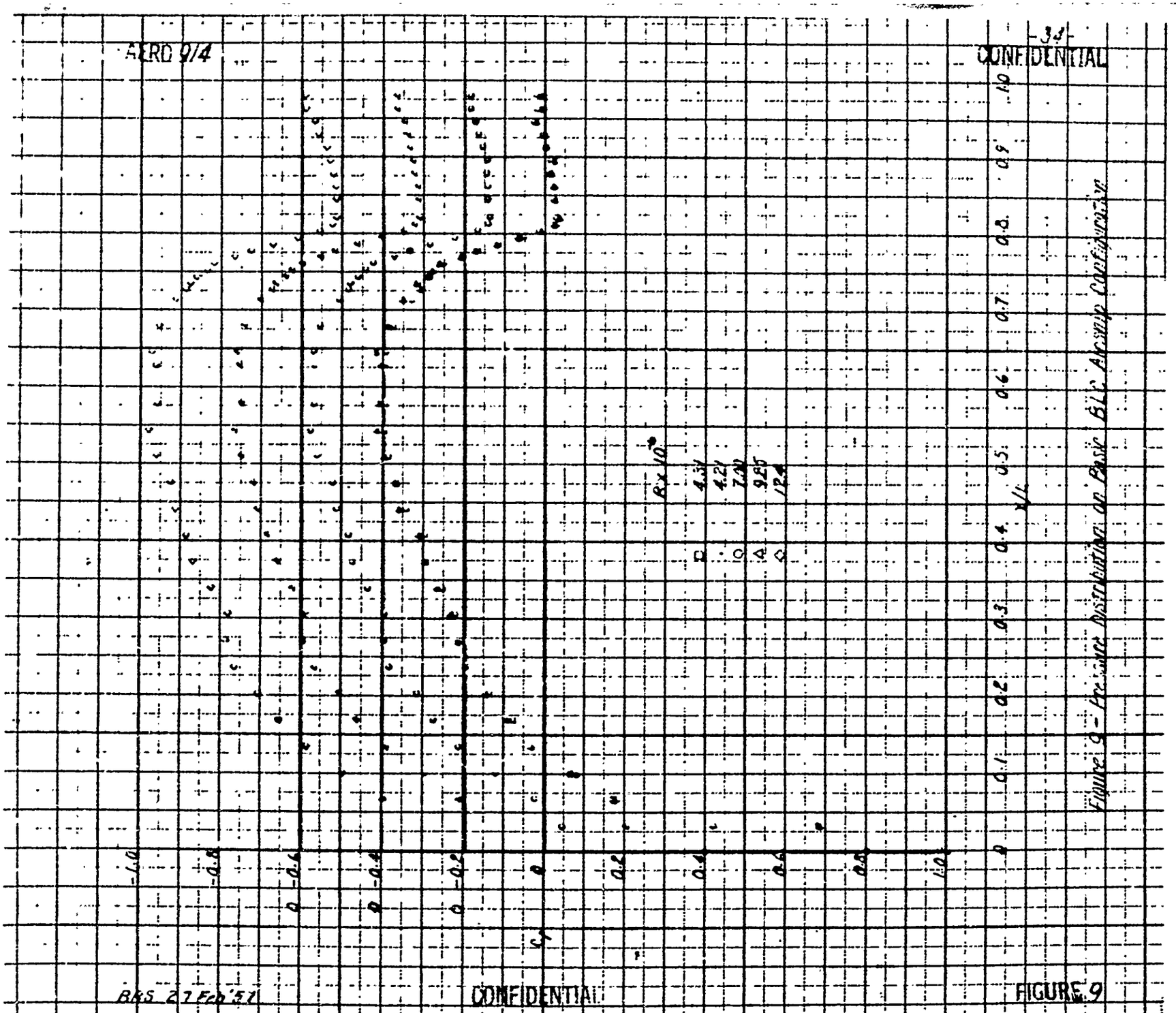

Figure 9 – Pressure Distribution on Base BLC Aerofoil Configuration

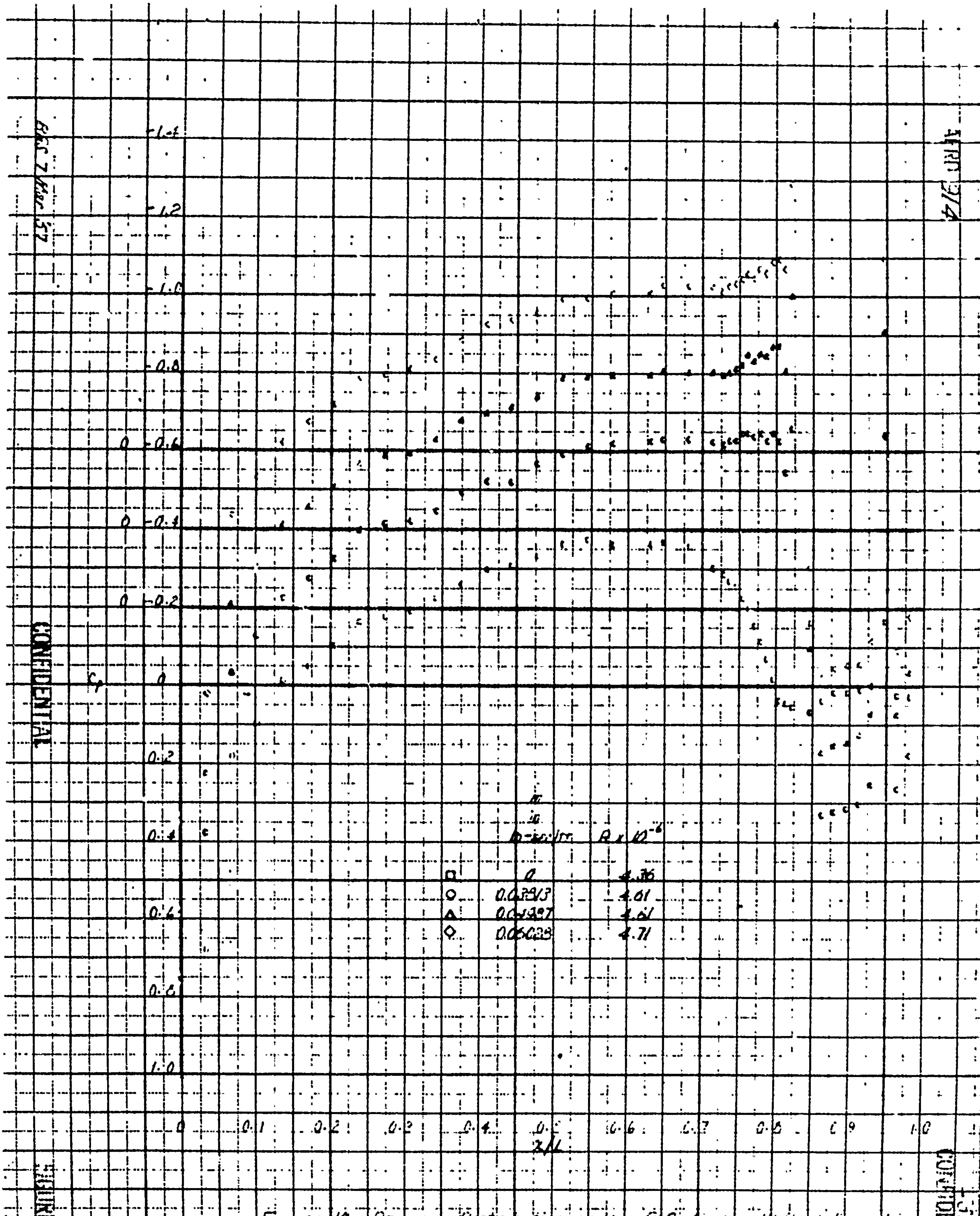

Figure 10 - Pressure Distribution on the B.C. Airship Without Shroud

(a) $a/L = 0.06$; $R \approx 46 \times 10^6$

CONFIDENTIAL

FIGURE 10a

AERO 974

BGS 7 Mar 57

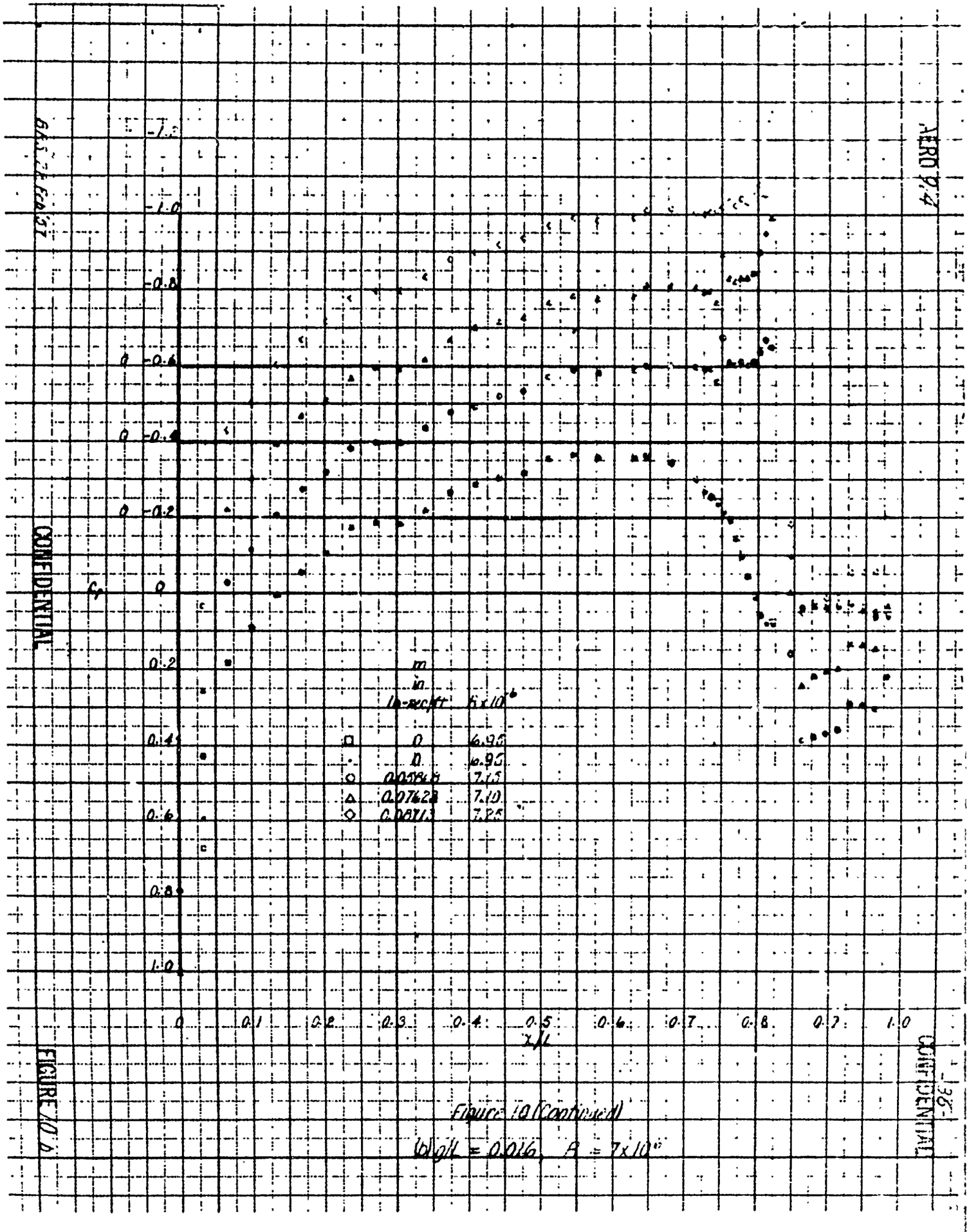

Figure 10 (Continued)

Wgt = 0.016, R = 7x10⁶

FIGURE 10 b

Figure 10 (Continued)

(c) $\phi_{ik} = 0.5\pi$, $R = 10 \times 10^6$

FIGURE 10 c

Figure 10 (Continued)

(d) $g/L = 0.816$, $k = 12.6 \times 10^{-6}$

Figure 10 (Continued)

(a) $\delta/L = .002$; $R = 4 \times 10^6$

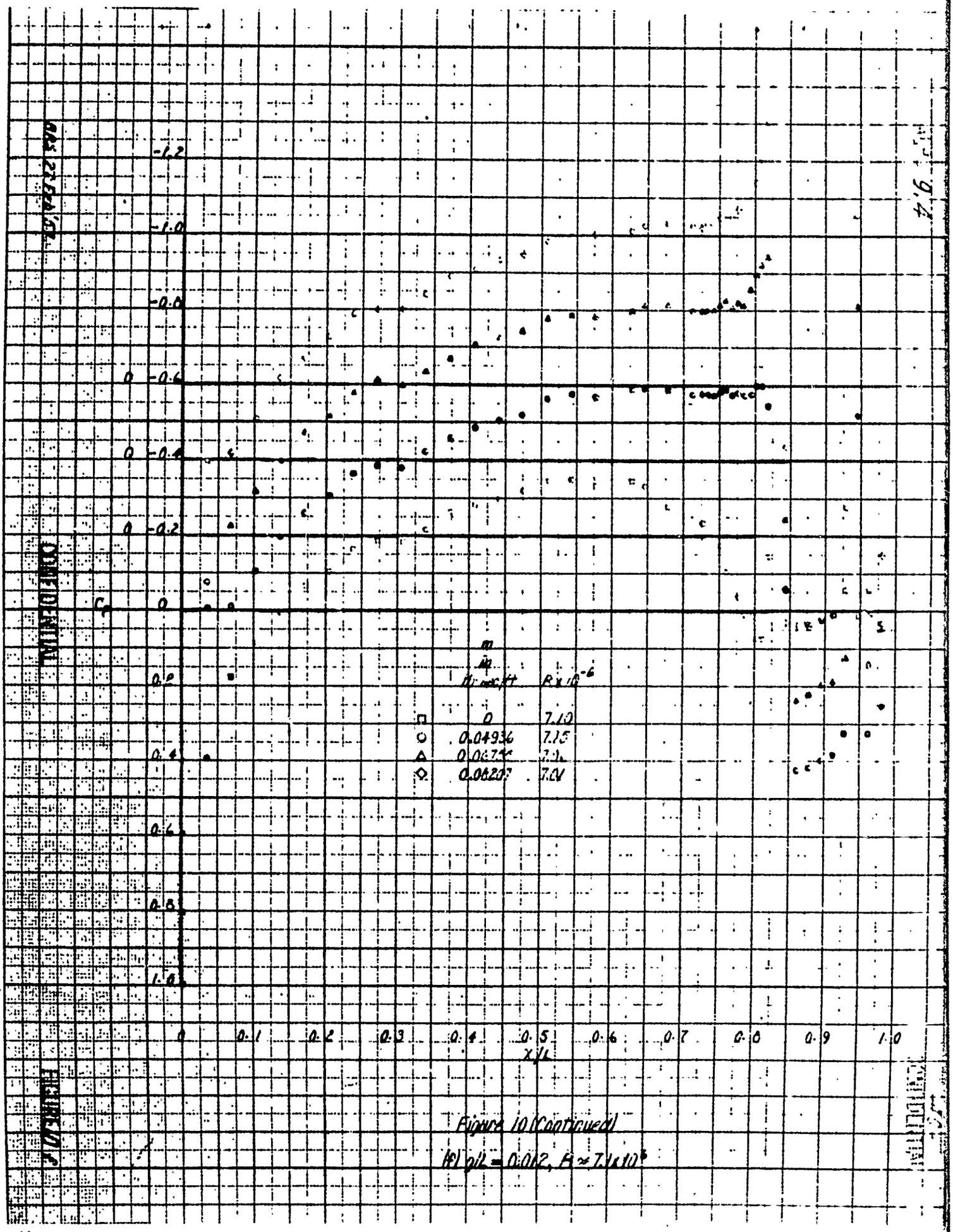

Figure 10 (Continued)

$\Delta l/l = 0.012$, $Re \approx 7.1 \times 10^6$

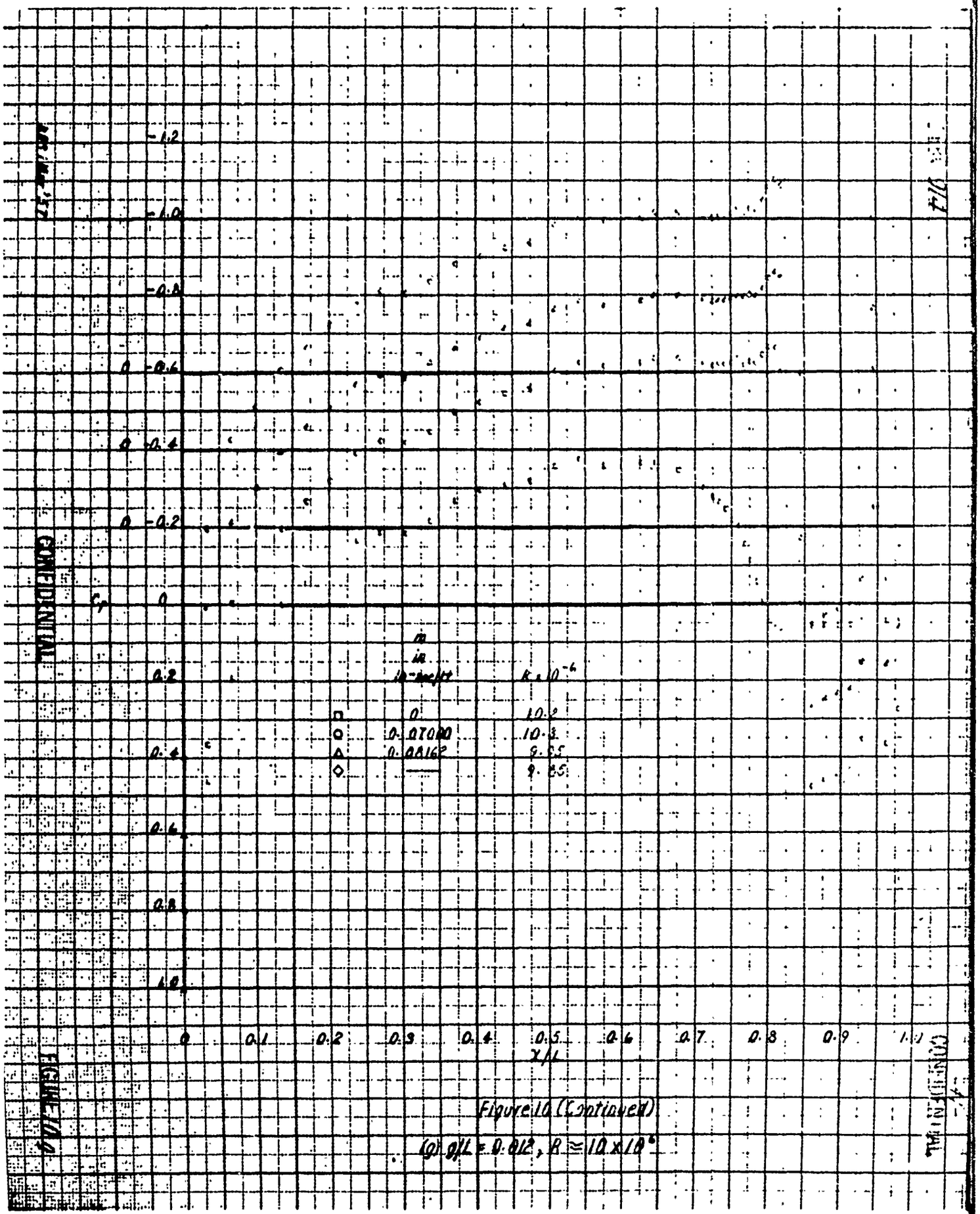

Figure 10 (Continued)

(g) $\alpha/L = 0.012$, $R \approx 10 \times 10^6$

CONFIDENTIAL
AERO 7/4

CONFIDENTIAL

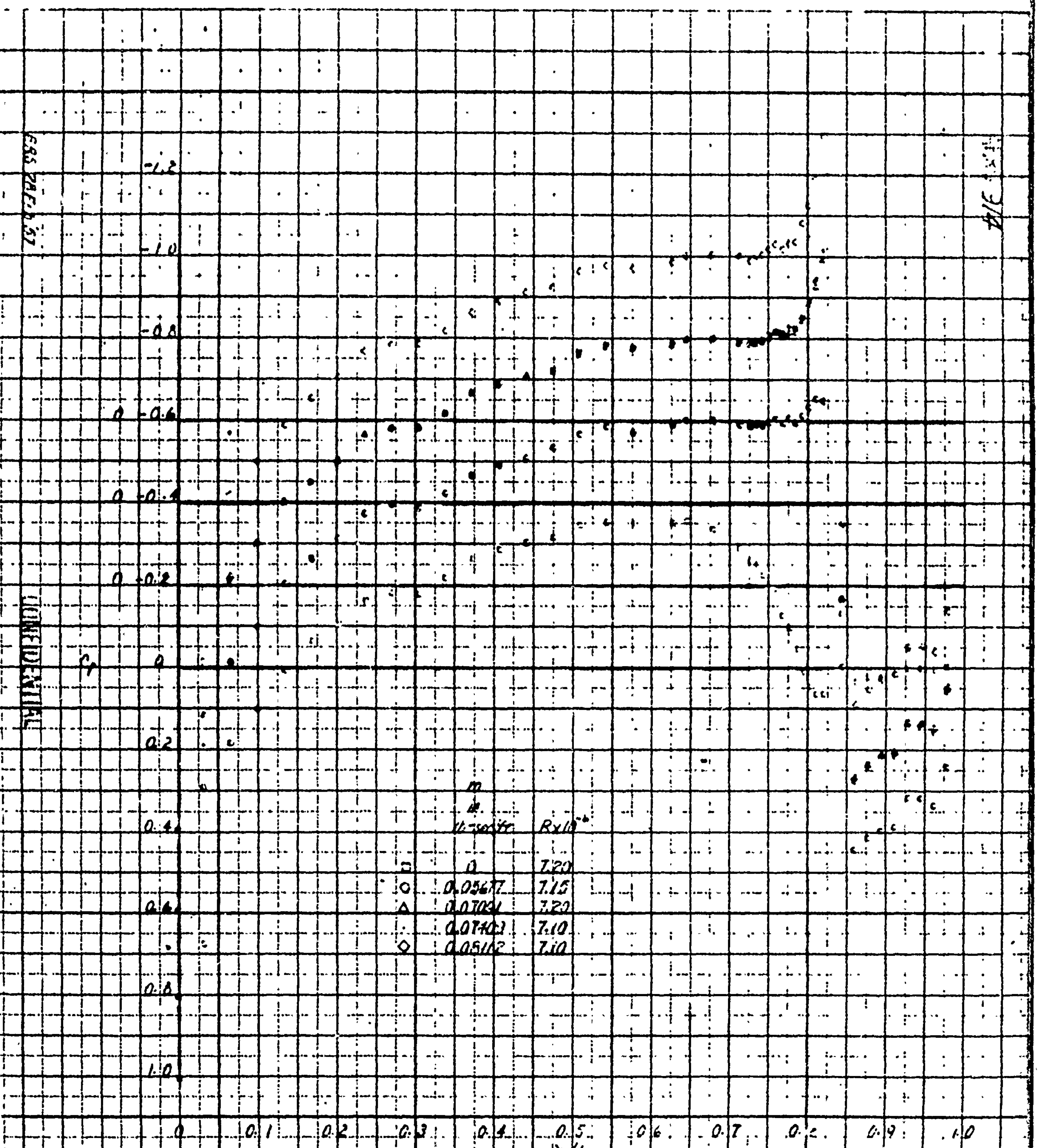

Figure 10 (Continued)

(i) h/l = 0.008, R = 7.1 × 10⁶

FIGURE 10(i)

CONFIDENTIAL

ERS 7AFeb.57

AERO 914

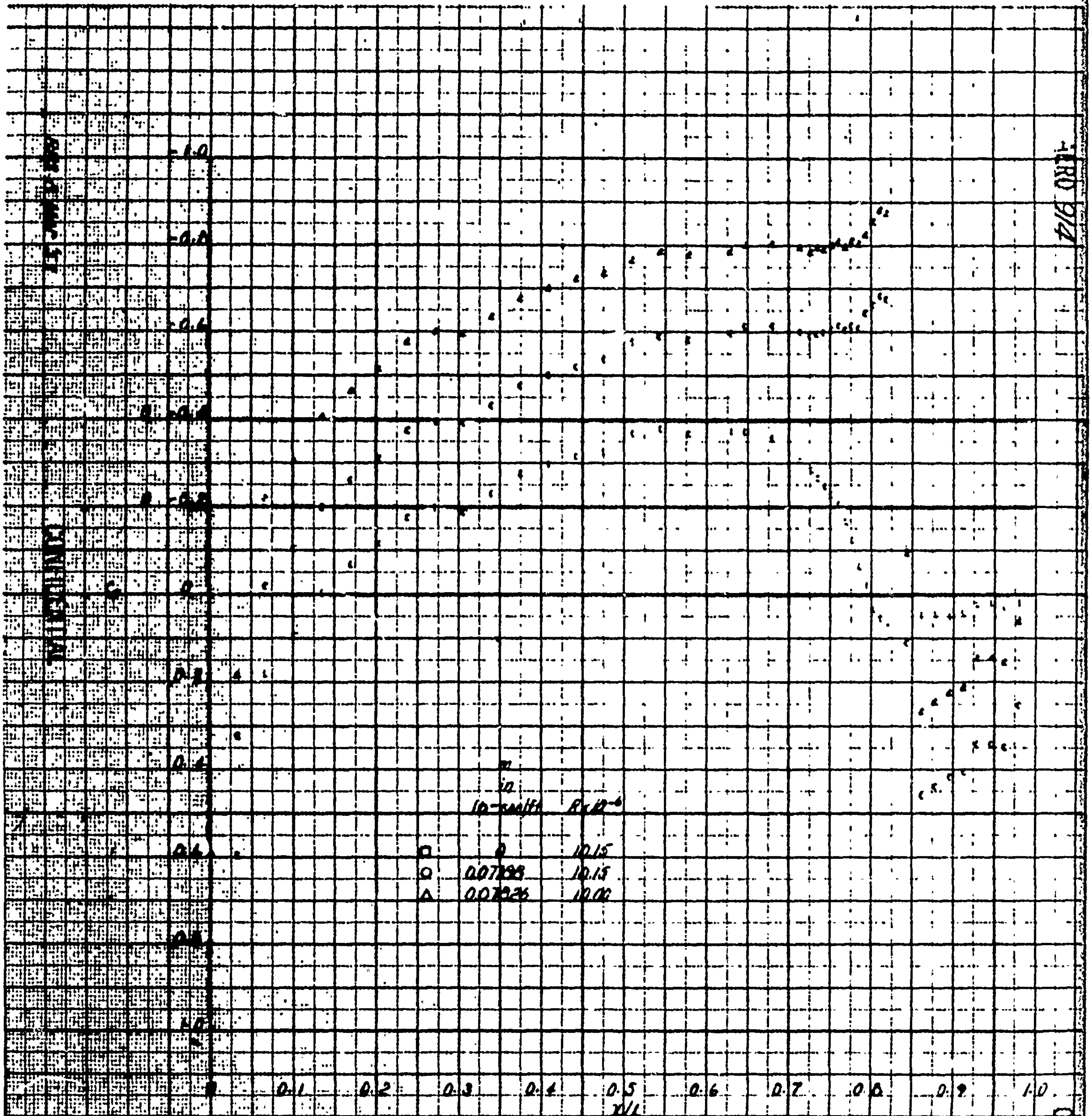

Figure 10 (Continued)

( ) a/l = 0.0[illegible], $R \approx 10.1 \times 10^6$

CONFIDENTIAL

CONFIDENTIAL

Figure 10 (Concluded)

(a) $\alpha/L = 0.514$, $R = 4.5 \times 10^6$

Figure 11 - Pressure Distribution on the Lee Airship Hull at (a) b/L = 0.342, R = 4.4 x 10^6

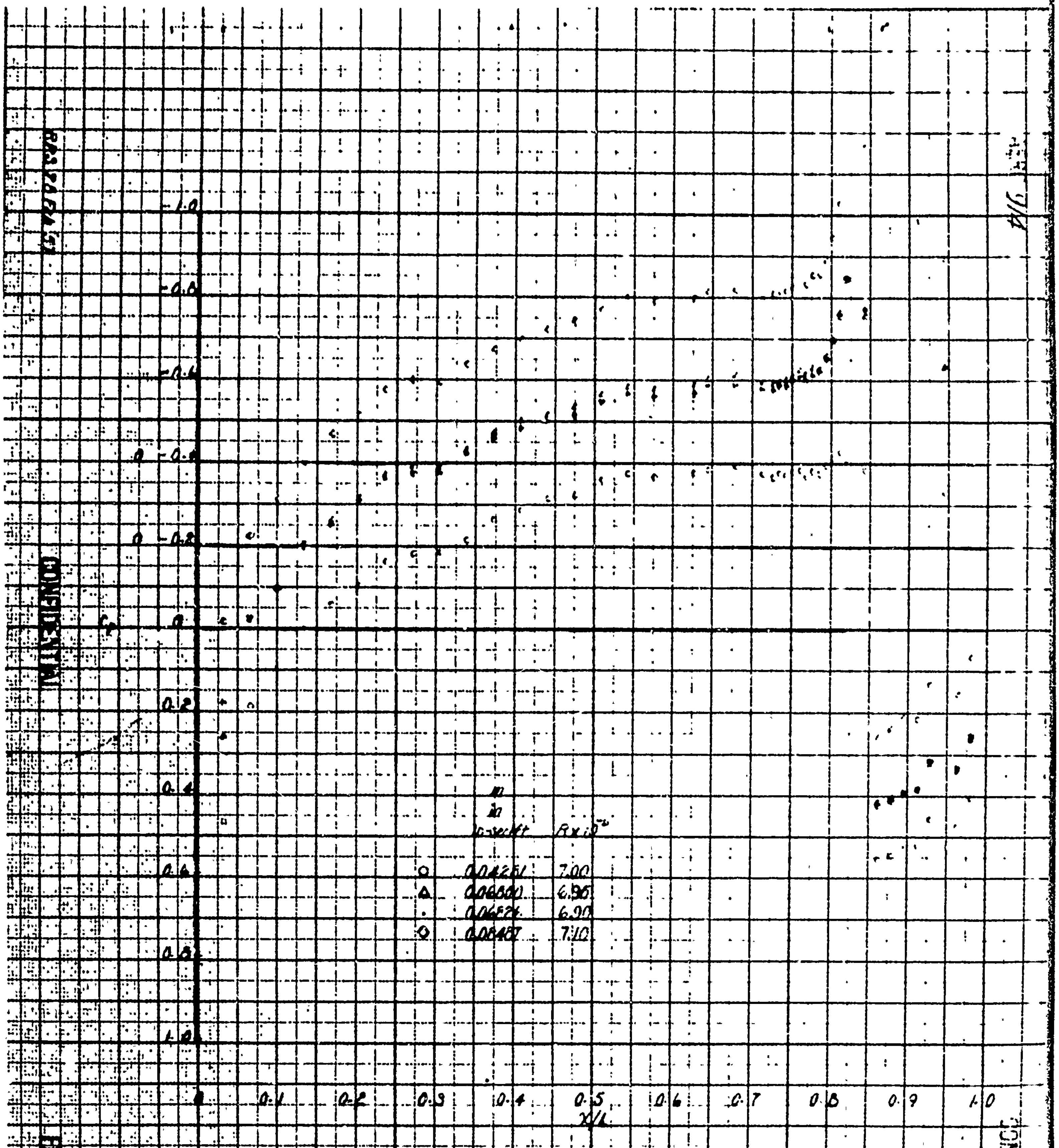

Figure 11 (Continued)

(i) g/L = 0.312, R ≈ 7 x 10⁶

Figure 11. (Continued)

(c) $q/L = 0.012$, $R = 12 \times 10^6$

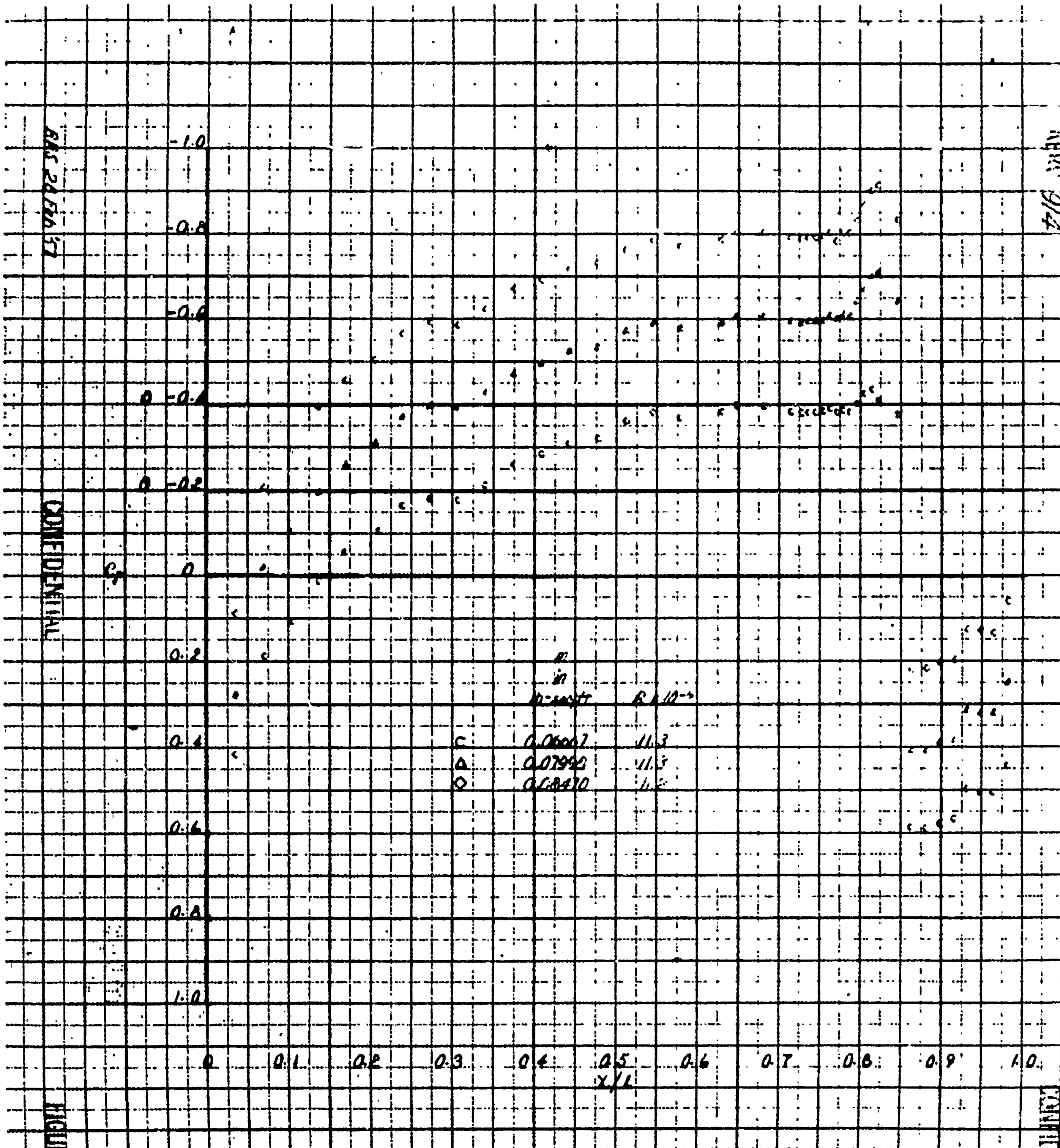

Figure 11 (Continued)

(d) $g/l = 0.012$, $R \approx 11.3 \times 10^6$

CONFIDENTIAL

FIGURE 11d

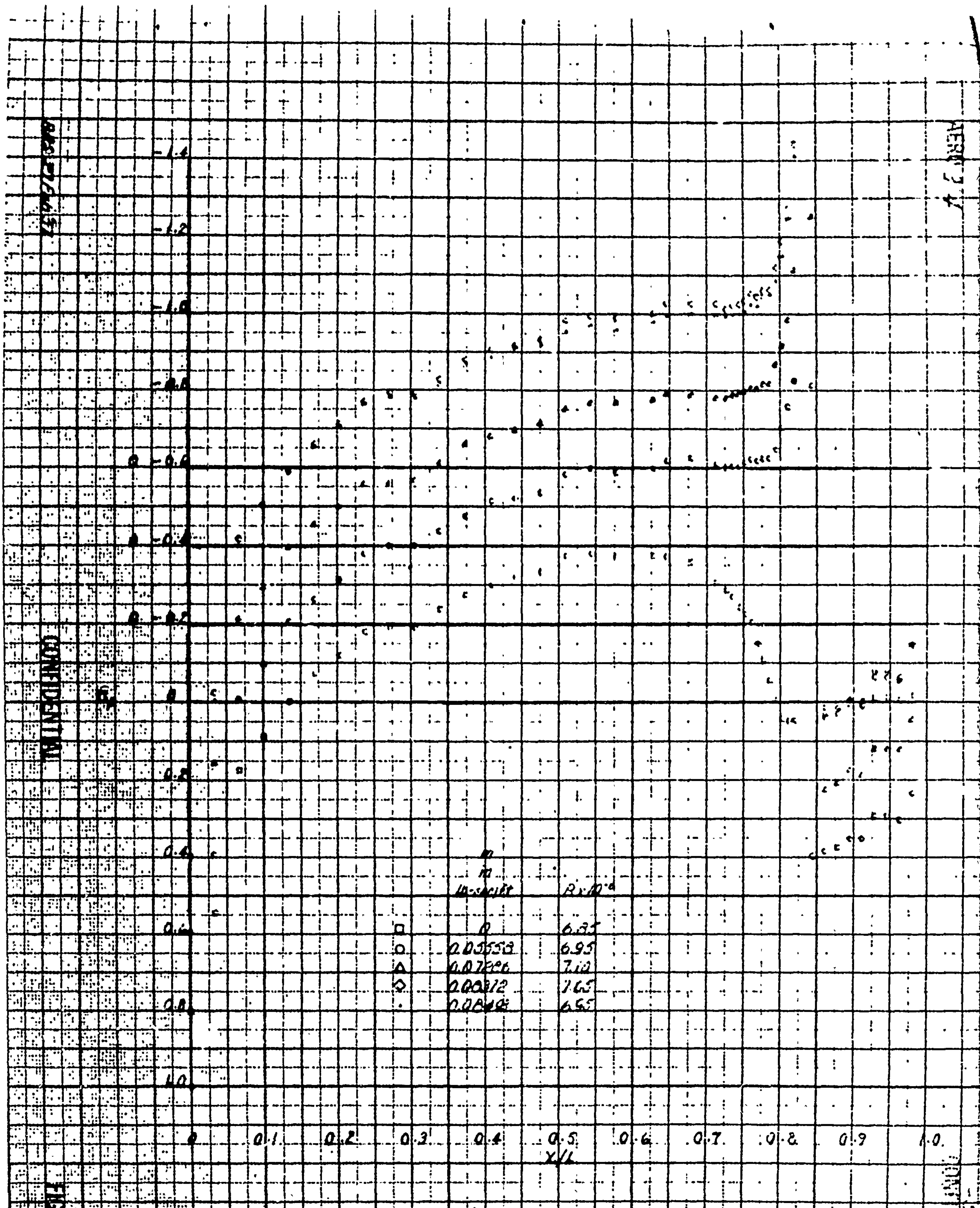

Figure 11 (Continued)

(c) α' = 0.006, R = 7 x 10^6

CONFIDENTIAL

AERO 914

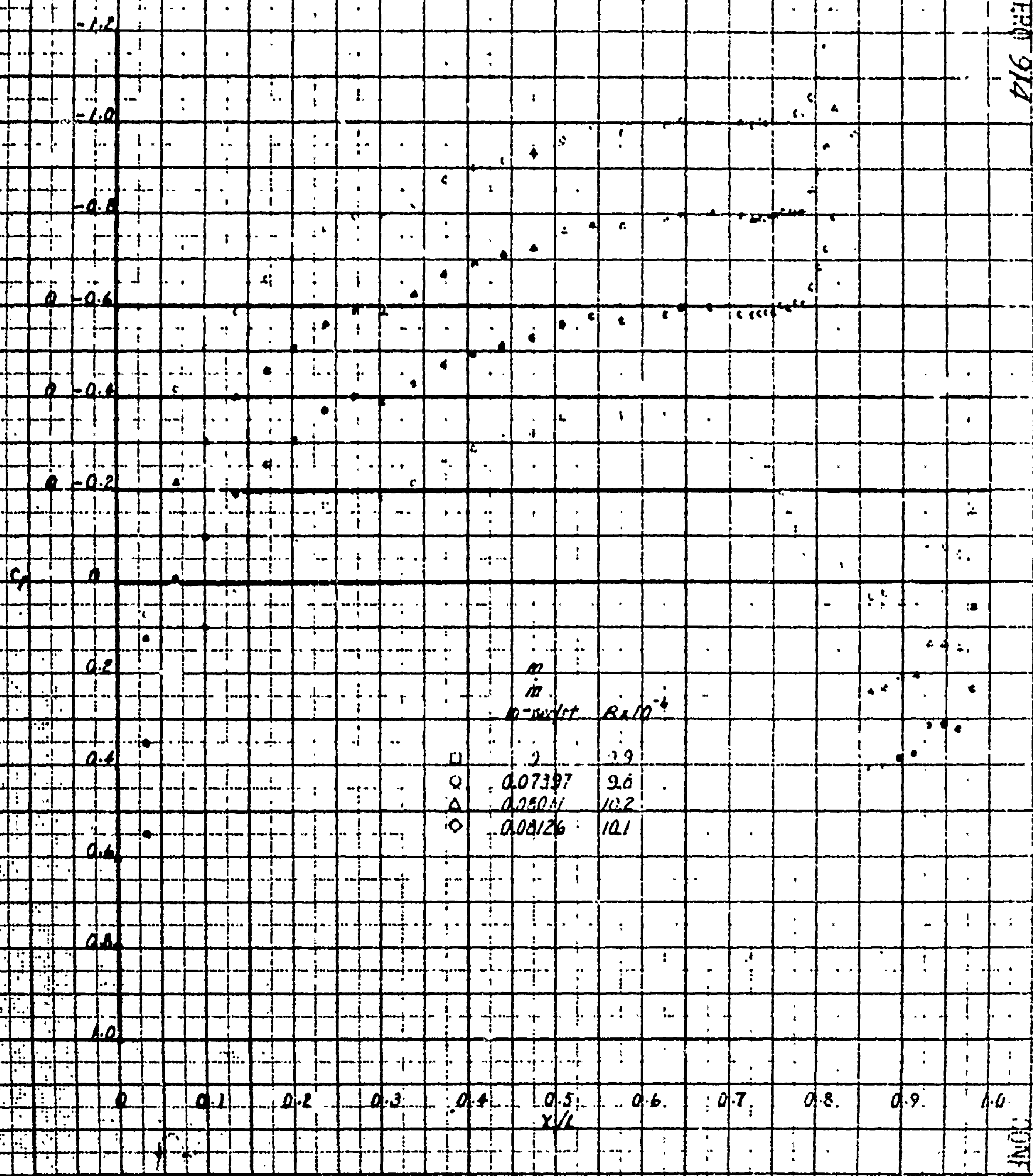

Figure 11 (Continued)

$l/l \; g/l = 0.006, R = 10 \times 10^6$

FIGURE 11 g

CONFIDENTIAL

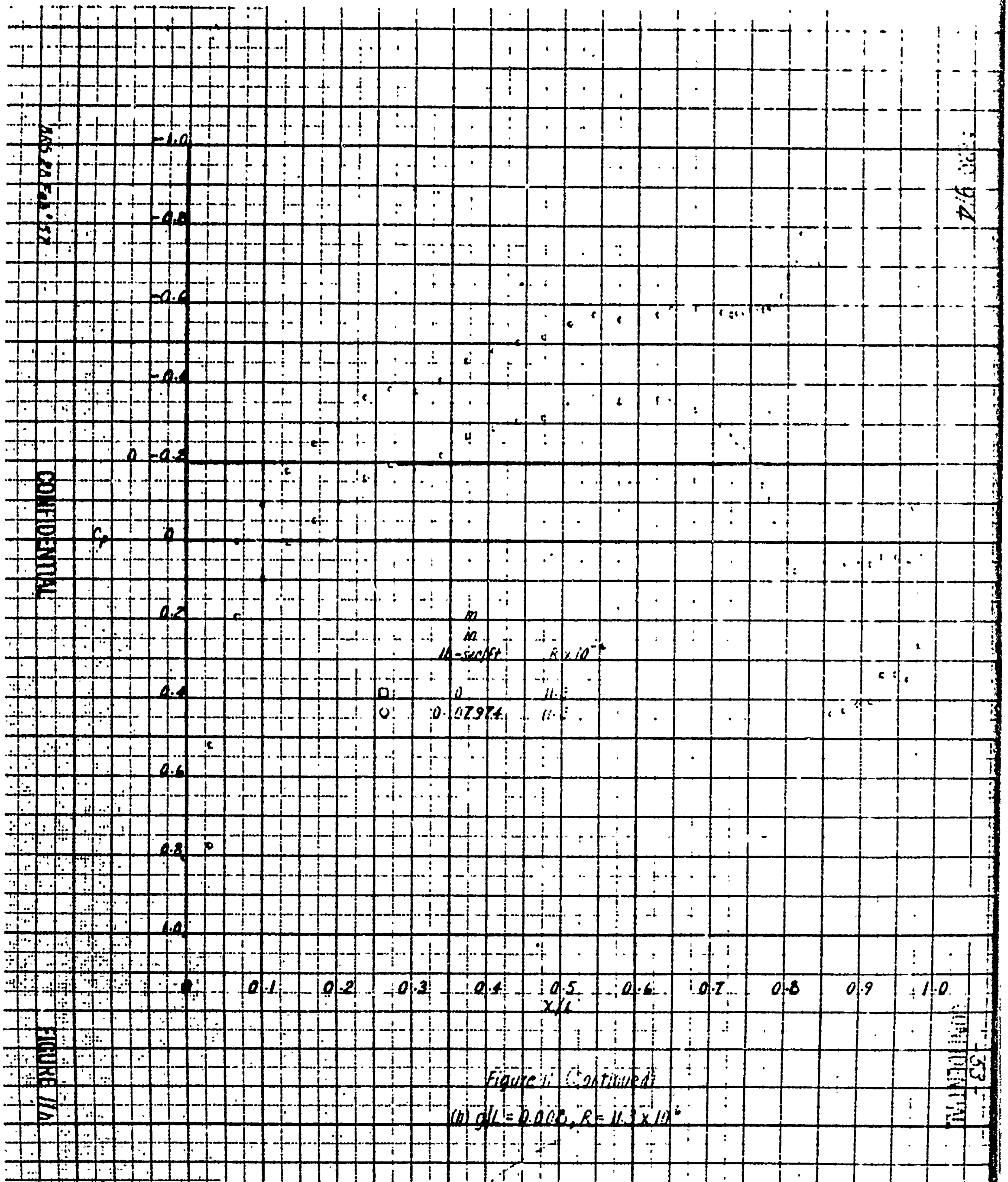

Figure 11 (Continued)

(d) d/l = 0.002, R = 11.3 x 10⁶

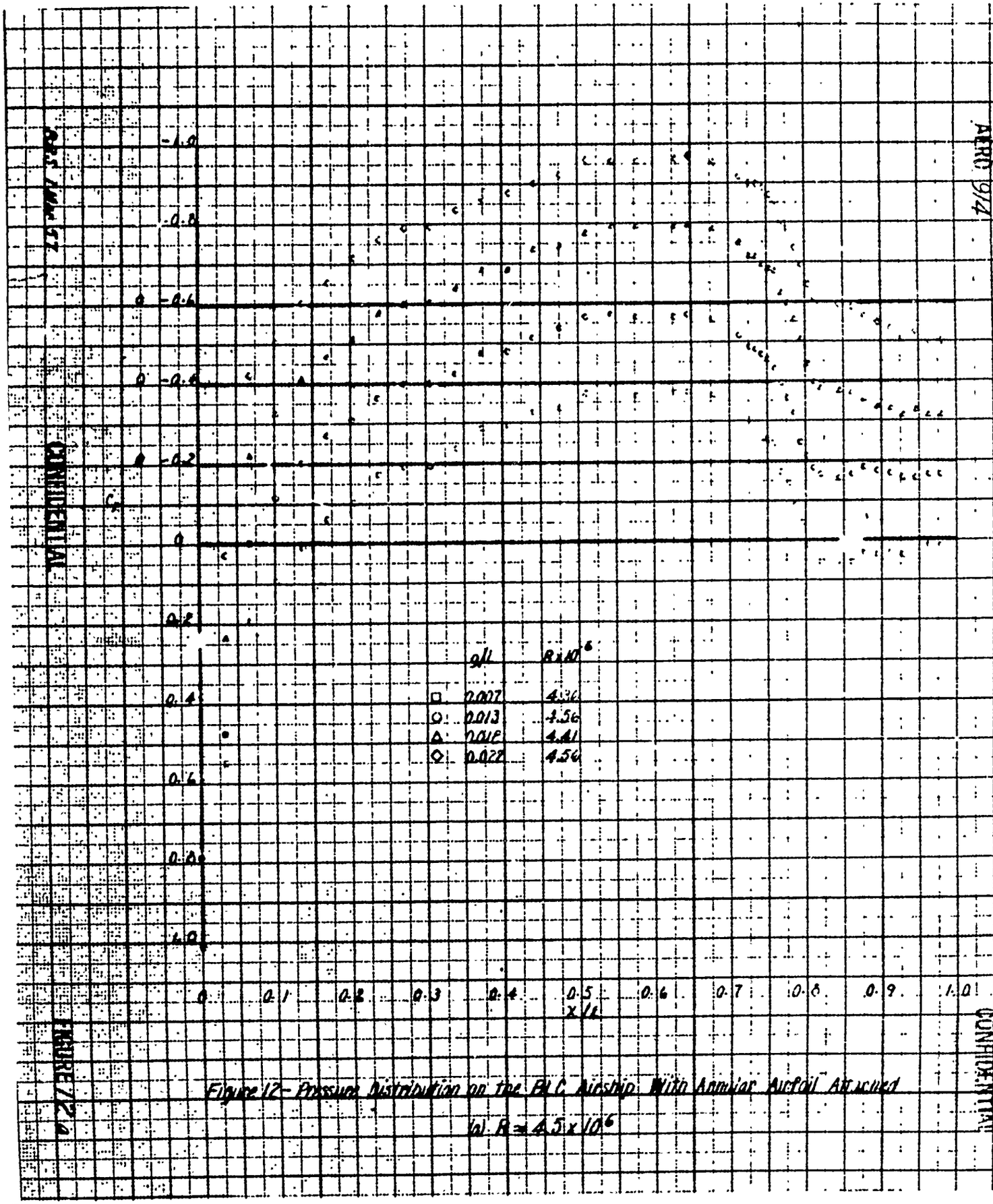

Figure 12- Pressure Distribution on the BLC Airship With Annular Airfoil Attached
(a) $R = 4.5 \times 10^6$

Figure 12 (Continued)

(b) $R_n = 7 \times 10^6$

	α/l	$R \times 10^{-6}$
□	0.003	7.01
○	0.013	6.76
△	0.016	6.93
◇	0.022	7.01

FIGURE 12 b

AERO 9/14

ARS 1 Mar 52

	α/L	$A \times 10^{-6}$
□	0.007	9.75
○	0.013	9.80
△	0.018	9.75
◇	0.022	9.80

Figure 12 (Continued)

$[c] B = 9.6 \times 10^{6}$

AERC 9/4

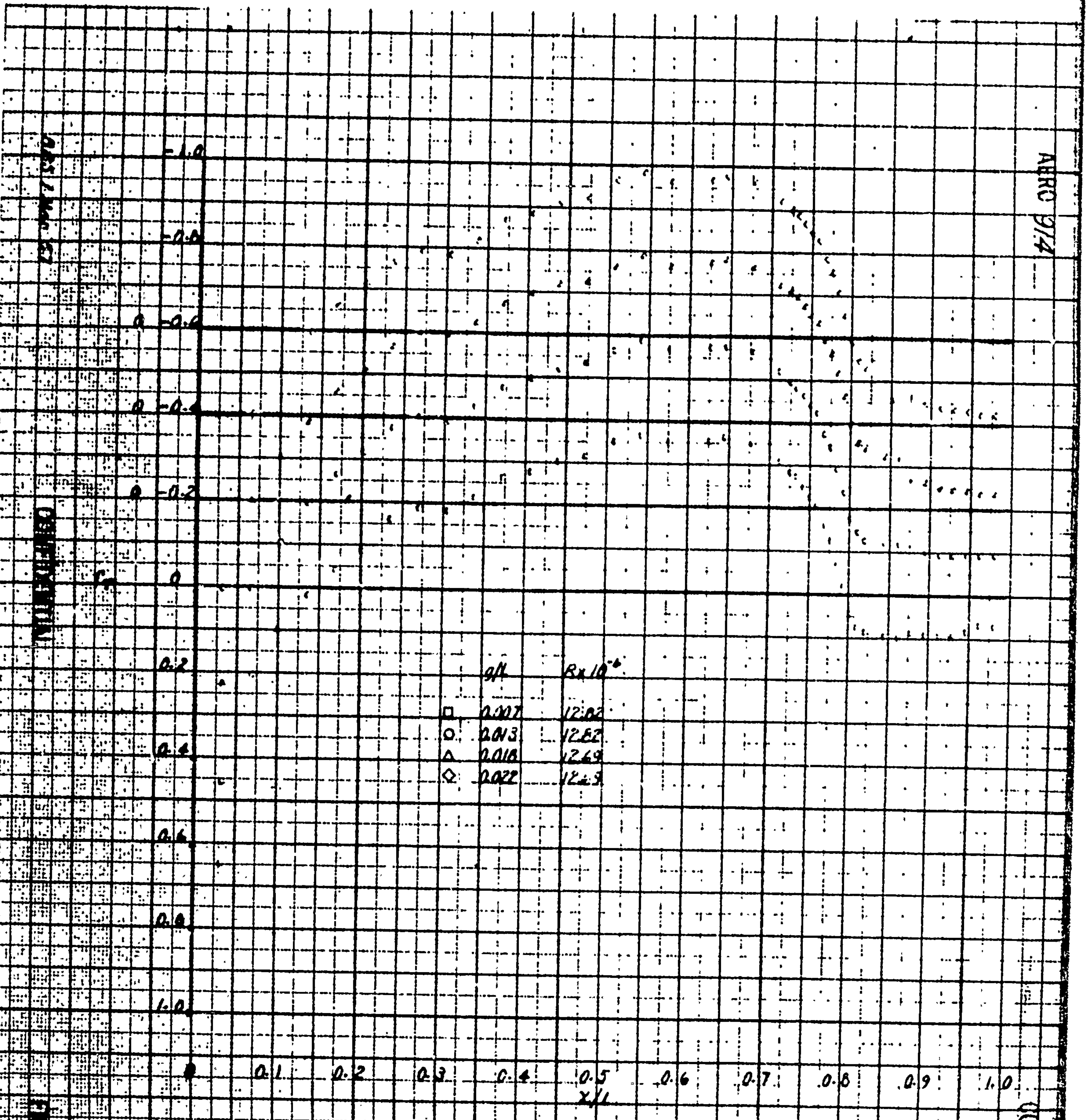

Figure 12 (Concluded)

(d) $R = 12.7 \times 10^6$

FIGURE 12 d

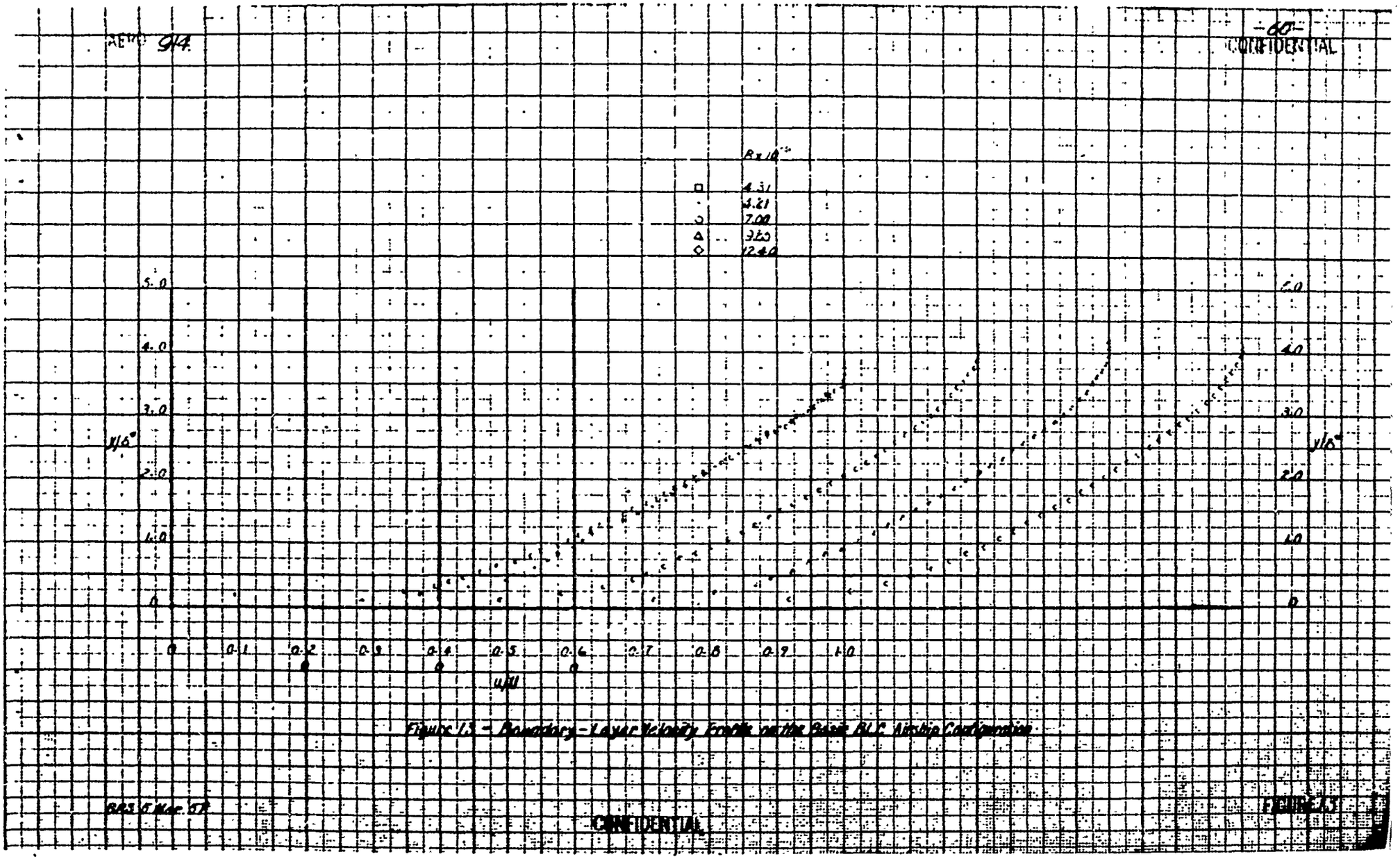

Figure 15 – Boundary-Layer Velocity Profile on the Basic BLC Airship Configuration.

AERO 944

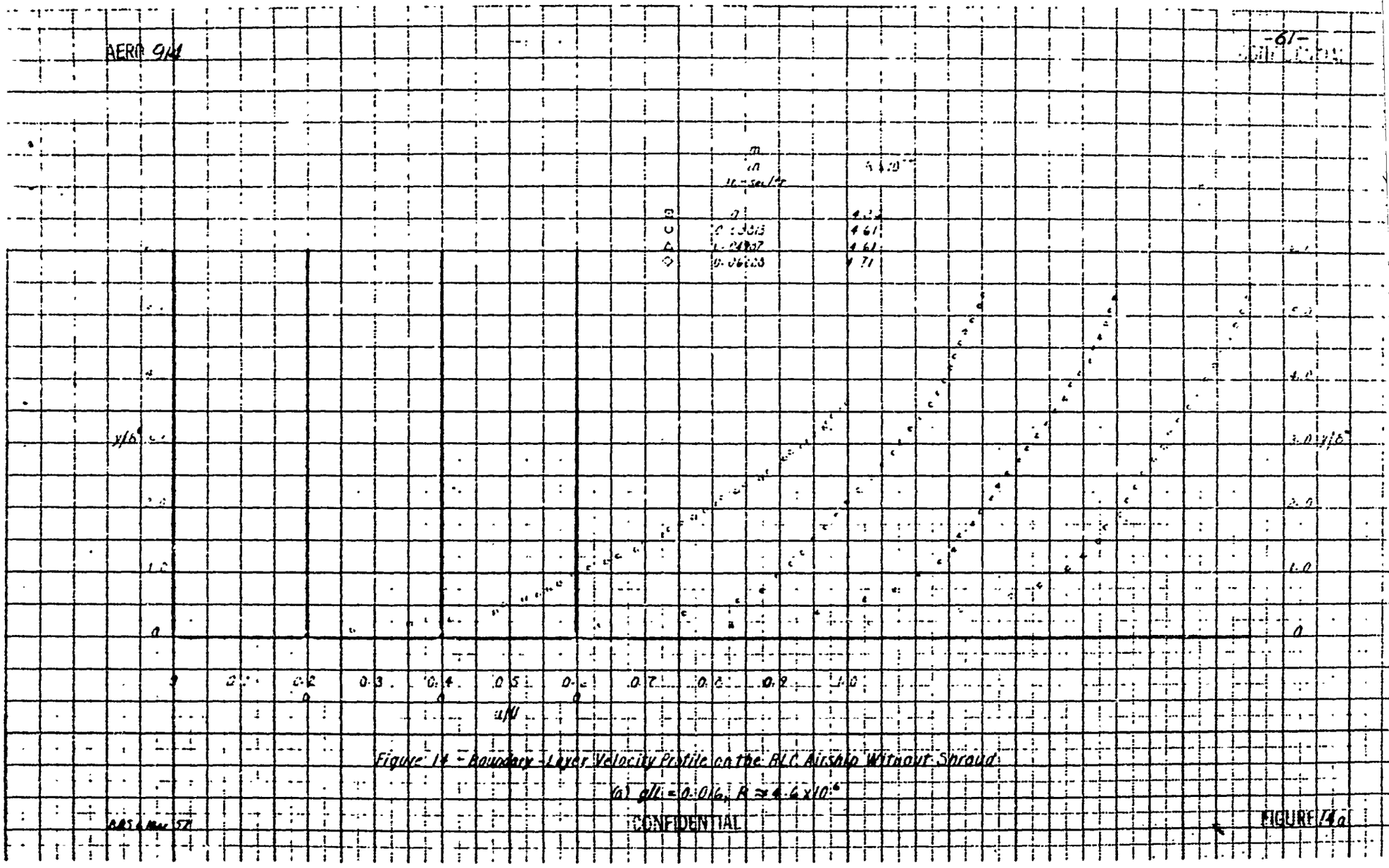

Figure 14 - Boundary Layer Velocity Profile on the RLC Airship Without Shroud

(a) $\delta/L = 0.016$, $R \approx 4.6 \times 10^6$

CONFIDENTIAL

FIGURE 14a

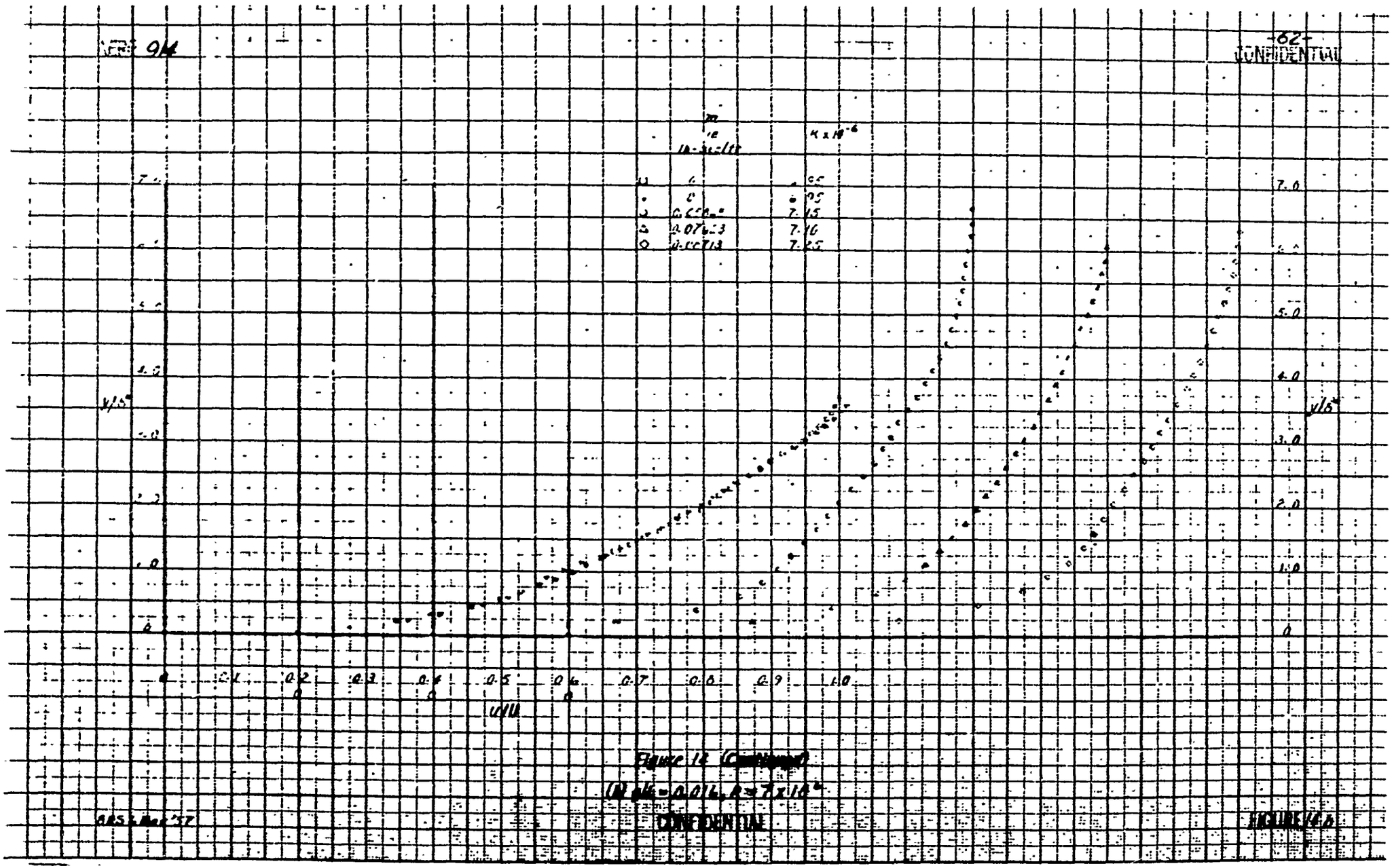

Figure 12 (Continued)

(f) $\alpha_K = 0.014$, $R = 7 \times 10^{-6}$

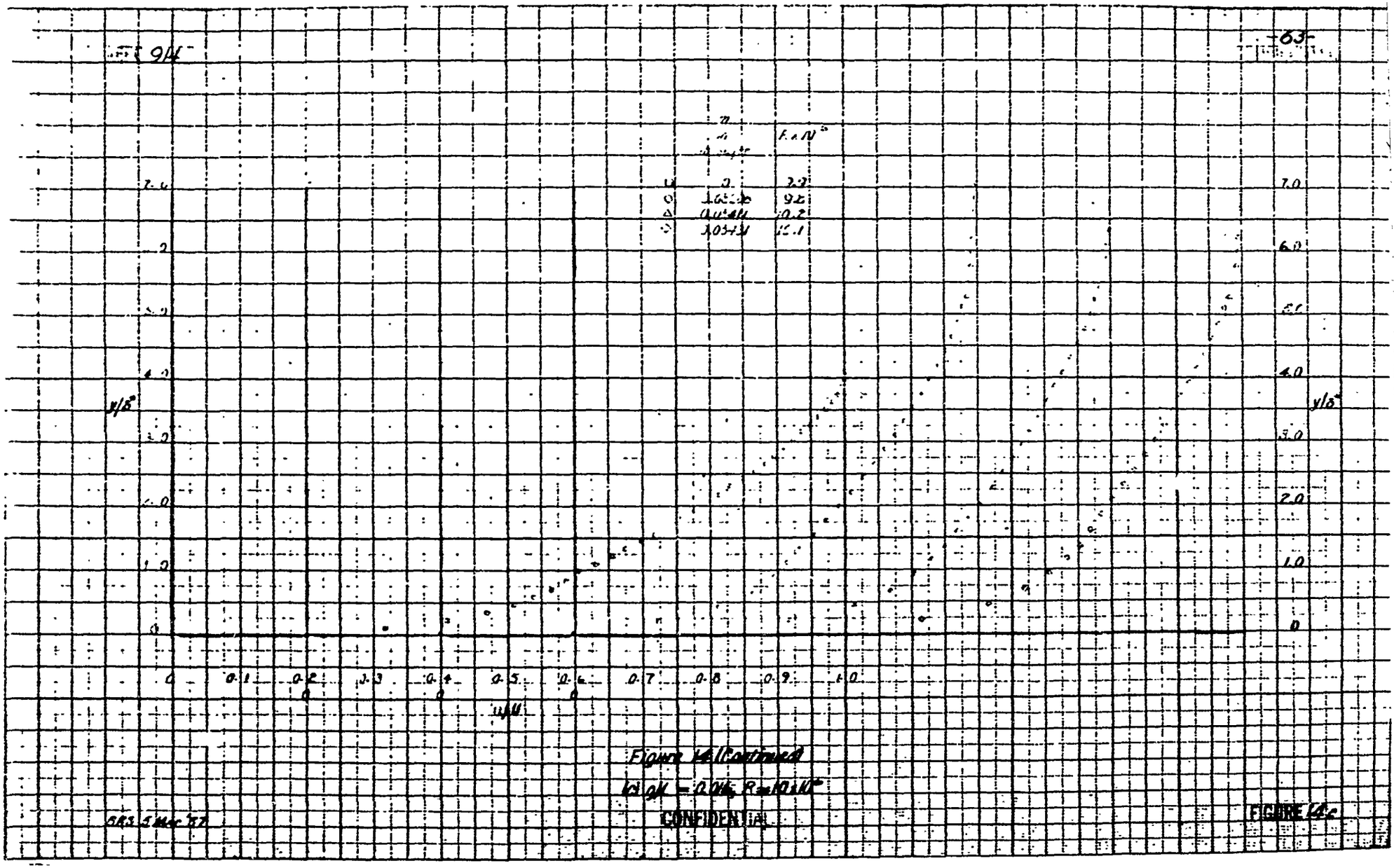

Figure 14 Continued

$M_\infty = 0.96$, $R = 10 \times 10^6$

CONFIDENTIAL

FIGURE 14c

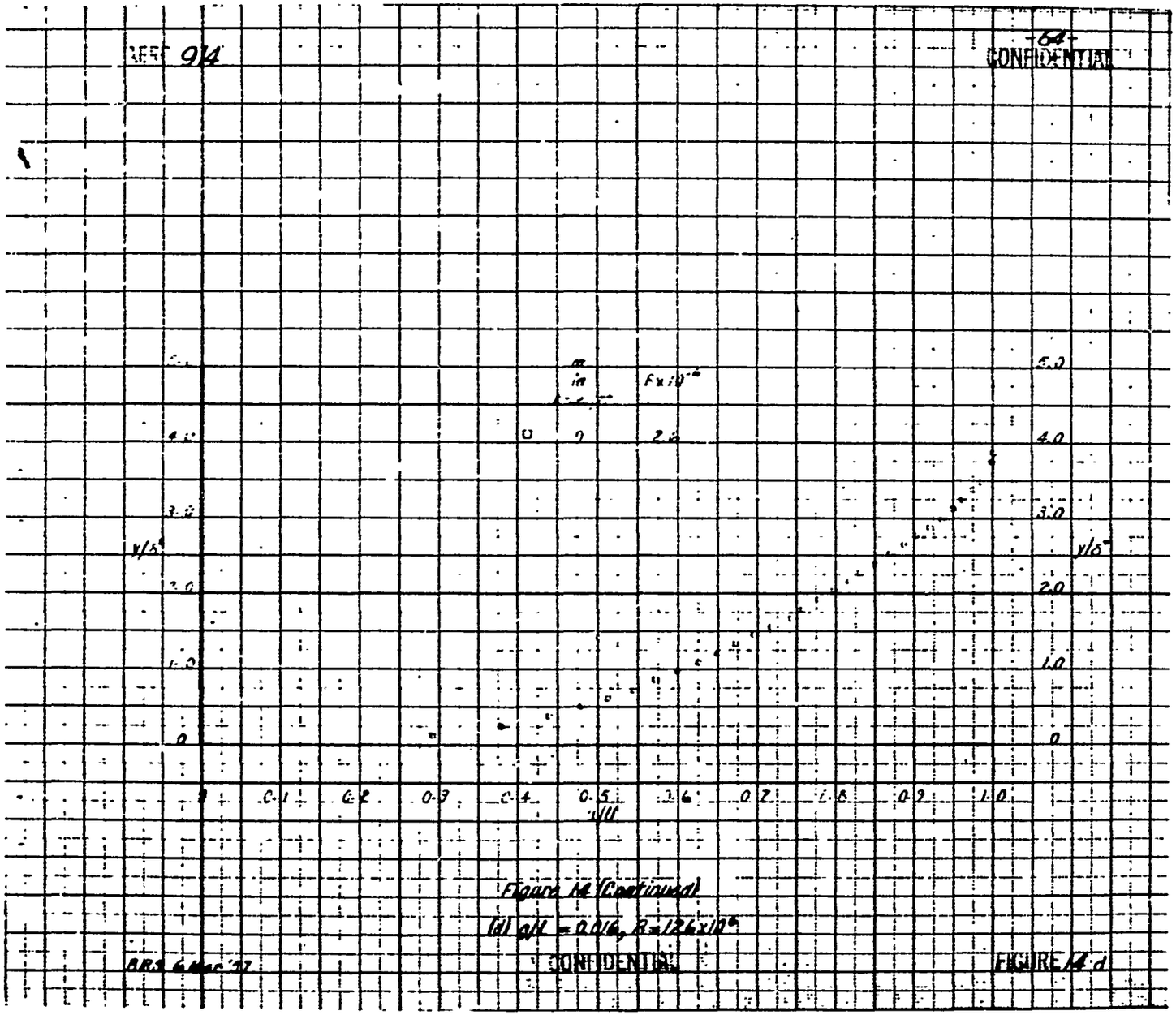

Figure 14 (Continued)

(d) $\alpha/t = 0.016$, $R = 1.26 \times 10^6$

FIGURE 14-d

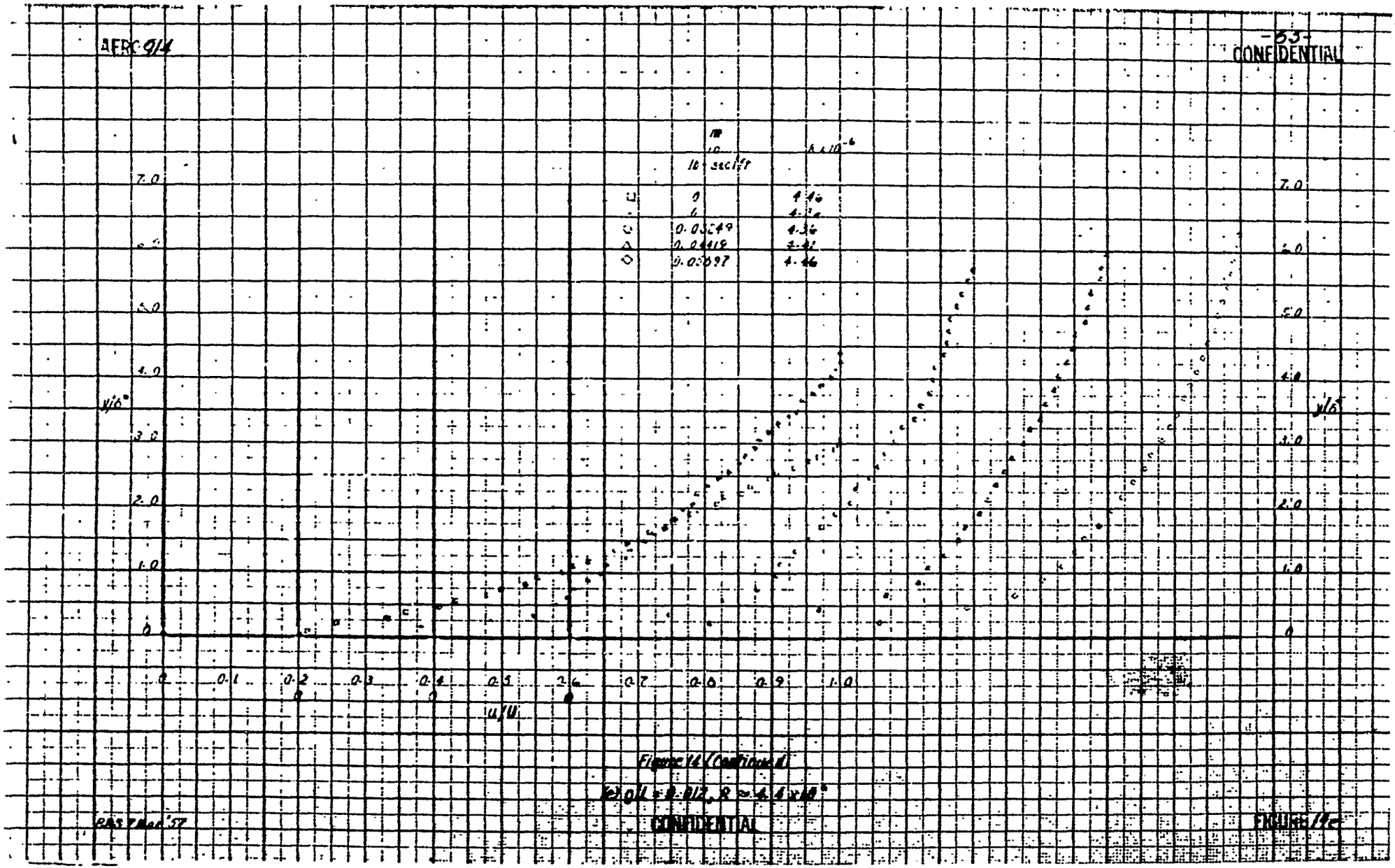

Figure 14 (Continued)

(c) $\delta/L = 0.012$, $R = 4.4 \times 10^6$

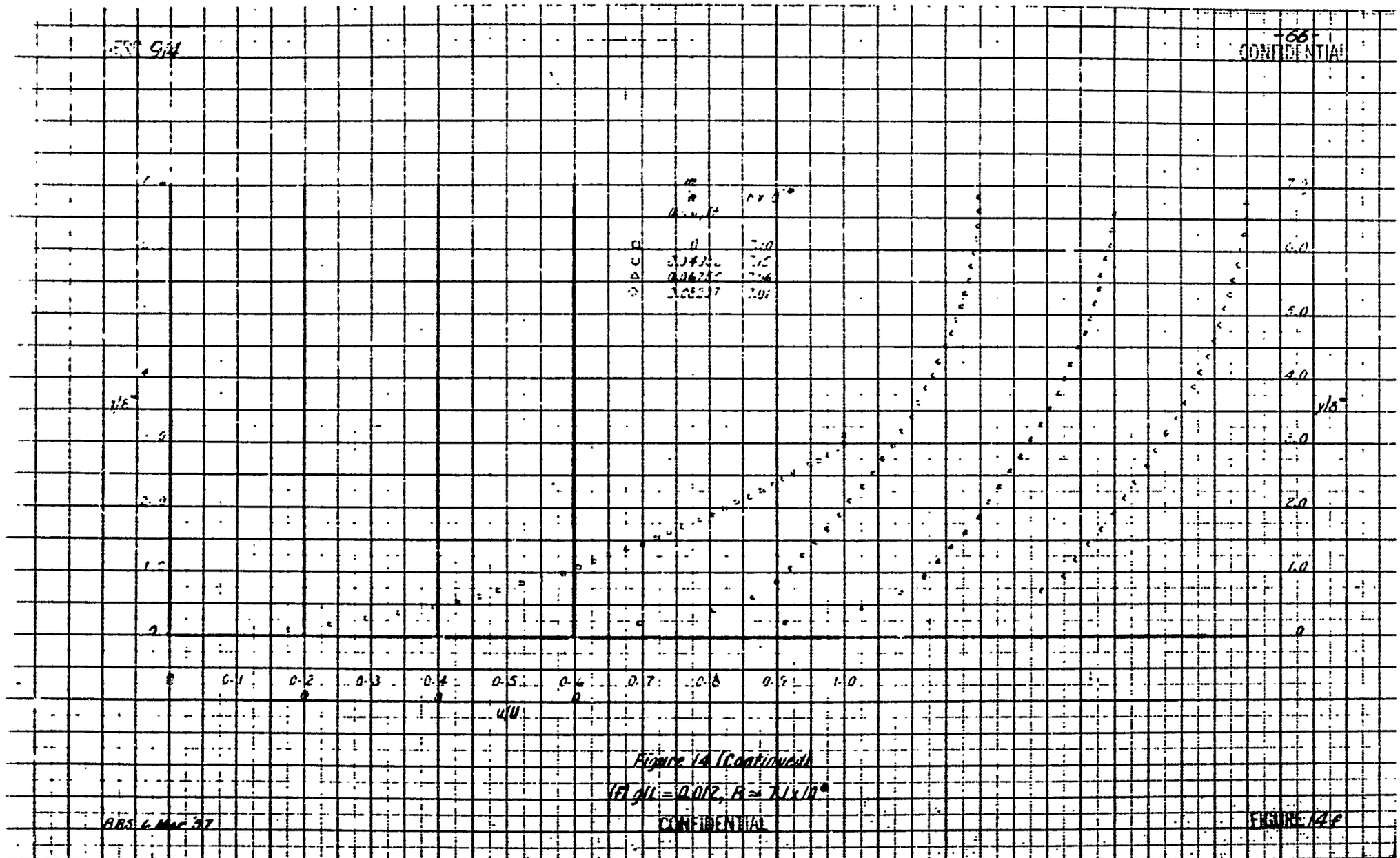

Figure 14 (Continued)

$\sqrt{\theta_{11}} = 0.012$; $R \approx 7.1 \times 10^4$

ABS 6 Mar 37

FIGURE 14 f

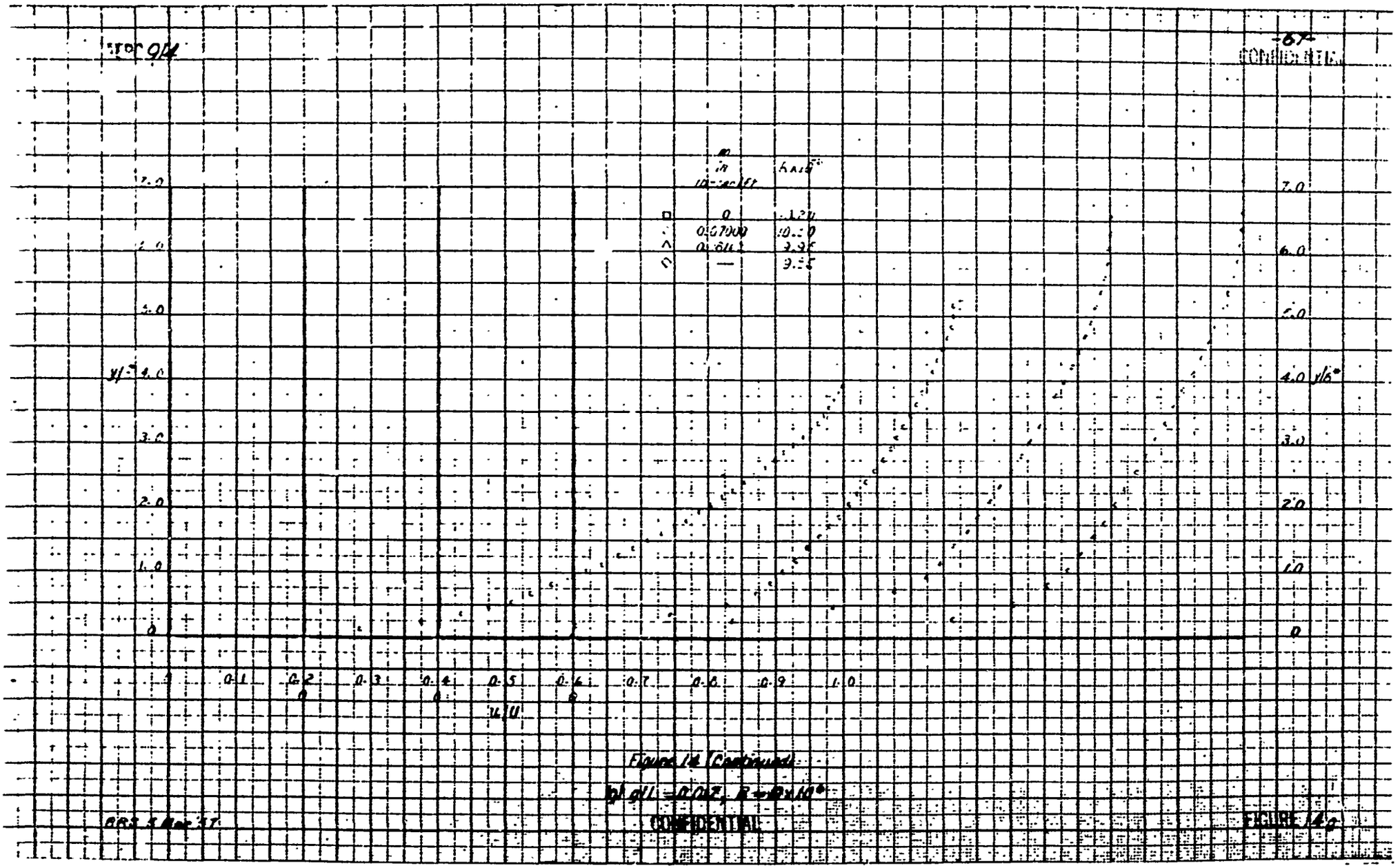

Figure 14 (Continued)

$\log \dot{q}/I = 0.012$, $R = 8 \times 10^6$

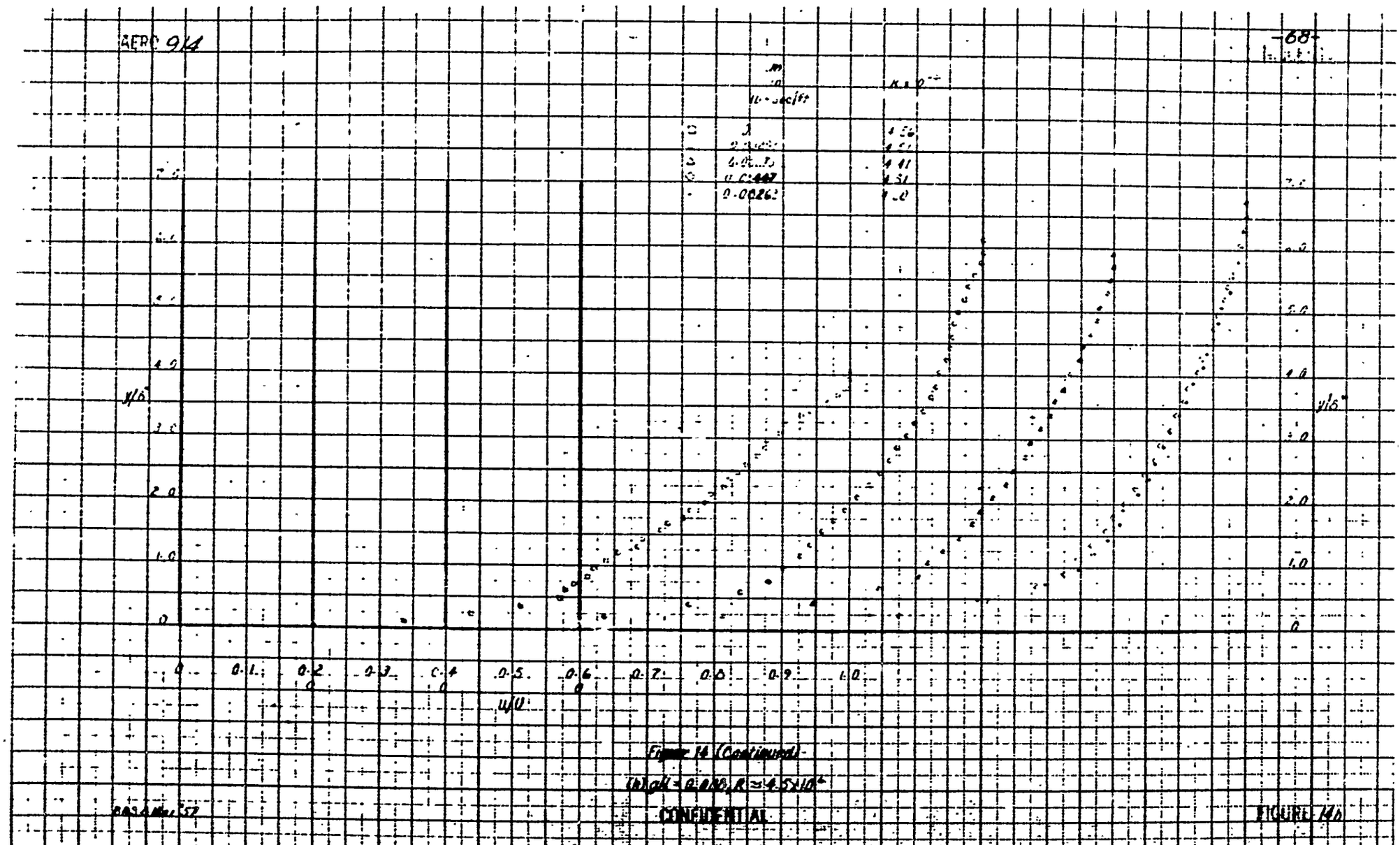

Figure 16 (Continued)

(b) $\alpha = 0.000$, $R \approx 4.5 \times 10^6$

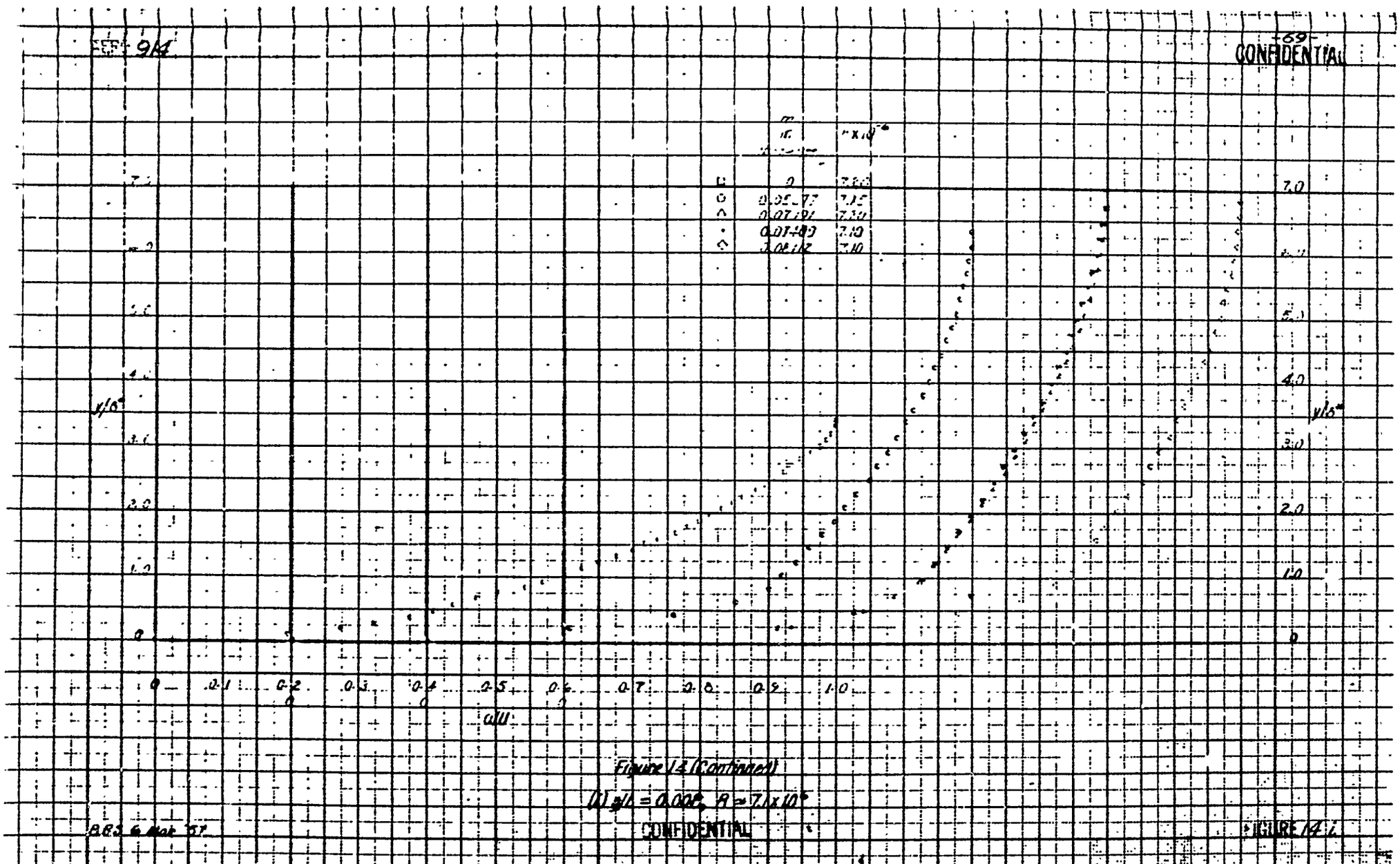

Figure 14 (Continued)

(k) $a/b = 0.005$, $R = 7.1 \times 10^{6}$

BRS 6 Mar 57

FIGURE 14 (k)

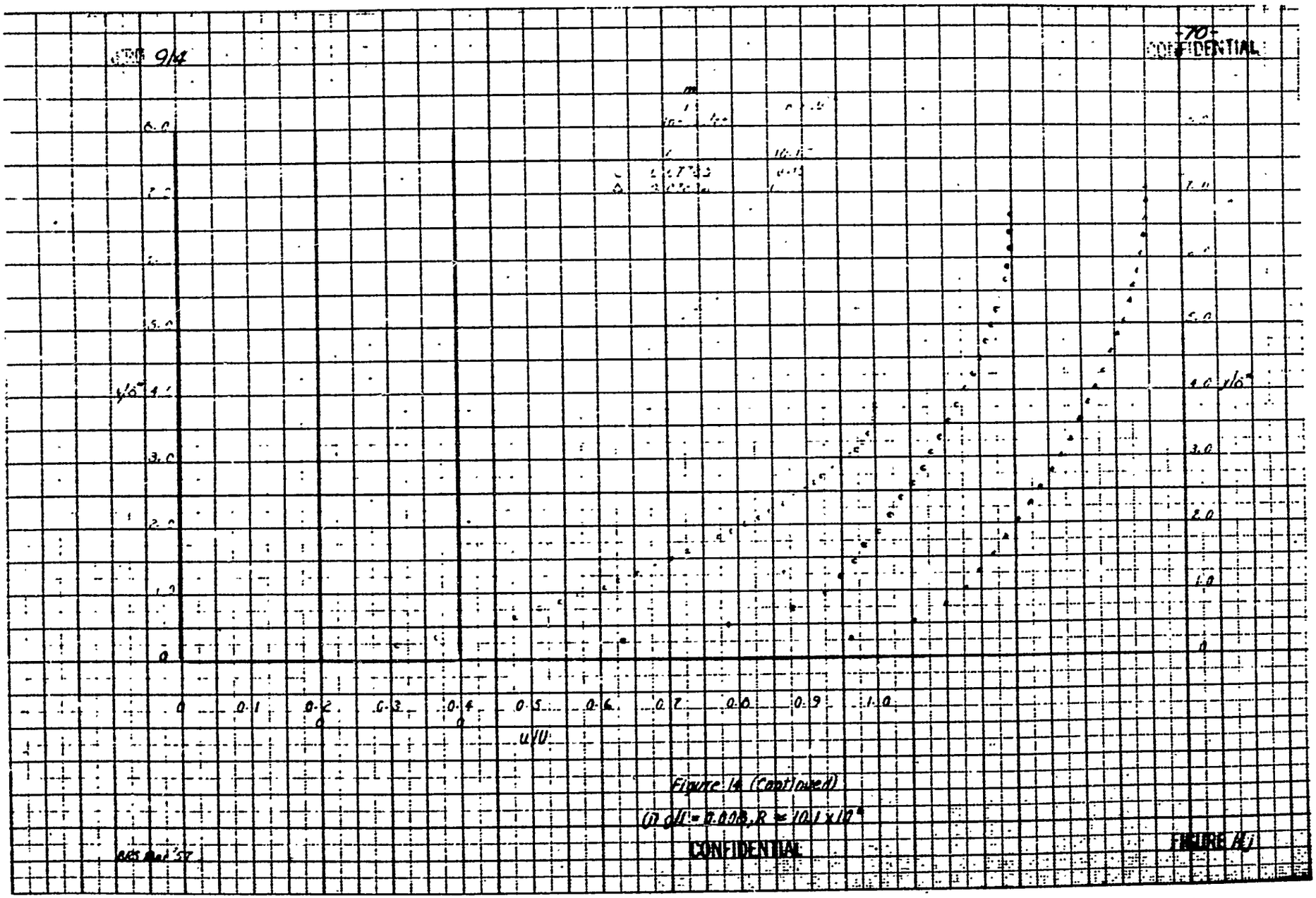

Figure 14 (Continued)

(j) $\partial U = 0.008$, $R = 10.1 \times 10^6$

FIGURE 14j

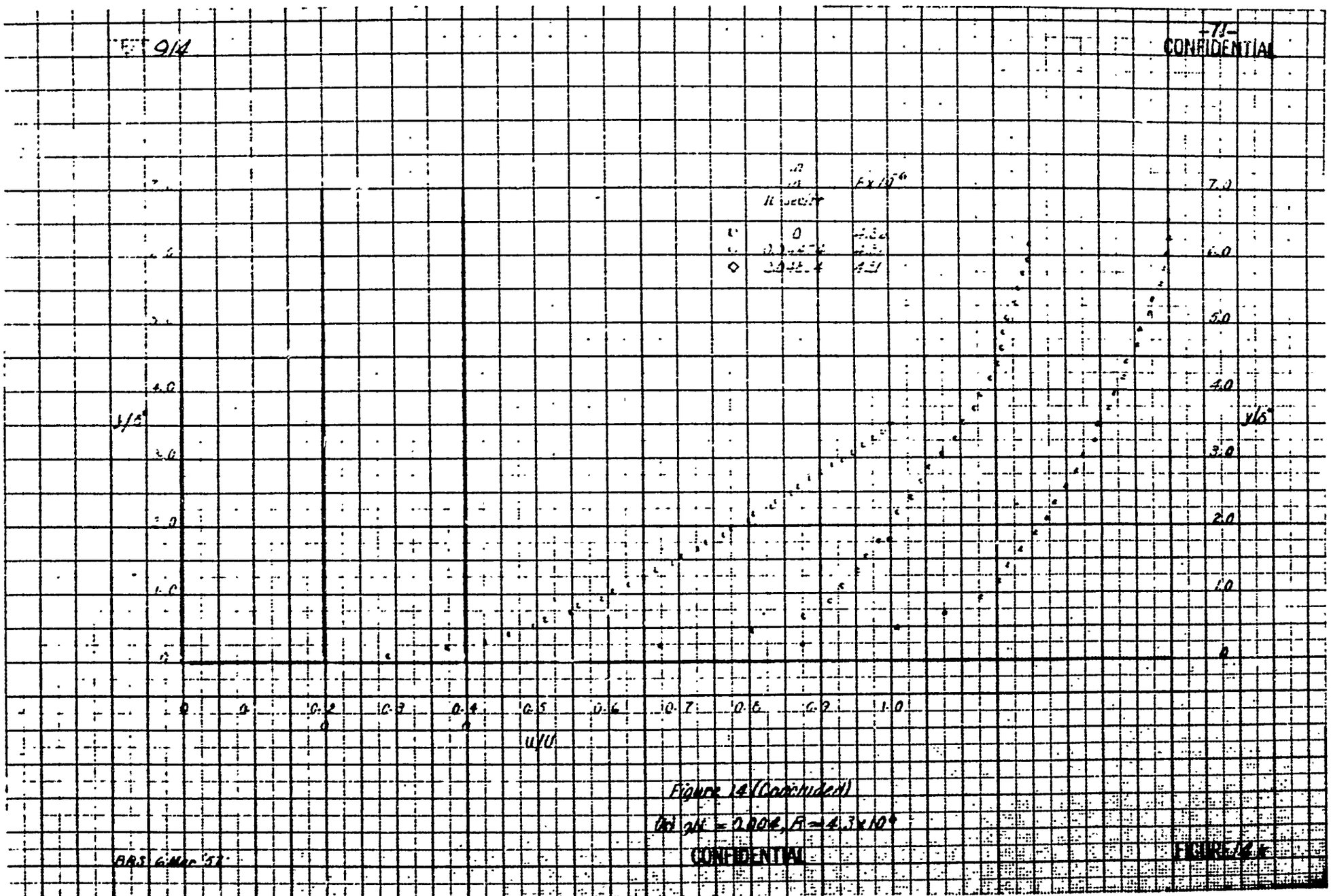

Figure 14 (Concluded)

(b) $\frac{2h}{\delta} = 2.004$, $R = 4.3 \times 10^4$

CONFIDENTIAL

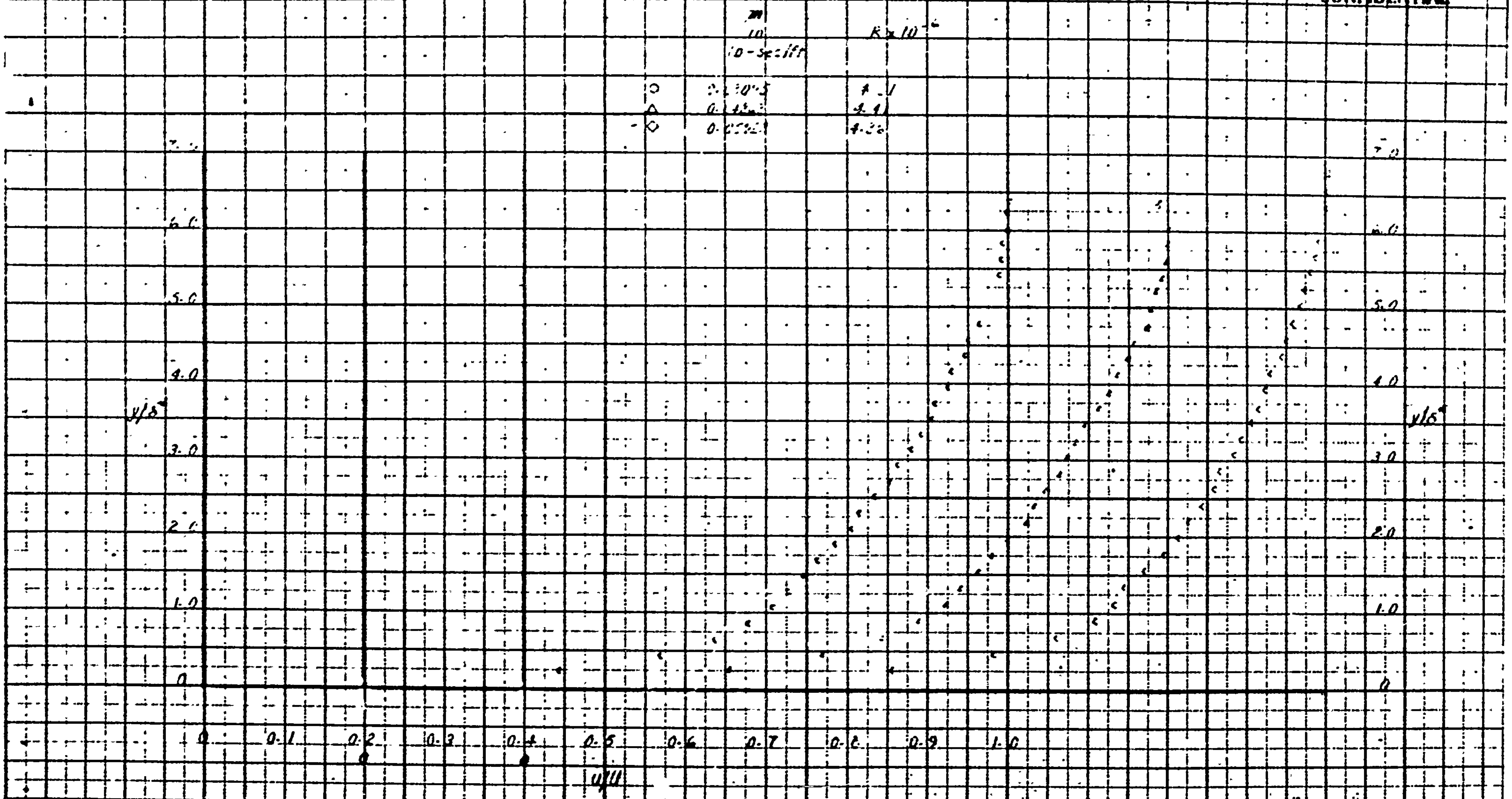

Figure 15 – Boundary-Layer Velocity Profile on the BLC Airship With Shroud

BBS 6 Mar 57

CONFIDENTIAL

FIGURE 15a

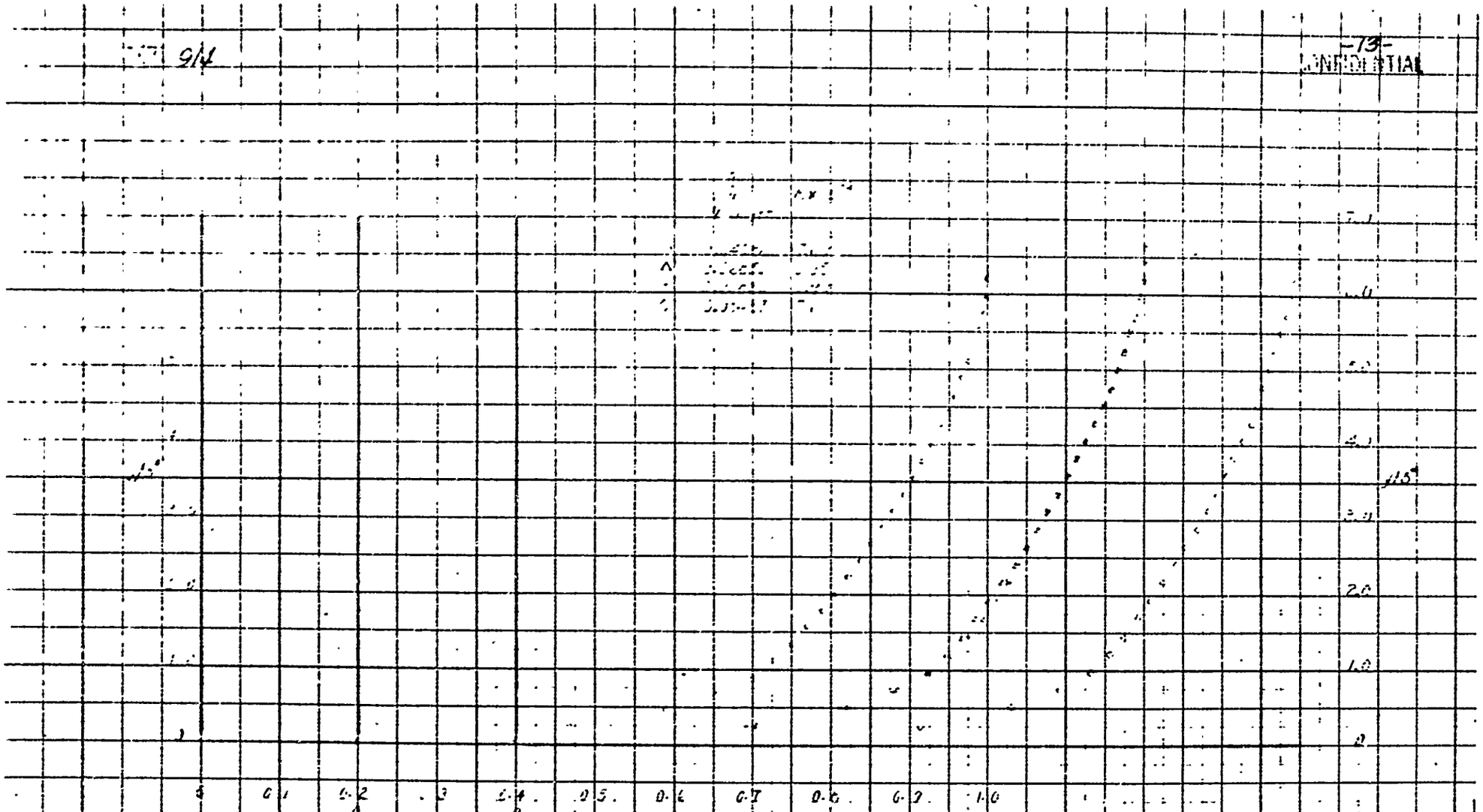

Figure 15 (Continued)

$(\partial u/\partial y)_{w} = 0.012$, $R \approx 7.0 \times 10^{6}$

FIGURE 15 b

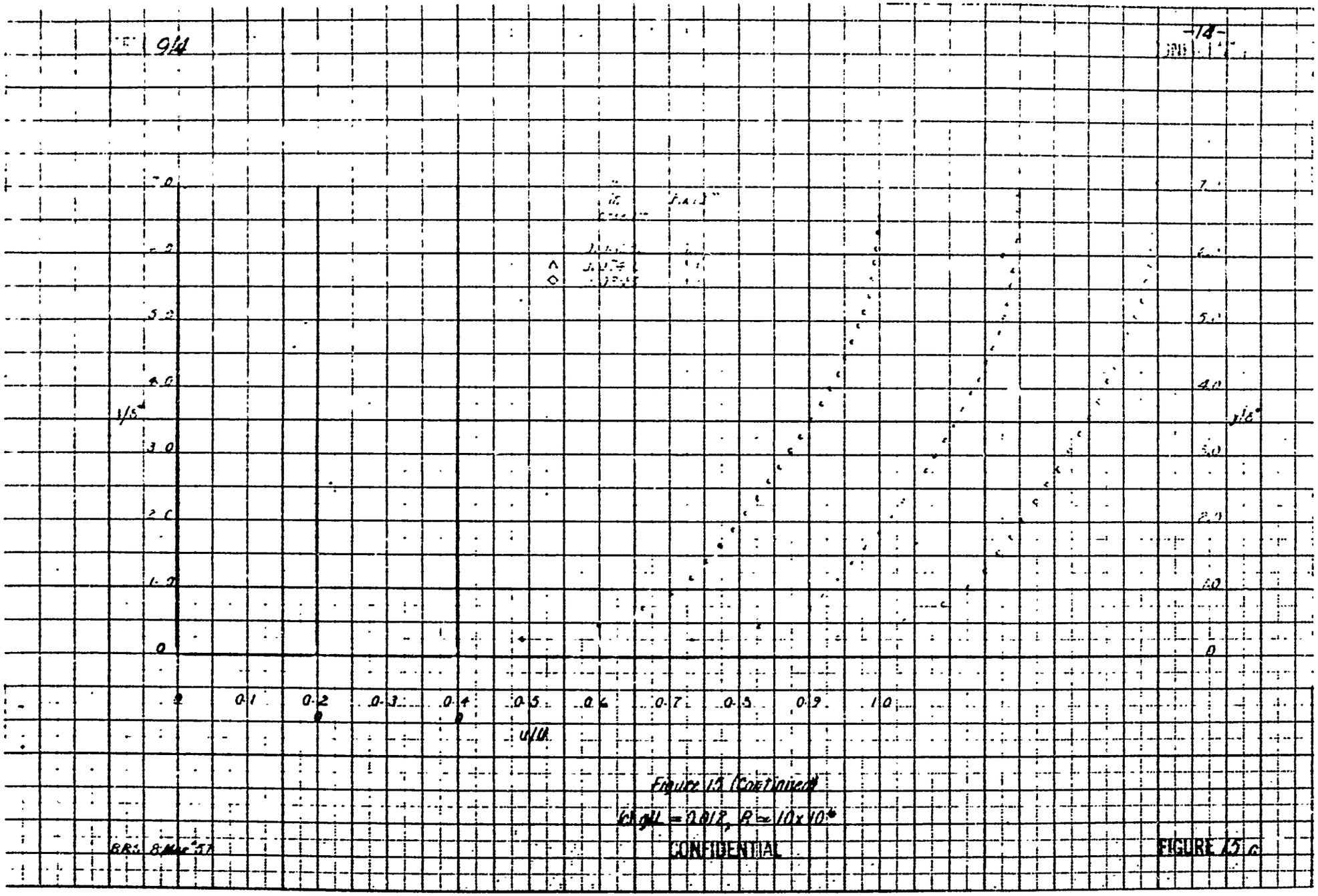

Figure 15 (Continued)

$C_{hgll} = 0.018$, $R \sim 10 \times 10^6$

FIGURE 15 c

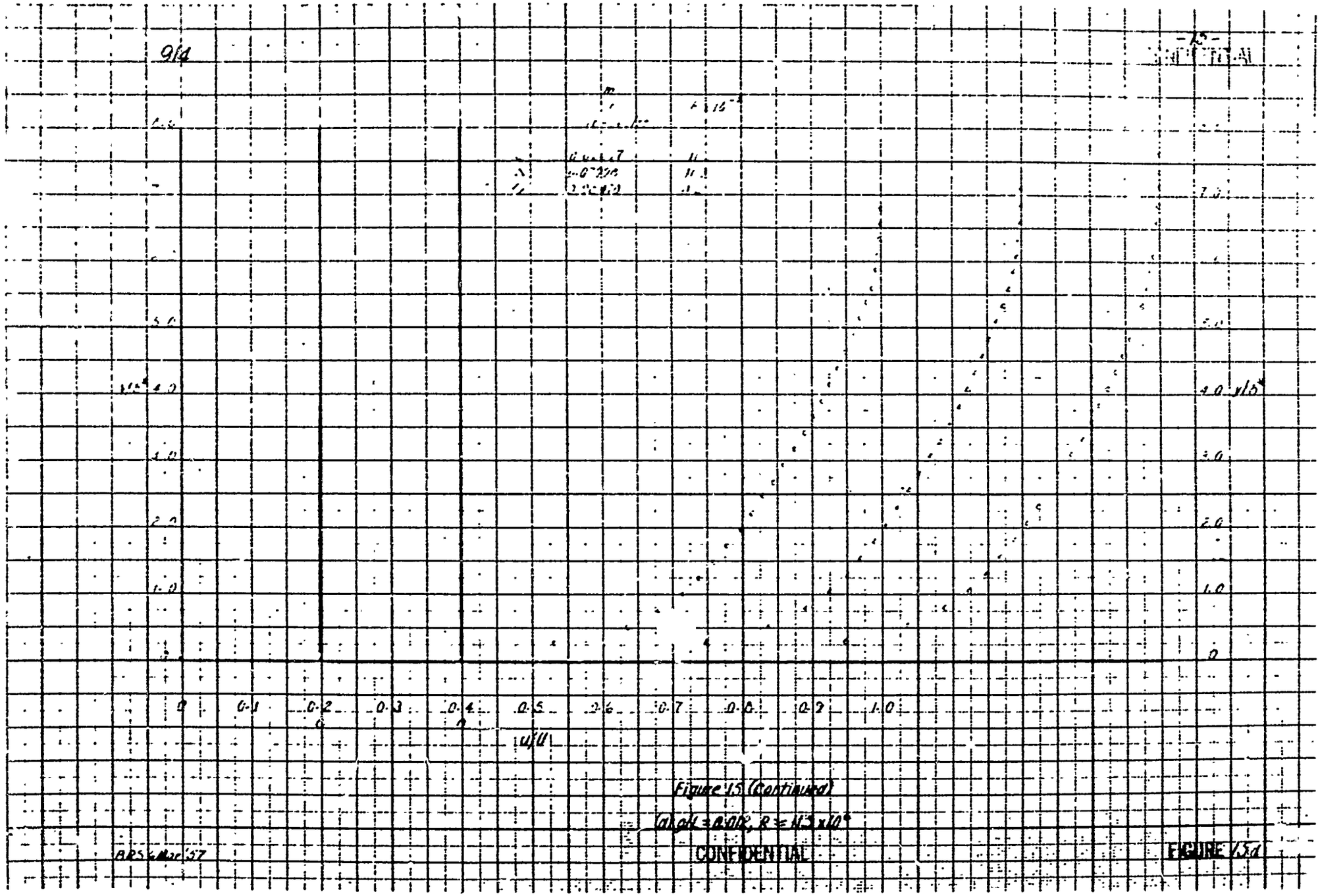

Figure 15 (Continued)

(a) $\alpha t = 0.002$, $R = 1.5 \times 10^4$

FIGURE 15d

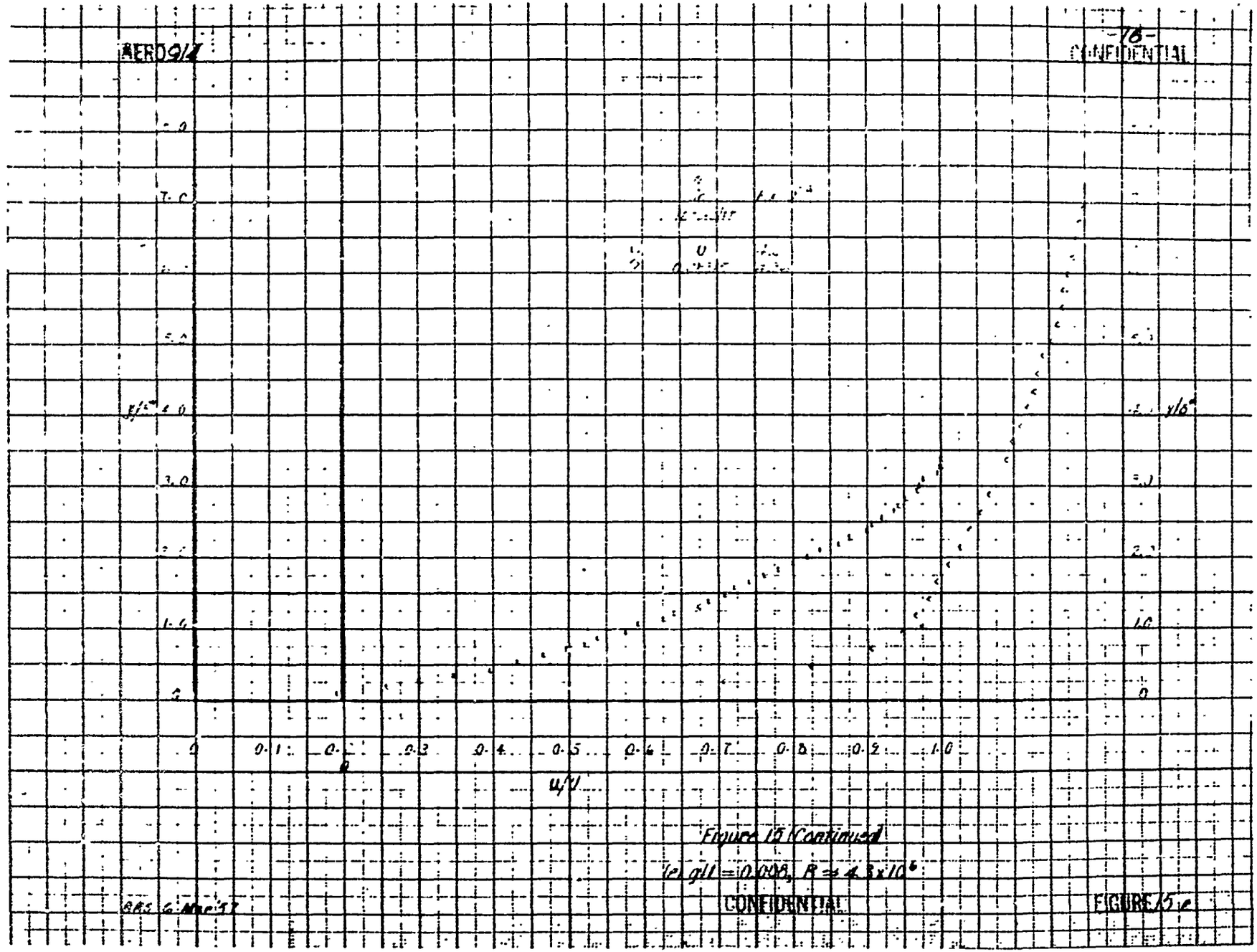

Figure 15 (Continued)

(e) $g/l = 0.008$, $R = 4.3 \times 10^6$

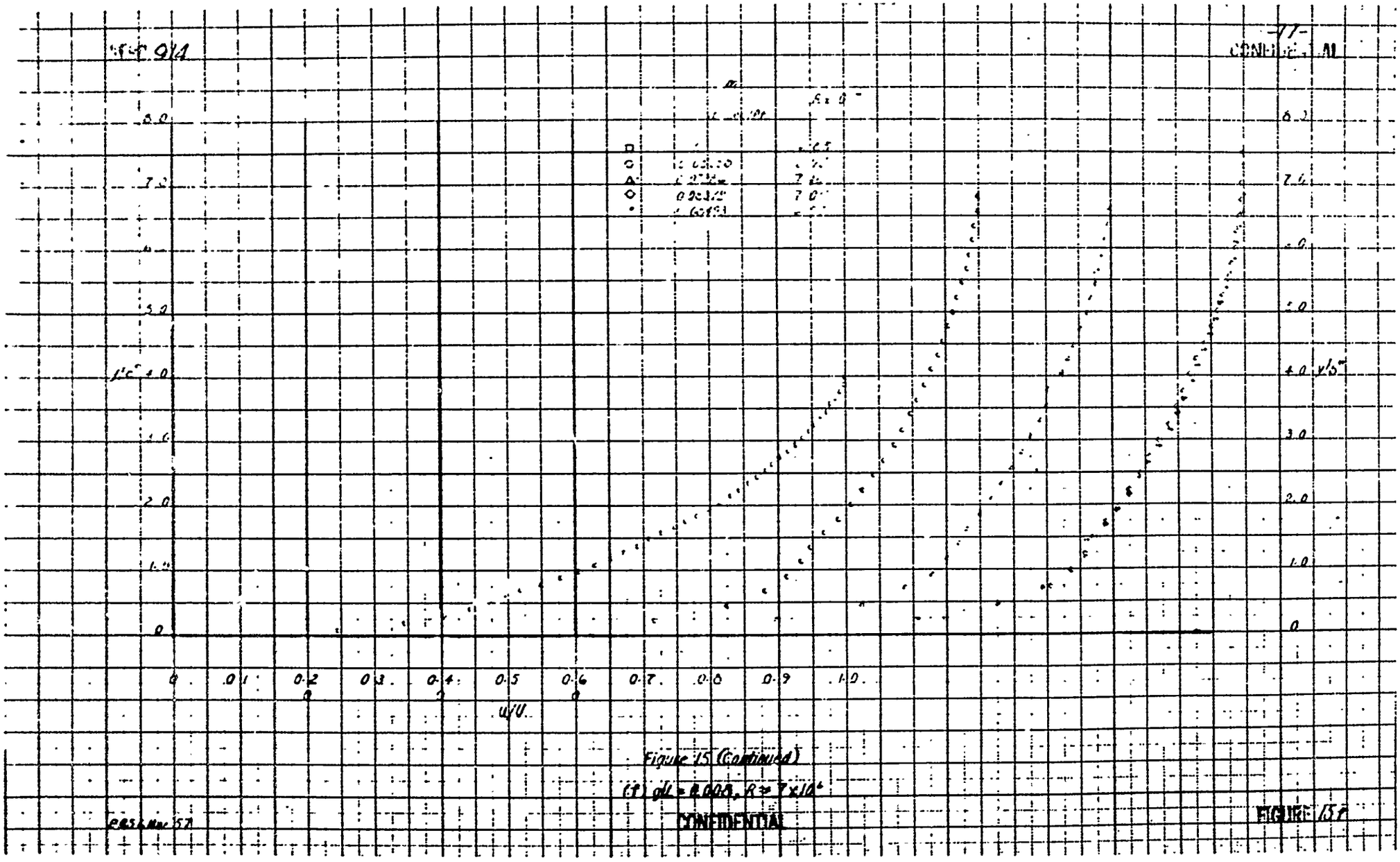

Figure 15 (Continued)

(f) $dU = 0.008$, $R = 7 \times 10^6$

FIGURE 15f

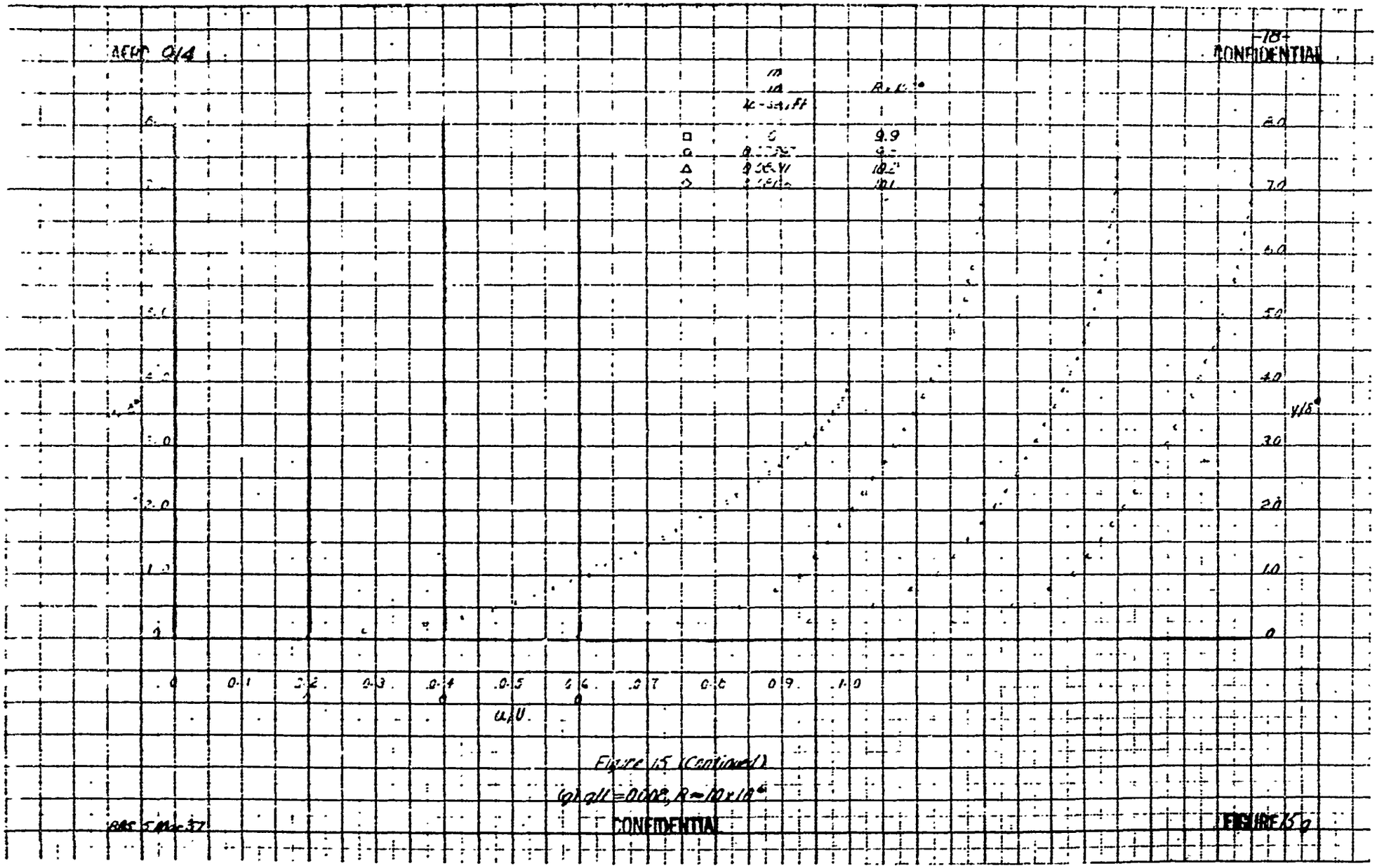

Figure 15 (Continued)

(g) q_∞ = 0.002, R = 10 x 10^6

FIGURE 15g

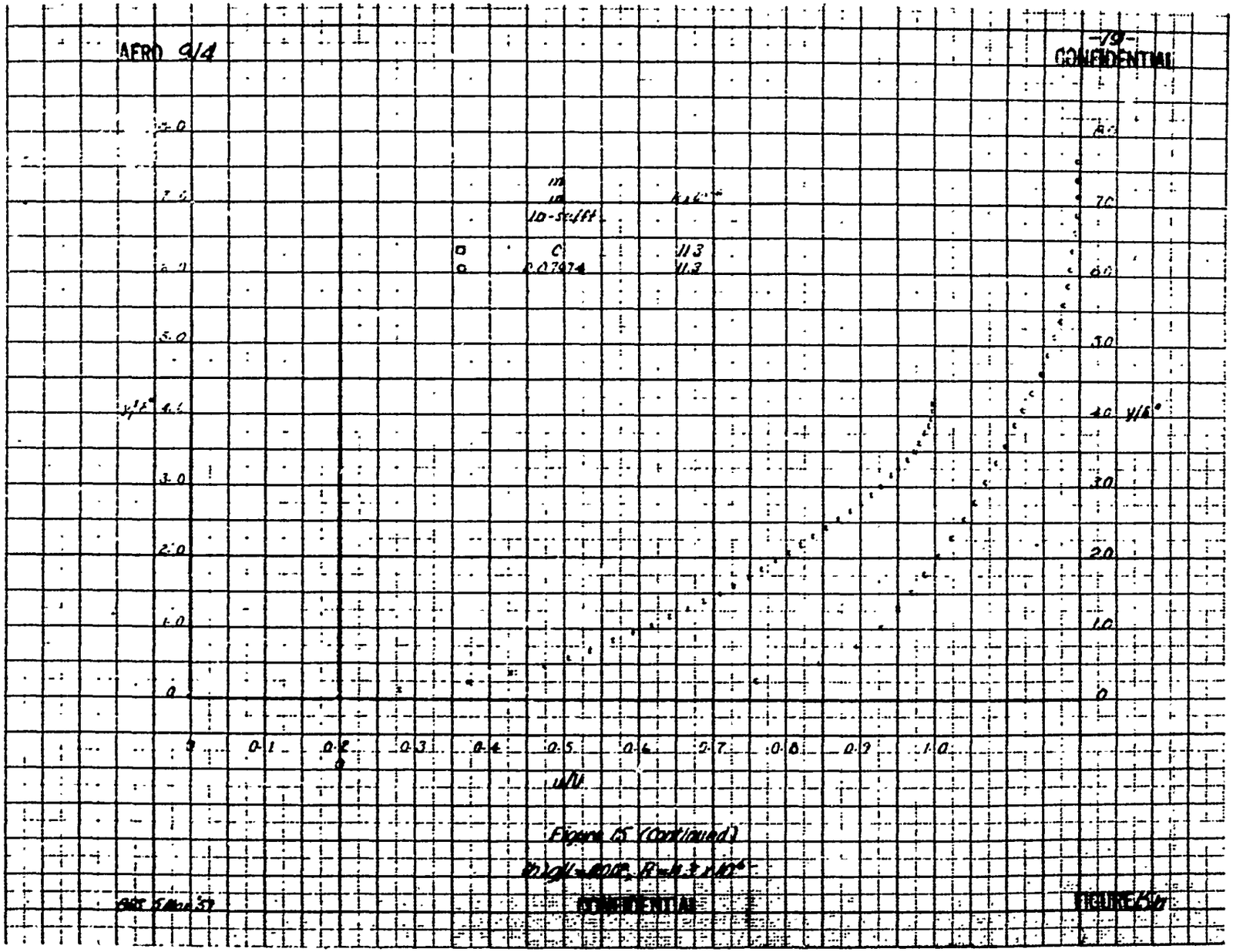

AERO 914

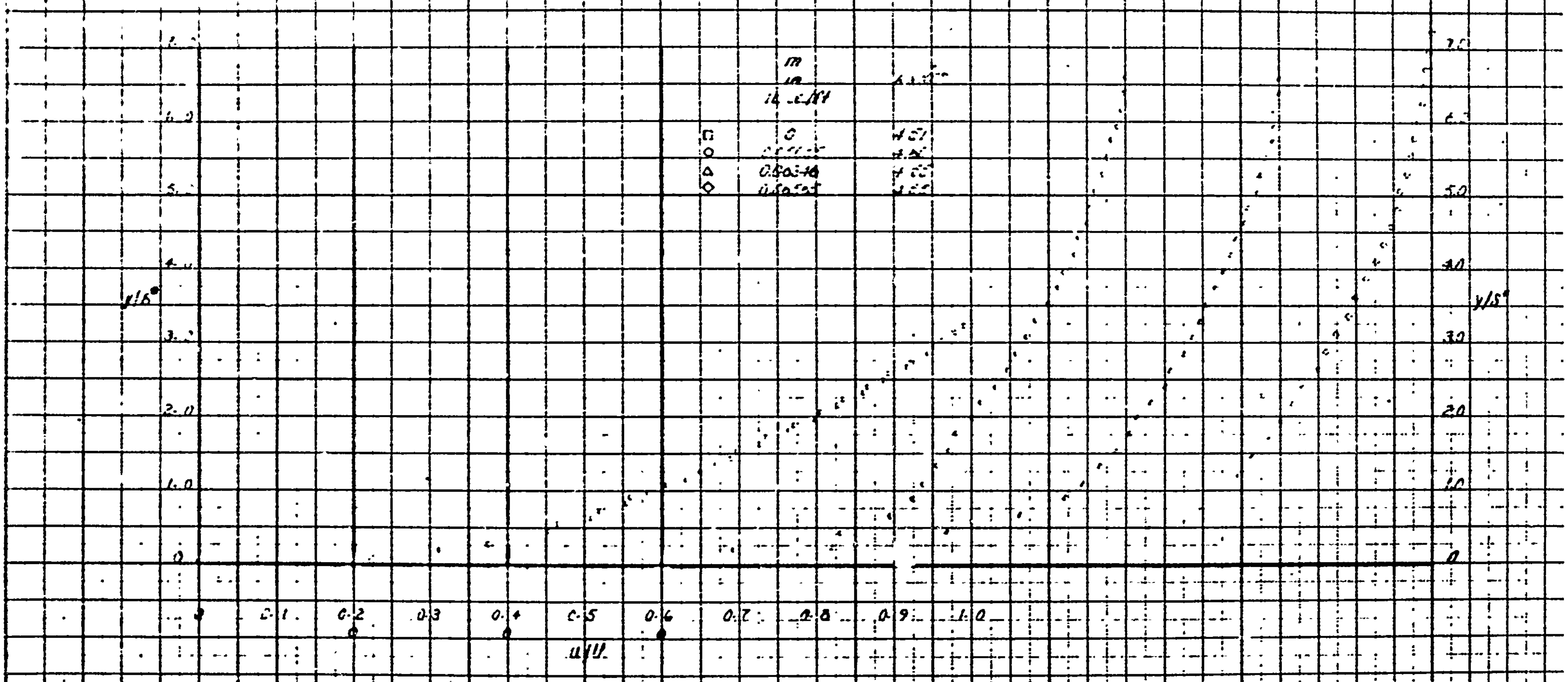

Figure 15 (Continued)

(i) $gH = 0.004$, $R = 4.5 \times 10^6$

CONFIDENTIAL

FIGURE 15 c

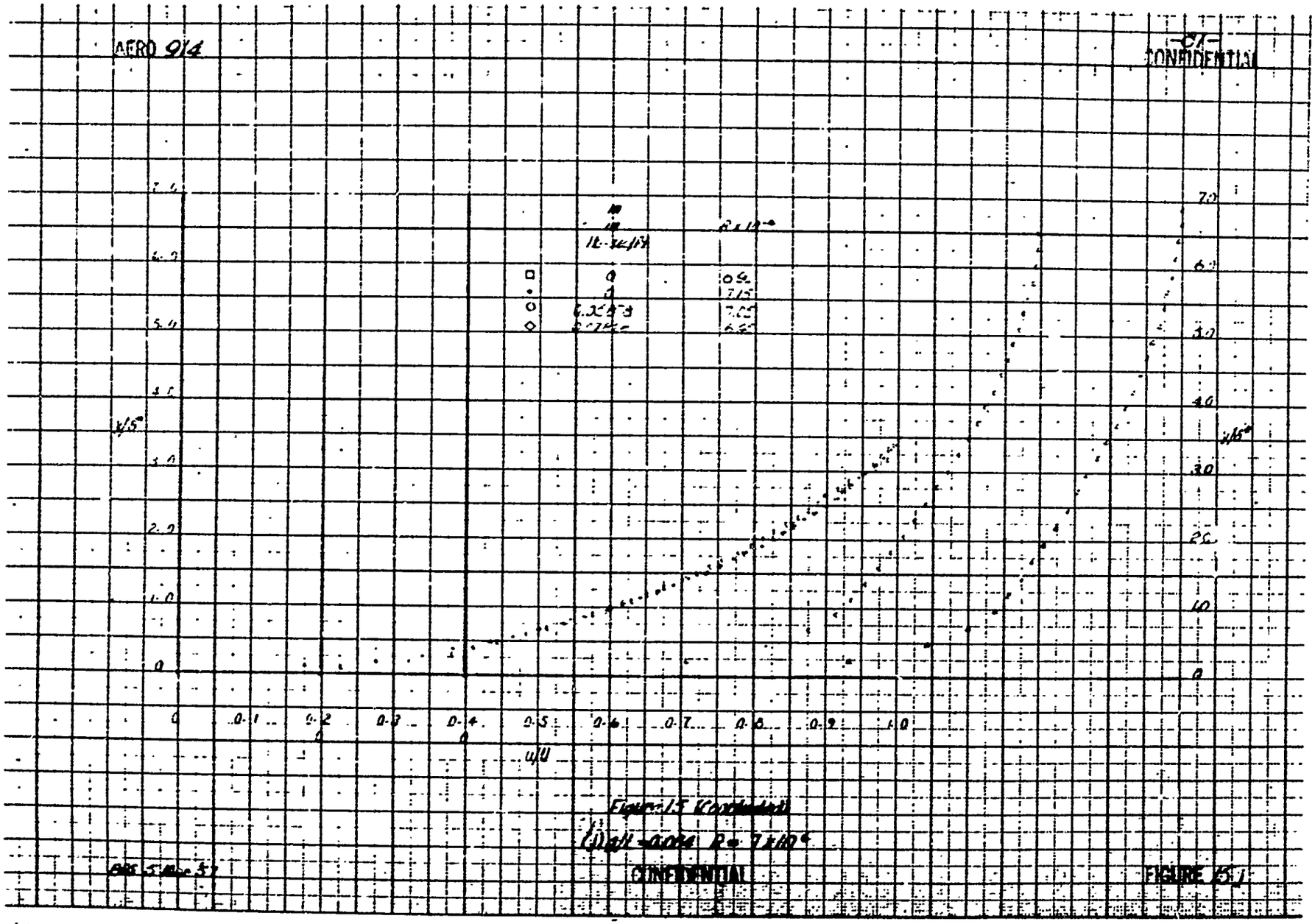

FIGURE 15.1

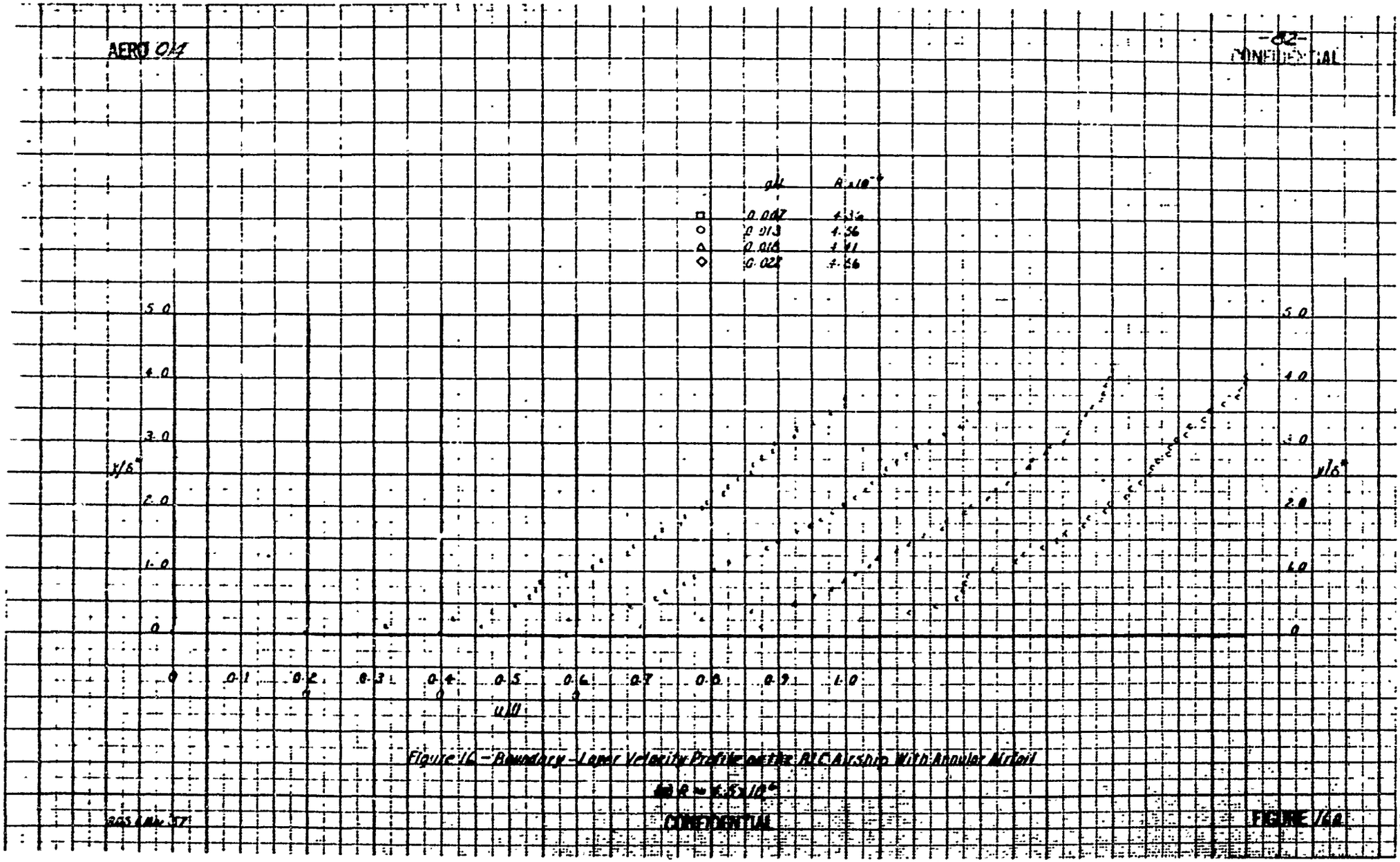

Figure 16 - Boundary - Layer Velocity Profile on the RIC Airship With Annular Airfoil

$R_{\delta^*} = 4.5 \times 10^6$

FIGURE 16

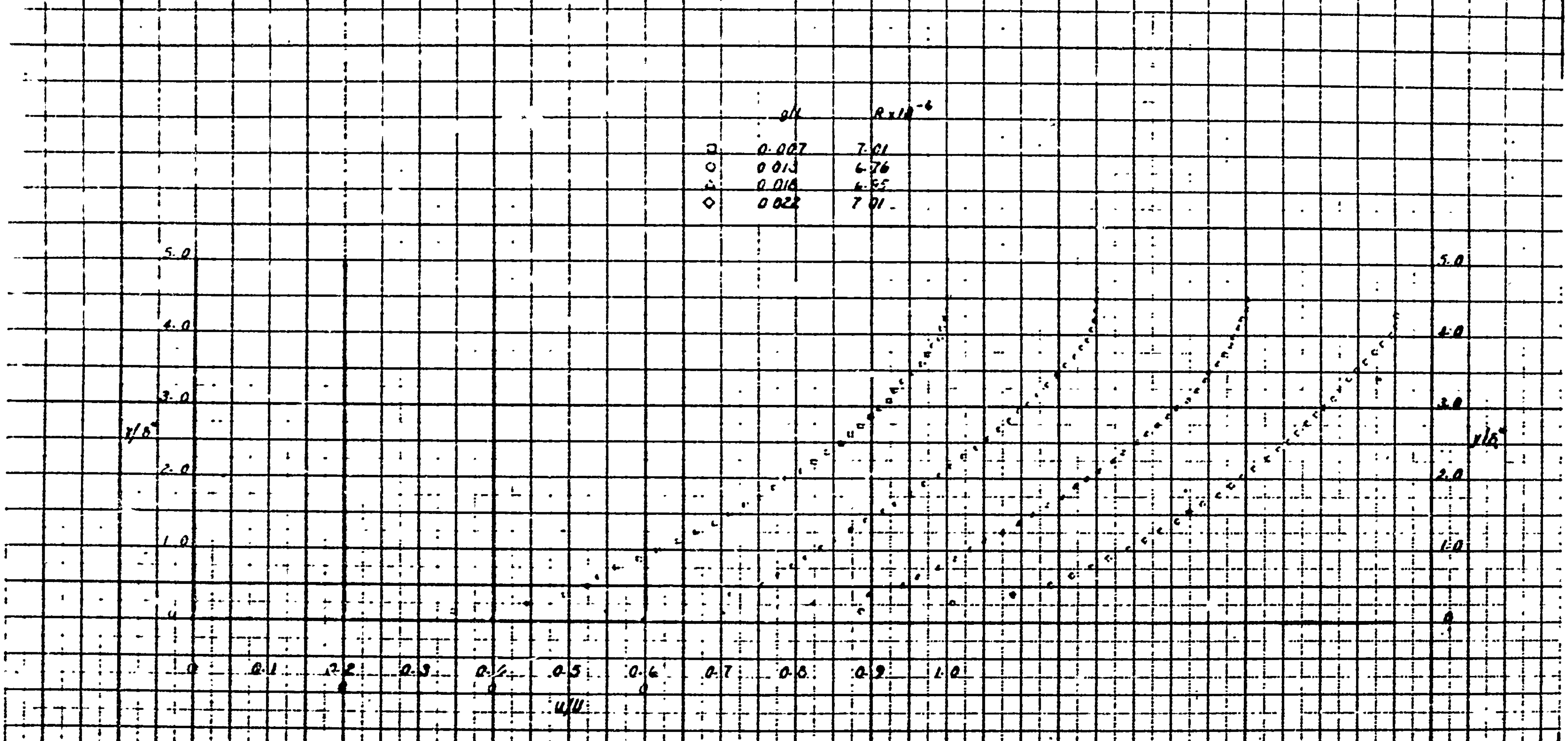

Figure 16 (Continued)

(b) R = 7 x 10^6

CONFIDENTIAL

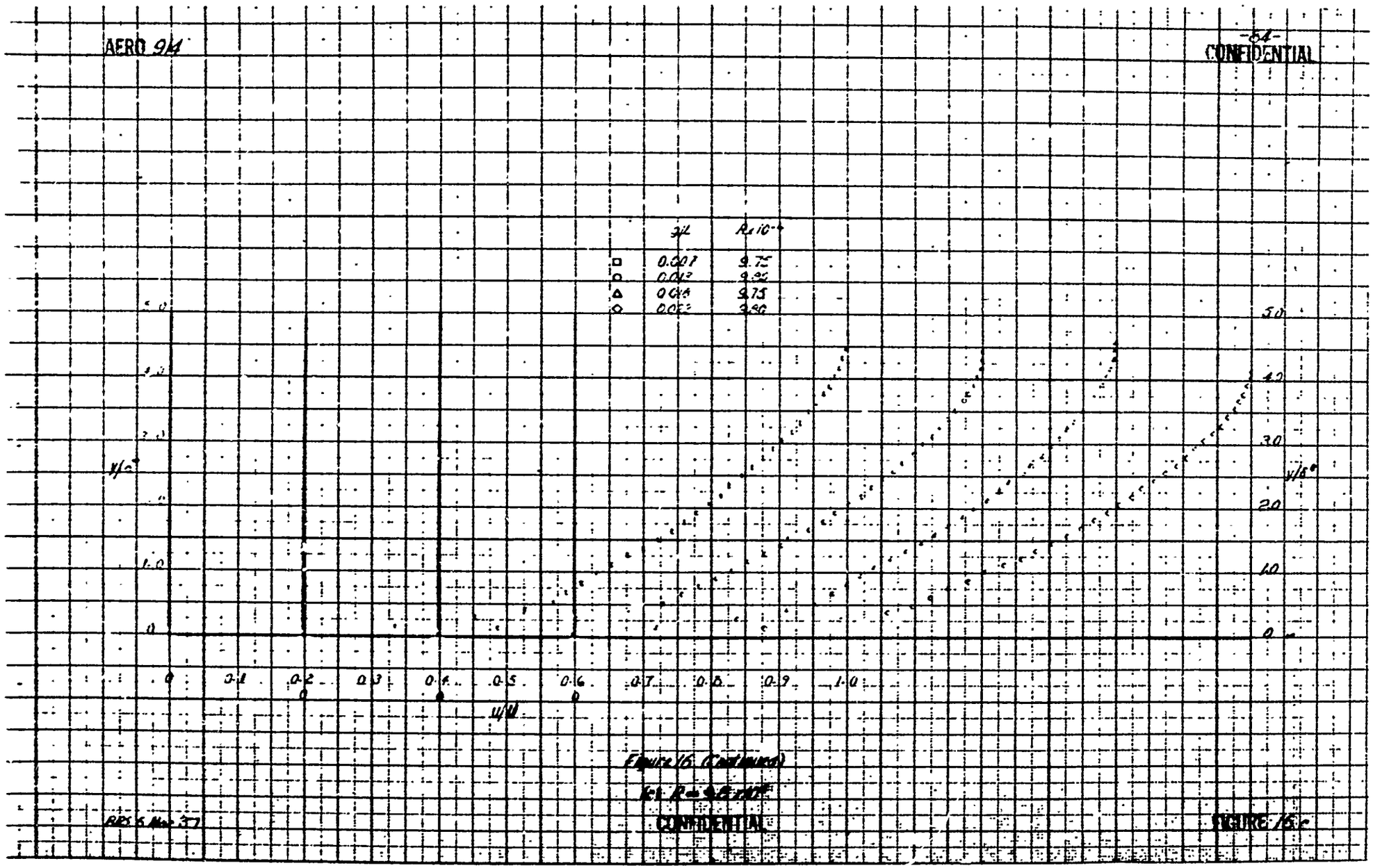

Figure 16. (Continued)

for R = 9.8 x 10⁶

CONFIDENTIAL

RPS 5 May 37

FIGURE 16-c

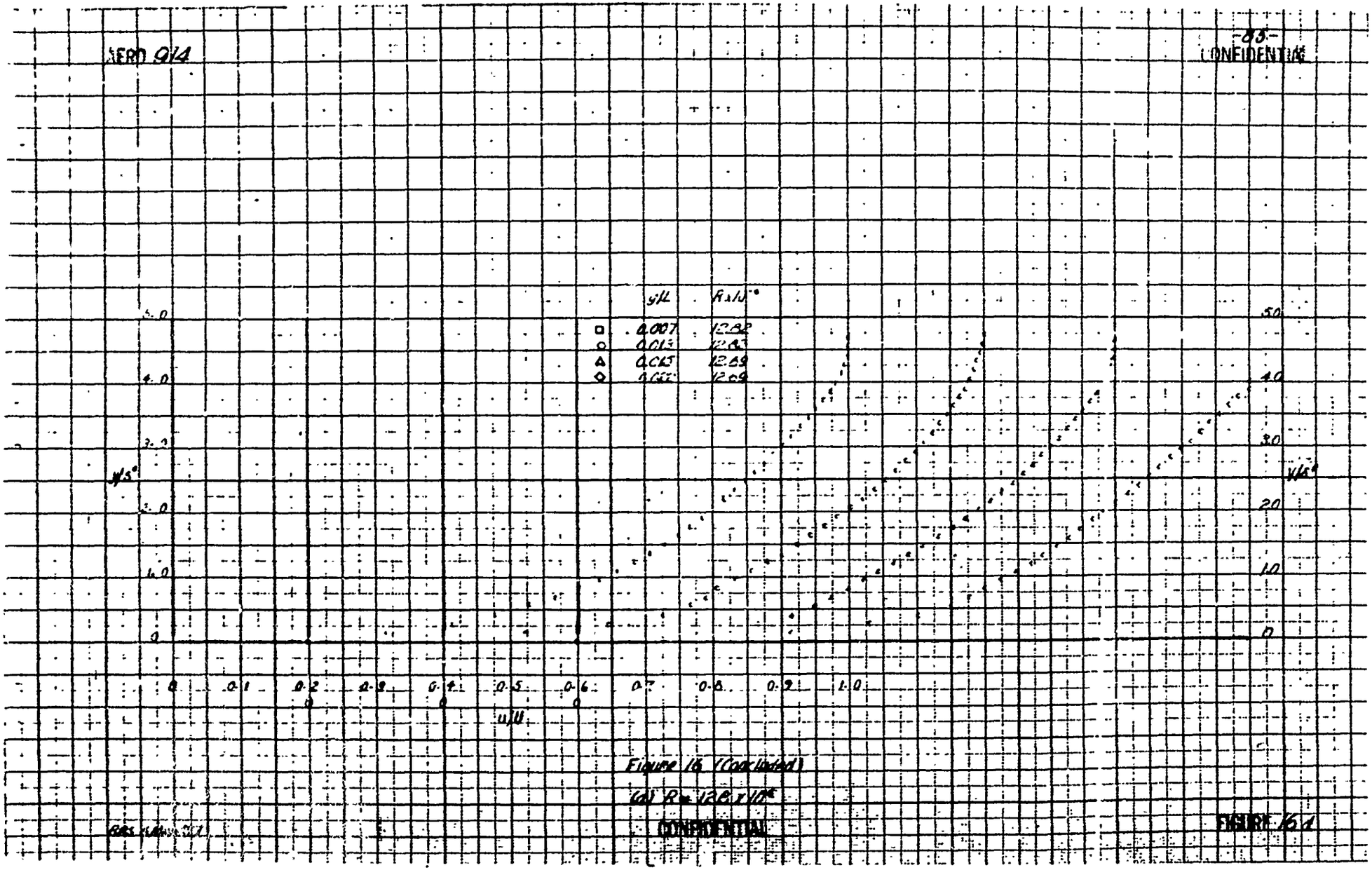

Figure 16 (Concluded)

(d) $R = 12.8 \times 10^6$

FIGURE 16d

CONFIDENTIAL

AD 127331

ERRATA

to

AERO REPORT 914

by

Peter A. Cerreta

March 1957

AD-127331

Enclosure (1) Bu Aer ltr ser 05E68
of

10 JUN 1957

4 3 1

ENCLOSURE (1)

CONFIDENTIAL

57AA 23581

Pen and ink changes:

Page 1, Line 14: Change "20 percent" to "30 percent"

Page 13, Line 1: Change "at least 20 percent" to "approximately 30 percent"

Substitute the following attached material for the corresponding pages in the Report:

Table 4,	Pages 18 - 21
Figure 5,	Pages 26 - 29
Figure 7,	Page 31
Figure 8a,	Page 32
Figure 12b,	Page 57
Figure 14b,	Page 62
Figure 14g,	Page 67

Table 4

Summary of Test Configurations and Calculated Results

Model	Airfoil	Shroud	BL	g/L	Rx10^{-6}	$\frac{m}{\text{in}}$ $\frac{\text{lb-sec}}{\text{ft}}$	C_{D_s}	C_{D_w}	C_{D_T}	δ^*	θ	$\frac{\delta^*}{\theta}$
XZS2G-1	None	None	Tripped	0	4.65	0	0	0.0284	0.0284	--	--	--
					8.57			0.0262	0.0262	--	--	--
					12.6			0.0267	0.0267	--	--	--
					18.3			0.0239	0.0239	--	--	--
BLC Airship	None	None	Tripped	0	4.31	0	0	0.0403	0.0403	0.2465	0.1423	1.7322
					7.00			0.0438	0.0438	0.1852	0.1076	1.7211
					9.85			0.0391	0.0391	0.1720	0.1010	1.7029
					12.4			0.0481	0.0481	0.1677	0.0987	1.6990
				0.016	4.36	0	0	0.0359	0.0359	0.2022	0.1155	1.7506
					4.61	0.03813	0.0182	0.0040	0.0222	0.1048	0.0696	1.5057
					4.61	0.04987	0.0198	0.0016	0.0214	0.1022	0.0676	1.5118
					4.71	0.06028	0.0195	0.0008	0.0203	0.0947	0.0627	1.5103
					6.95	0	0	0.0372	0.0372	0.1836	0.1030	1.7825
					6.95	0	0	0.0308	0.0308	0.1770	0.0987	1.7933
					7.15	0.05868	0.0168	0.0032	0.0200	0.0964	0.0651	1.4807
					7.10	0.07623	0.0180	0.0018	0.0198	0.0920	0.0623	1.4767
					7.25	0.08713	0.0184	0.0007	0.0191	0.0883	0.0602	1.4667
					9.9	0	0	0.0438	0.0438	0.1657	0.0974	1.7012
					9.8	0.08208	0.0161	0.0014	0.0175	0.0906	0.0620	1.4612
					10.2	0.08411	0.0160	0.0013	0.0173	0.0883	0.0606	1.4570
					10.1	0.08431	0.0161	0.0014	0.0175	0.0870	0.0595	1.4621
					12.6	0	0	0.0255	0.0255	0.1667	0.0950	1.7547

CONFIDENTIAL

Table 4 (Continued)

Model	Airfoil	Shroud	BL	g/L	Rx10^{-6}	$\frac{m}{\text{in}}$ $\frac{\text{lb-sec}}{\text{ft}}$	C_{D_s}	C_{D_w}	C_{D_T}	δ^*	θ	$\frac{\delta^*}{\theta}$
BLC Airship	None	None	Tripped	0.012	4.46	0	0	0.0484	0.0484	0.2218	0.1136	1.9524
					4.36	0	0	0.0314	0.0314	0.1648	0.1051	1.5680
					4.36	0.03249	0.0165	0.0042	0.0207	0.1055	0.0698	1.5114
					4.41	0.04419	0.0181	0.0026	0.0207	0.0940	0.0627	1.4992
					4.46	0.05897	0.0198	0.0008	0.0206	0.0922	0.0623	1.4799
					7.10	0	0	0.0350	0.0350	0.2177	0.1079	2.0176
					7.15	0.04936	0.0142	0.0041	0.0183	0.0936	0.0641	1.4602
					7.06	0.06755	0.0166	0.0018	0.0184	0.0850	0.0584	1.4554
					7.01	0.08207	0.0179	0.0013	0.0192	0.0826	0.0570	1.4491
					10.2	0	0	0.0558	0.0558	0.1739	0.0999	1.7407
					10.3	0.07000	0.0176	0.0054	0.0230	0.1157	0.0778	1.4871
					9.95	0.08162	0.0153	0.0032	0.0185	0.0854	0.0566	1.5088
					9.85	--	--	0.0027	--	0.0781	0.0544	1.4356
		Attached	Tripped	0.012	4.51	0.03095	0.0155	0.0040	0.0195	0.0963	0.0631	1.5261
					4.41	0.04263	0.0178	0.0022	0.0200	0.0929	0.0618	1.5032
					4.36	0.05922	0.0199	0.0007	0.0206	0.0918	0.0620	1.4806
					7.00	0.04281	0.0133	0.0052	0.0185	0.0898	0.0605	1.4842
					6.95	0.06850	0.0165	0.0017	0.0182	0.0840	0.0575	1.4608
					7.10	0.08487	0.0180	0.0010	0.0190	0.0837	0.0579	1.4455
					6.90	0.06826	0.0164	0.0014	0.0178	0.0833	0.0568	1.4665
					10.1	0.06286	0.0132	0.0027	0.0159	0.0854	0.0575	1.4852
					10.0	0.07410	0.0147	0.0027	0.0174	0.0870	0.0588	1.4795
					10.0	0.08385	0.0143	0.0049	0.0193	0.0788	0.0543	1.4511
					11.3	0.06667	0.0131	0.0026	0.0157	0.0826	0.0567	1.4567
					11.3	0.07998	0.0145	0.0019	0.0164	0.0794	0.0550	1.4436
					11.2	0.08470	0.0147	0.0019	0.0166	0.0793	0.0547	1.4497

CONFIDENTIAL

Table 4 (Continued)

Model	Airfoil	Shroud	BL	g/L	$R \times 10^{-6}$	$\frac{\dot{m}}{\text{in}}$ lb-sec/ft	C_{D_s}	C_{D_w}	C_{D_T}	δ^*	θ	$\frac{\delta^*}{\theta}$
					4.56	0	0	0.0326	0.0326	0.1692	0.1042	1.6238
					4.51	0.03891	0.0179	0.0028	0.0207	0.1047	0.0705	1.4851
					4.41	0.05273	0.0197	0.0018	0.0215	0.0947	0.0622	1.5225
					4.51	0.05447	0.0193	0.0009	0.0202	0.0888	0.0609	1.4581
					4.60	0.08263	0.0191	0.0003	0.0194	0.0827	0.0553	1.4954
					7.20	0	0	0.0274	0.0274	0.2104	0.1082	1.9445
		None	Tripped	0.008	7.15	0.05577	0.0158	0.0030	0.0188	0.0948	0.0624	1.5192
					7.20	0.07091	0.0166	0.0014	0.0180	0.0833	0.0572	1.4562
					7.10	0.07409	0.0167	0.0010	0.0177	0.0802	0.0562	1.4270
					7.10	0.08112	0.0177	0.0009	0.0186	0.0878	0.0584	1.5034
					10.[illegible]5	0	0	0.0574	0.0574	0.1910	0.1011	1.8892
					10.15	0.07788	0.0149	0.0019	0.0168	0.0848	0.0563	1.5062
BLC Airship	None				10.0	0.07826	0.0147	0.0020	0.0167	0.0793	0.0553	1.4339
					4.31	0	0	0.0291	0.0291	0.2252	0.1154	1.9582
					4.36	0.08315	0.0207	0.0005	0.0212	0.0833	0.0582	1.4312
					6.85	0	0	0.0291	0.0291	0.2020	0.1142	1.7688
					6.95	0.05558	0.0157	0.0024	0.0181	0.0880	0.0608	1.4473
					7.10	0.07286	0.0171	0.0013	0.0184	0.0846	0.0581	1.4561
					7.05	0.08372	0.0180	0.0008	0.0188	0.0799	0.0558	1.4318
		Attached	Tripped	0.008	6.95	0.08493	0.0177	0.0009	0.0186	0.0819	0.0562	1.4572
					9.9	0	0	0.0557	0.0557	0.1766	0.1011	1.7467
					9.8	0.07397	0.0146	0.0027	0.0173	0.0795	0.0550	1.4454
					10.2	0.08011	0.0147	0.0026	0.0173	0.0777	0.0537	1.4469
					10.1	0.08126	0.0152	0.0026	0.0178	0.0791	0.0552	1.4329
					11.3	0	0	0.0500	0.0500	0.1726	0.0989	1.7451
					11.3	0.07974	0.0142	0.0020	0.0162	0.0786	0.0547	1.4369

CONFIDENTIAL

Table 4 (Concluded)

Model	Airfoil	Shroud	BL	g/L	$Rx10^{-6}$	$\frac{m}{\text{in}}$ $\frac{\text{lb-sec}}{\text{ft}}$	C_{D_s}	C_{D_w}	C_{D_T}	δ^*	θ	$\frac{\delta^*}{\theta}$
					4.36	0	0	0.0901	0.0901	0.1931	0.1107	1.7443
	None	None	Tripped	0.004	4.31	0.04474	0.0186	0.0014	0.0200	0.0905	0.0615	1.4731
					4.31	0.04864	0.0184	0.0019	0.0203	0.0856	0.0582	1.4707
					4.51	0	0	0.0325	0.0325	0.2214	0.1208	1.8327
					4.60	0.05055	0.0189	0.0029	0.0218	0.0903	0.0625	1.4448
					4.55	0.06346	0.0203	0.0024	0.0227	0.0904	0.0603	1.4991
	None	Attached	Tripped	0.004	4.55	0.06565	0.0190	0.0005	0.0195	0.0827	0.0572	1.4458
					6.90	0	0	0.0286	0.0286	0.1941	0.1048	1.8520
					7.05	0.05878	0.0167	0.0033	0.0200	0.0854	0.0584	1.4623
					6.95	0.07826	0.0175	0.0035	0.0210	0.0805	0.0558	1.4426
					7.15	0	0	0.0288	0.0288	0.2047	0.1074	1.9059
					4.36			0.0465	0.0465	0.1726	0.1025	1.6904
BLC Airship				0.007	7.01	0	0	0.0472	0.0472	0.1605	0.0970	1.6546
					9.75			0.0503	0.0503	0.1446	0.0888	1.6283
					12.82			0.0472	0.0472	0.1463	0.0879	1.6643
					4.56			0.0485	0.0485	0.1769	0.1013	1.7462
				0.013	6.76	0	0	0.0554	0.0554	0.1567	0.0961	1.6305
					9.80			0.0633	0.0633	0.1546	0.0912	1.6951
					12.82			0.0580	0.0580	0.1436	0.0878	1.6355
	Attached	None	Tripped		4.41			0.0587	0.0587	0.1688	0.1000	1.6880
					6.95			0.0587	0.0587	0.1607	0.0970	1.6567
				0.018	9.75	0	0	0.0755	0.0755	0.1494	0.0906	1.6490
					12.69			0.0628	0.0628	0.1468	0.0905	1.6220
					4.56			0.0607	0.0607	0.1770	0.1066	1.6604
					7.01			0.0622	0.0622	0.1589	0.0955	1.6638
				0.022	9.80	0	0	0.0557	0.0557	0.1648	0.0949	1.7365
					12.69			0.0639	0.0639	0.1492	0.0896	1.6651

CONFIDENTIAL

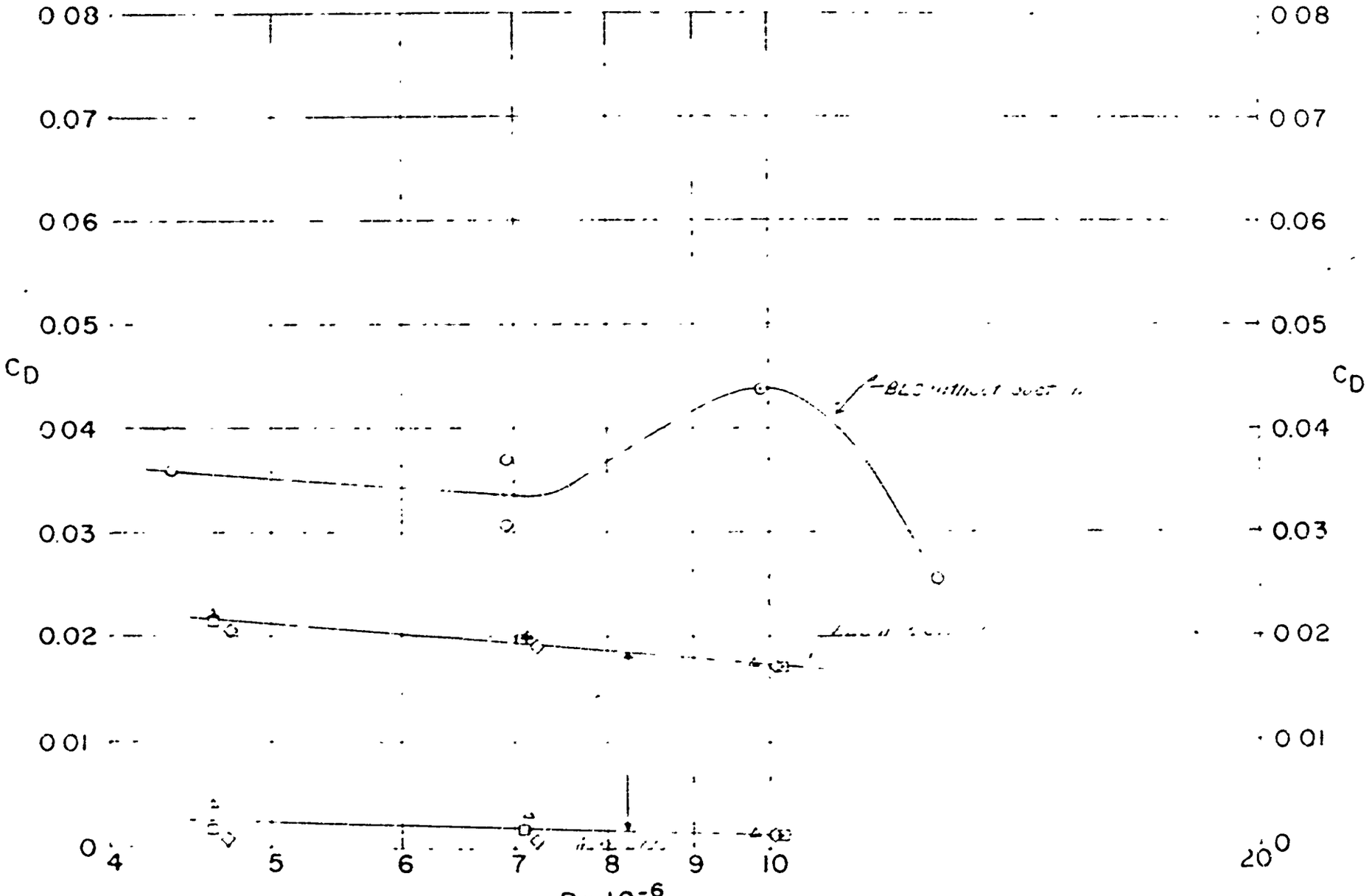

Fig. 5 Drag Coefficient with Reynolds Number for Section with Single Suction
(a) $\mu L = 0.016$

AERO 914

CONFIDENTIAL

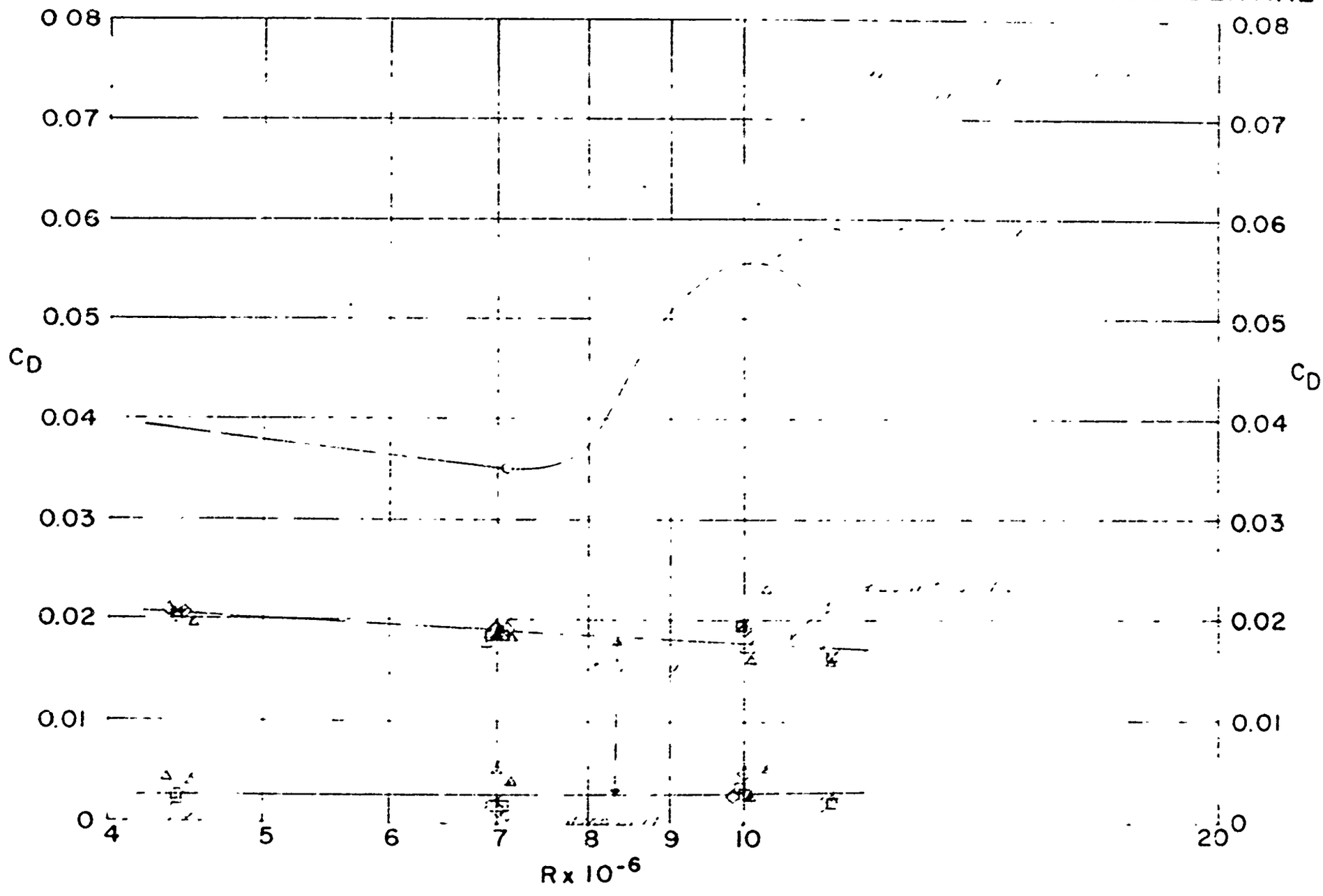

Figure 35 (Continued)
(b) $q/L = 1.012$

CONFIDENTIAL

FIGURE 35

AERO 914

CONFIDENTIAL

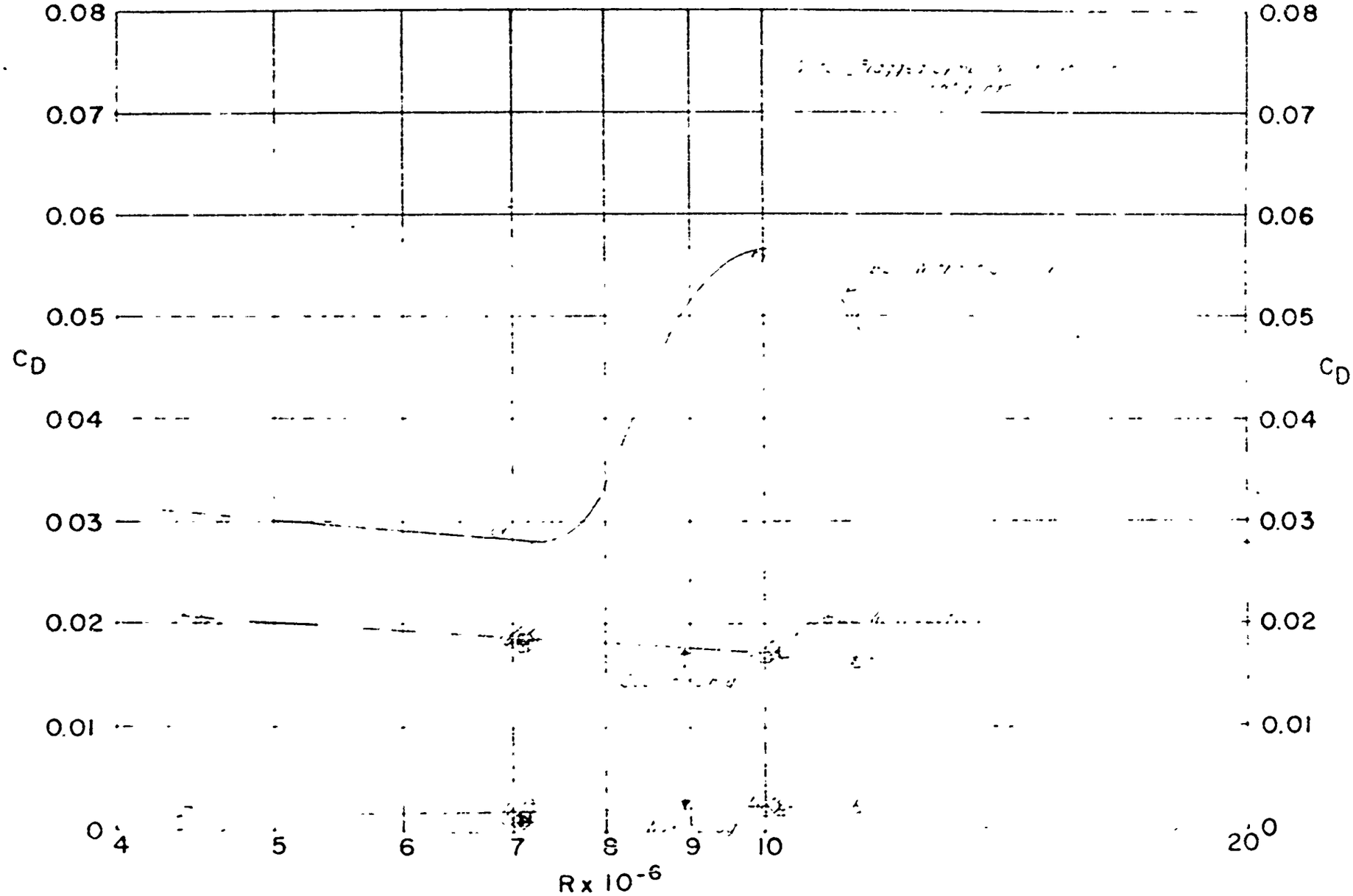

CONFIDENTIAL

FIGURE ___

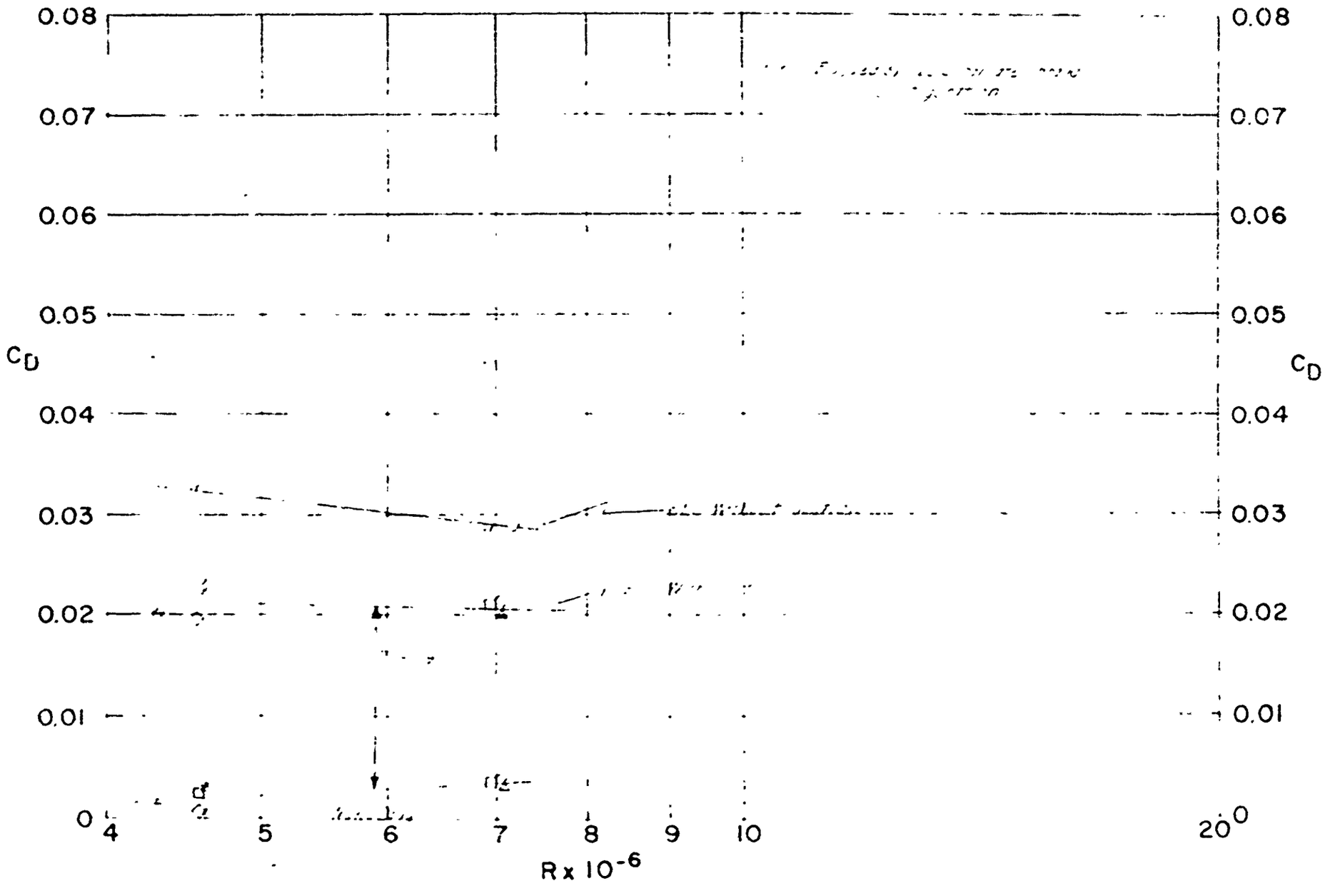
0.08
0.07
0.06
0.05
C_D
0.04
0.03
0.02
0.01
0
4
5
6
7
8
9
10
$R \times 10^{-6}$
α
20^0

FIGURE 5d

AERO 914

CONFIDENTIAL

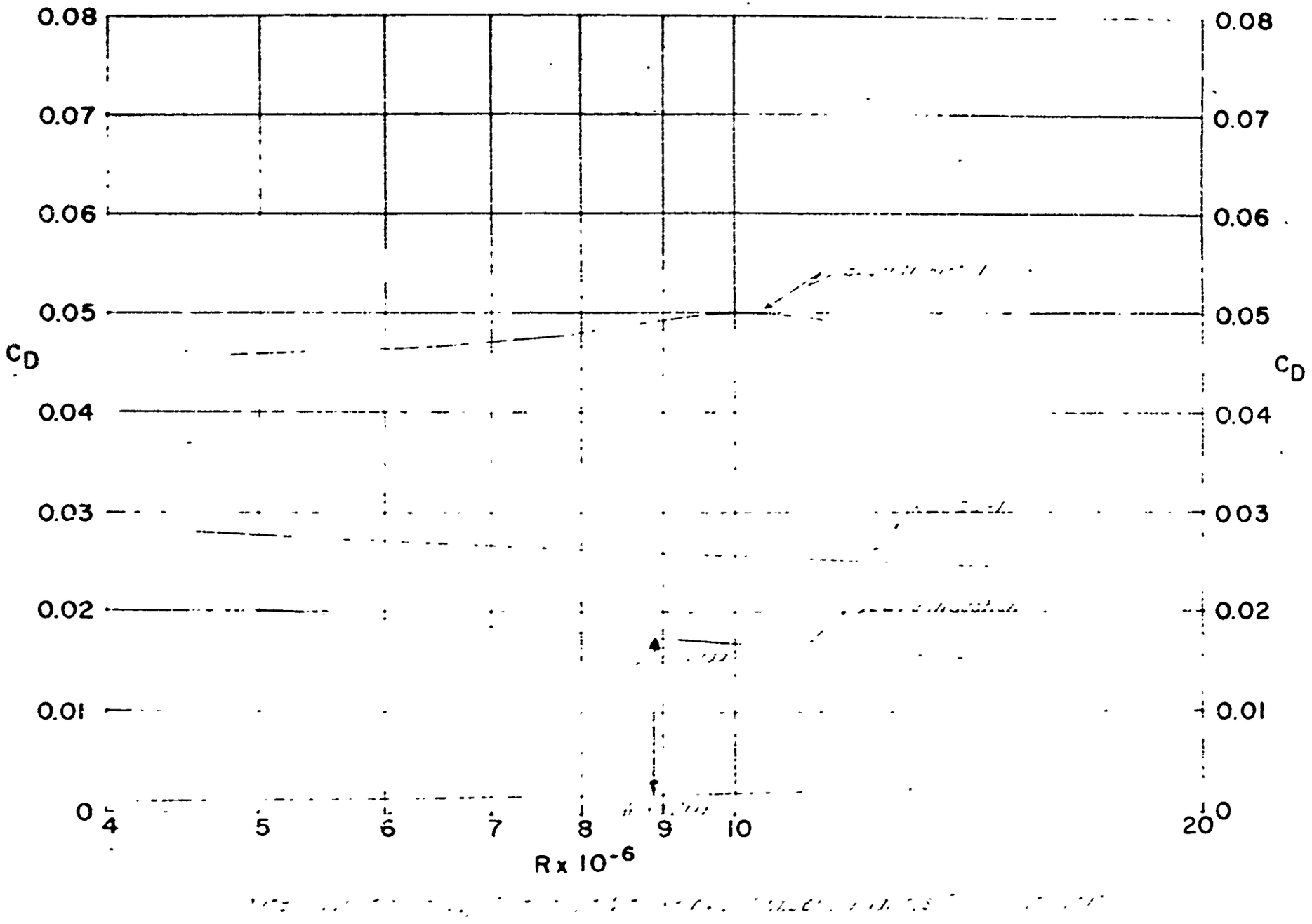

CONFIDENTIAL

FIGURE 1

Figure 8 - Pressure Distribution on the X-15A-1 Airship

(a) Meridional Transition

CONFIDENTIAL
Figure 12 (Continued)
(d) R = 7 x 10⁶
z/L
0.1
0.2
0.3
0.4
0.5
0.6
0.7
0.8
0.9
1.0
CONFIDENTIAL
FIGURE 12 b

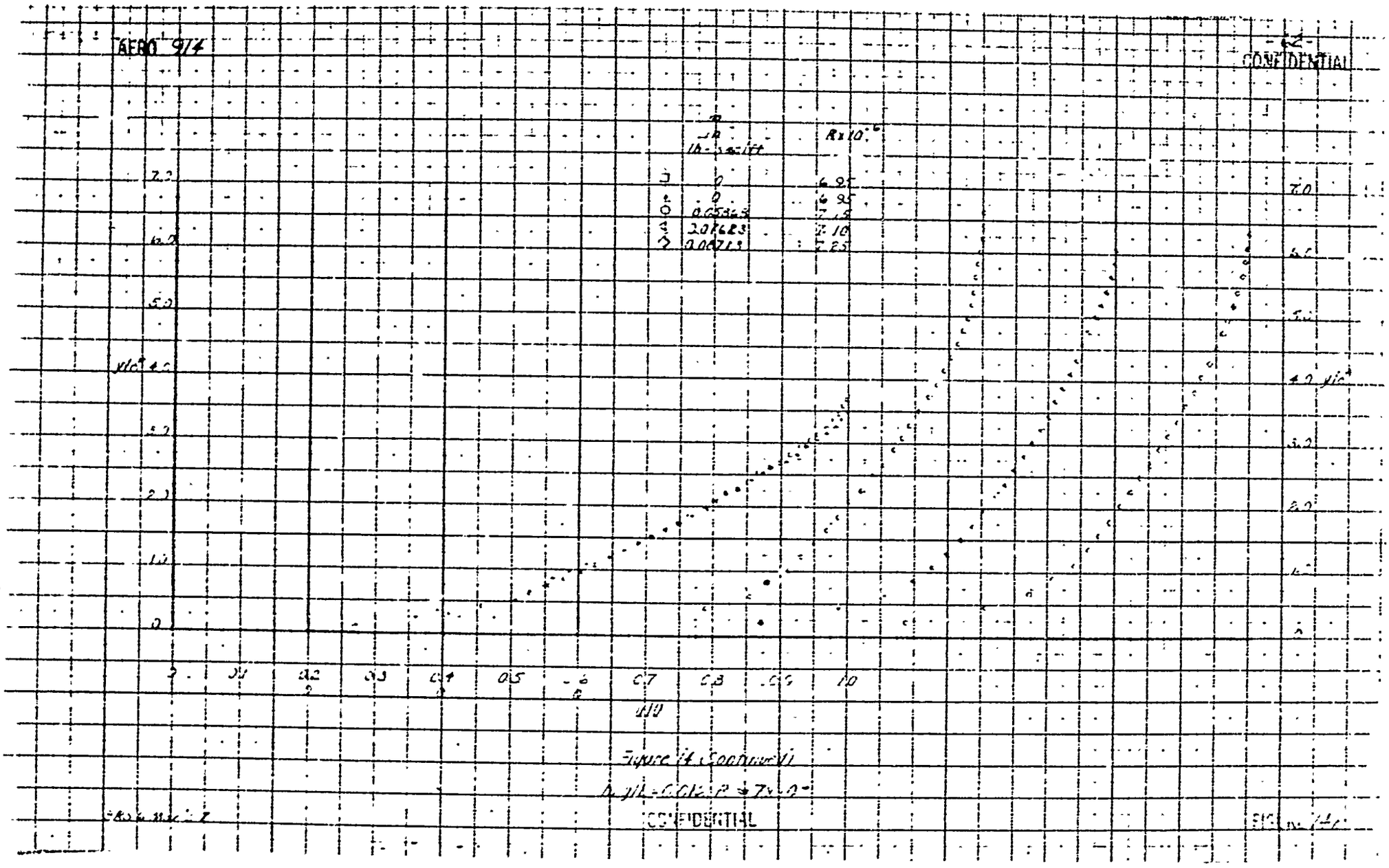

Figure 14 (Continued)